3D Remote Sensing technologies for Precision Forestry

UNIVERSITÀ
DEGLI STUDI
FIRENZE

DOTTORATO DI RICERCA IN GESTIONE SOSTENIBILE DELLE RISORSE AGRARIE FORESTALI E ALIMENTARI

Curriculum: ECONOMIA, PIANIFICAZIONE FORESTALE E SCIENZE DEL LEGNO

CICLO XXX

COORDINATORE Prof. Susanna Nocentini

3D Remote Sensing technologies for Precision Forestry

Settore Scientifico Disciplinare AGR/05

Francesca Giannetti

Tutor

Prof. Gherardo Chirici

Prof. Davide Travaglini

Anni 2015/2017

PhD Candidate
Francesca Giannetti
francesca.giannetti@unifi.it
francesca-giannetti@outlook.it

PhD supervisors
Prof. Gherardo Chirici
Dipartimento di Gestione dei Sistemi Agrari Alimentari e Forestali
Università degli Studi di Firenze
Via San Bonaventura, 13, 50145 Firenze
Prof. Davide Travaglini
Dipartimento di Gestione dei Sistemi Agrari Alimentari e Forestali
Università degli Studi di Firenze
Via San Bonaventura, 13, 50145 Firenze

Reviewers
Prof. Anna Barbati
Department for Innovation in Biological, Agro-food and Forest systems
DIBAF - University of Tuscia
S. Camillo de Lellis snc, 01100, Viterbo, Italy
Prof. Terje Gobakken
Faculty of Environmental Sciences and Natural resource Management
Norwegian University of Life Science
P.O. Box 5003, No, Ås, Norway

Evaluation Committee
Prof. Enrico Corrado Borgogno Mondino
Università di Torino
Prof. Piermaria Corona
Università della Tuscia
Prof. Mats Nilsson
Swedish University of Agricultural Sciences

Acknowledgements
This thesis was practically carried out in the framework of the FRESh LIFE project “Demonstrating Remote Sensing integration in sustainable forest management” (LIFE14/IT000414).

Acknowledgements

First of all, I would like to thank my PhD supervisors and co-authors in all papers Prof. Gherardo Chirici and Prof. Davide Travaglini for their support and guidance and Prof. Susanna Nocentini coordinator of the PhD program. The works included in this thesis are the result of their support with financial and intellectual resources. I am very grateful for being given complete intellectual freedom in finding my research interests. The past three years have been an invaluable learning and work experience. Moreover, thank you for buying my best UAV robot friend, "eBee"!

Special thanks go to my colleagues, co-authors and very good friends Dr Francesca Bottalico and Dr Martina Cambi who have help me to understand the research world. They have been an irreplaceable source of ideas and support. Martina e Francesca, to laugh and work together was an honour!

Thank you to all my co-authors: Prof. Enrico Marchi, Dr Nicola Puletti, Prof. Piermaria Corona, Dr Stefano Puliti, Prof. Terje Goabakken, Prof. Erik Naesset, and Dr Valerio Quatrini for their help in guiding me in the complex work of writing papers.

I am also grateful to Prof. Terje Goabakken and Dr Stefano Puliti for their kind help during my Norwegian PhD period. It has been very precious to work with you and to learn many new things.

Thank you also to the reviewers of this thesis, Prof. Anna Barbati and Terje Goabakken for their valuable comments.

I would like to thank my colleagues at GeoLAB, at GESAAF, and For&co group for creating an open and friendly working environment. The

lunch and coffee breaks, the short and long chats in the kitchen helped me to laugh and smile these three years. Thank you, Patrizia Rossi for your kind support and for the delicious coffee!

I want to thank also my family, my nephews Pietro e Jacopo, my mum, and my sisters Lucia e Camilla who have always supported me. Thank you for believing always in me and for following me along my complex and confused dreams!

Thanks to Maria Luisa for her kind support and enthusiasm in supporting my experiences!

Thanks to my swim coach colleagues, Filippo, Eugenia, Stefania e Geraldine for sharing the sporting life with me and for reminding me how education is important everywhere. Thanks to my athletes of Viola Swim Team that think of me as a doctor of trees or a UAV pilot superhero.

Last but not the least, thank you to all my friends, especially Giulia Maso and Vale that helped me when I needed distractions!

Firenze, 30th October 2017

Francesca Giannetti

Contents

Abstract

Precision forestry is a new approach for more sustainable forest management. Modern technologies are important to the development of new tools and applications to conduct site-specific management practices. 3D remote sensing technologies are new tools and have new applications useful for improving the data collection, work efficiency and quality of forest information that can be used to take better management decisions.

This thesis is aimed at assessing the use of 3D data to develop new tools and procedures useful for forest inventories and for the estimation of soil disturbances caused by forest operations. In so doing, this study attempts to close the gaps underlined by previous studies.

The thesis is divided into two main sections. The first one comprises the studies I, II, and III related to forest inventory optimization, while the second section comprises the studies IV and V related to estimation of soil disturbances caused by forest operations.

Study I demonstrates how a 3D point cloud acquired by a Terrestrial Laser Scanner (TLS) and a Hand-Held Mobile Laser Scanner (HMLS) can be used to automatically derive forest single tree variables such as diameter at breast height (DBH) and tree position (TP). Moreover, the study underlines how the integration of TLS with Airborne Laser Scanner (ALS) point clouds improves the estimation of tree top height (H) and crown base projection (CPA).

In study II a novel approach is presented for the extraction of explanatory variables from unmanned aerial vehicle (UAV) 3D photogrammetric data for predicting forest biophysical properties without relying on a digital terrain model. This study assesses the use of DTM-independent variables to predict forest biophysical proprieties using as a benchmark two more traditional sets of variables: (i) height and density variables from UAV photogrammetric data normalized using a DTM

acquired using airborne laser scanning (ALS) (Image-DTM_{ALS} variables), and (ii) height and density variables extracted from normalized ALS data (ALS variables). We obtained comparable results between the models developed with DTM-independent models and the ones obtained with the other two types of variables (i.e. Image-DTM_{ALS} and ALS) to predict: Growing Stock Volume (V), Basal Area (G), Number of trees (N), Dominant Height (H_{dom}) and Lory's height (H_l).

Study III used the new set of DTM-independent variables developed in study II to predict area-based (ABA) forest structure variables (e.g. V, G, Mean Diameter (DBH_{mean}), Gini coefficient of DBH (Gini), standard deviation of DBH(σ_{dbh}), H_{dom}, H_l and standard deviation of H (σ_h)) using as benchmarks the variables from ALS. The results underline comparable results between the two types of metrics in the estimation of forest structure variables. Moreover, the models developed with DTM-independent metrics were used to create two maps of two forest structure indices.

In study IV and V we tested the utility of multi-temporal high resolution DTM derived by Personal Laser Scanner (PLS) (IV) and by close range photogrammetry (V) to measure and quantify soil disturbances caused by forest operation. These studies underline how multi-temporal high resolution (DTM) can be used to quantify rut deep, bulges, and soil volume changes.

In conclusion, 3D RS data appears useful in the development of new methods to collect and measure forest ecosystem components such as vegetation and soils.

Keywords: precision forestry, 3D Remote Sensing data, Airborne Laser Scanner, Terrestrial Laser Scanner, Photogrammetry, Portable Laser Scanner, Structure from Motion, Forestry, Forestry inventories, forest operations, forest management

List of papers

Forest inventory applications

Paper I

Giannetti, F., Puletti, N., Quattrini, V., Bottalico, F., Travaglini D., Corona, P., Chirici G. (2017). Integrating terrestrial and airborne laser scanning for the assessment of single tree attributes in Mediterranean forest stands. *Submitted*

Paper II

Giannetti, F., Chirici, G., Gobakken, T., Næsset, E., Travaglini, D., Puliti, S. (2017). Development and assessment of DTM-independent variables for prediction of forest biophysical properties using UAV photogrammetric data. *Submitted*

Paper III

Giannetti, F., Puletti, N., Puliti, S., Travaglini, D., Chirici, G. (2017). UAV photogrammetric DTM-independent variables can be used to predict forest structural indices? A case of study in mixed temperate forests. *Manuscript*

Soil disturbance applications

Paper IV

Giannetti, F., Chirici, G., Bottalico, F., Travaglini, D., Marchi, E., Cambi, M. (2017). Assessment of soil disturbance caused by forest operations by means of Portable Laser Scanner and soil physical parameters *Soil Science Society of America Journal DOI: 10.2136/sssaj2017.02.0051. Published online October 19, 2017*

Paper V

Cambi, M., Giannetti, F., Bottalico, F., Travaglini, D., Nordfjell, T., Chirici, G., Marchi, E. (2017). Estimating soil impact in logging skid trails via close-range photogrammetry and soil parameters: a case study in central Italy. *Accepted iForest*

1. Introduction

1.1. Precision Forestry

Forests are complex environments characterized by high biological and genetic biodiversity (Dinerstein et al., 1995) that provide multifunctional services simultaneously to satisfy social, cultural, economic, and environmental demands (Chirici et al., 2012; FOREST EUROPE, 2015; O'Farrell and Anderson, 2010). Many forest ecosystem components (e.g. vegetation, soil, and water) need to be monitored and measured simultaneously to quantify the health and the state of forests (FOREST EUROPE, 2015) and to create multiple objective management plans (Arabatzis, 2010; Fotakis et al., 2012; Ozdemir, 2008). At present, *precision forestry* is a new direction for better forest management (Corona et al., 2017; Fardusi et al., 2017; Kovácsová and Antalová, 2010). Precision forestry's fundamentals are founded on *precision agriculture*. Indeed, the term "precision" was introduced for the first time in the 1990s in agriculture and it was referred to practices and solutions to improve and to optimize site-specific management practices considering spatial and temporal variability with the aim of increasing productivity and reducing environmental risks (Tran and Nguyen, 2006). *Precision agriculture* was defined as "the integration of technology in the collection, interpretation, and analysis of data to support the decision-making system, in order to improve the agricultural processes by precisely managing each step to ensure maximum agricultural production while maintaining the sustainability of natural resources" (Dyck, 2003). Only in the early 2000s in the US, was "precision" introduced in forestry to develop sustainable forest management (SFM) systems and improve the work efficiency of forest operations. Taylor et al. (2002) first defined *precision forestry* as "planning and conducting site-specific forest management activities and operation to

improve wood production quality and utilization, reduce waste, and increase profits, and maintain the quality of the environment". Indeed, in 2014 the Joint Research Centre of the European Commission modified the definition of *precision*, (e.g. agriculture and forests) as the "environment friendly system solution that optimizes product quality and quantity while minimizing cost, human impact and intervention, and the variation caused by unpredictable nature", placing more importance on the sustainable development strategies.

Several authors underline how modern technologies are important to developing *precision forestry* applications (Fardusi et al., 2017; Kovácsová and Antalová, 2010; Taylor et al., 2002). The definition given in 2014 during the First International Conference on Precision Forestry underlines how "Precision Forestry uses high technology sensing and analytical tools to support site-specific, economic, environmental, and sustainable decision-making for the forestry sector supporting the forestry value chain from bare land to the customer buying a sheet of paper or board" (IUFRO, 2015, 2014). Thanks to modern technologies it is possible to conduct silvicultural operations in a cost-effective manner (Fardusi et al., 2017; Kovácsová and Antalová, 2010; Talbot et al., 2016; Taylor et al., 2002). Kovácsová and Antalová (2010a) in their review describe precision forestry with a diagram drawing precision forestry as a chain that uses data, tools, and information to take better decisions (Figure 1).

In this regard, the demands for global-level and small-scale forest information have increased (Chirici et al., 2012; Corona et al., 2017; Fardusi et al., 2017; Kovácsová and Antalová, 2010). The development of new geospatial-information tools and techniques for data collection and analysis are therefore considered essential (Fardusi et al., 2017; Talbot et

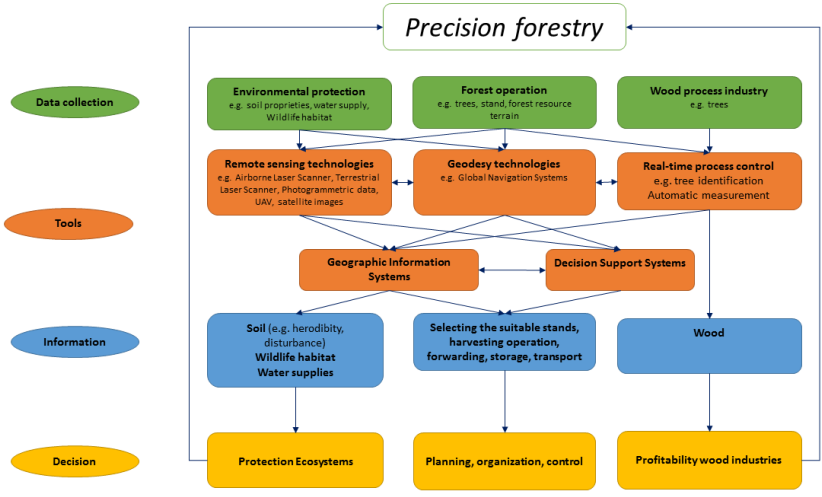

Figure 1: diagram of precision forestry (modified from Kovácsová and P Antalová, (2010b)).

al., 2016). Moreover, several authors have reported that new methods and tools that permit the integration of spatial and temporal dimensions to measure, monitor, and manage forests ecosystem components could be useful in the development of decision support systems (Corona et al., 2017; Fardusi et al., 2017; Kovácsová and Antalová, 2010). Detailed and continuous information is, instead, necessary for supporting and for implementing precision forestry practices (Fardusi et al., 2017; Fotakis et al., 2012; Holopainen et al., 2014; Kovácsová and Antalová, 2010; Taylor et al., 2002) and to develop the multiple objectives of conservation and management forest strategies, plans, actions, and decisions (Arabatzis, 2010; Corona et al., 2017; Fardusi et al., 2017; Holopainen et al., 2014; Kurttila, 2001).

measure, monitor, and manage

forests ecosystem components could be useful to develop decision support systems (Corona et al., 2017; Fardusi et al., 2017; Kovácsová and Antalová, 2010). Detailed and continuous information are, instead, necessary for supporting and for implementing *precision forestry* practices (Fardusi et al., 2017; Fotakis et al., 2012; Holopainen et al., 2014; Kovácsová and Antalová, 2010; Taylor et al., 2002) to develop multiple objectives conservation and management forest strategies, plans, actions, and decisions (Arabatzis, 2010; Corona et al., 2017; Fardusi et al., 2017; Holopainen et al., 2014; Kurttila, 2001).

1.2. 3D Remote Sensing technologies in precision forestry

Remote Sensing (RS) technologies, providing high-quality geospatial information about forests, are considered crucial to improving highly repeatable measurements, actions, and processes in precision forestry (Dyck, 2003; Holopainen et al., 2014; Kovácsová and Antalová, 2010). RS technologies have the ability to acquire information of an object without physical contact with it. Many authors have already underlined how RS technologies are essential to measuring, monitoring, and mapping forest ecosystem components (Bottalico et al., 2017; Corona and Fattorini, 2008; Koreň et al., 2015; Liang et al., 2016; Maack et al., 2015; Mura et al., 2015; Næsset and Økland, 2002; Pierzchała et al., 2014) and for planning forest operation activities (Talbot et al., 2016). Across a variety of RS technologies, multisource three dimensional (3D) RS data are considered to be a viable data source to derive high-quality geospatial information (Bohlin et al., 2015; Corona et al., 2017; Fardusi et al., 2017; Holopainen et al., 2014; Kovácsová and Antalová, 2010; Liang et al., 2016; Lim et al., 2003; Puliti et al., 2017b; Ryding et al., 2015). Generally, 3D RS information can be derived

with three different approaches: triangulation, interferometry, and measuring the time differences between a transmitted and received energy pulse. The last two approaches are applicable only when RS active sensors are used (e.g. laser scanner or radar) while triangulation can be applied from both active or passive sensors on board satellite or aerial platforms.

3D RS technologies have the ability to derive information about distances of objects from the sensor, deriving accurate three-dimensional (3D) information for different forest ecosystem components, such as vegetation (Dandois and Ellis, 2010; Dash et al., 2016; Puliti et al., 2015; Ryding et al., 2015), and soil (Barneveld et al., 2013; Kamphorst et al., 2000; Koreň et al., 2015; Pierzchała et al., 2014). Measures can be provided at different scales from the millimetre and centimetre range (e.g. soils displacement) (Koreň et al., 2015; Pierzchała et al., 2014), to kilometre range (e.g. stand volume) (Bottalico et al., 2017; Dandois and Ellis, 2013; Fardusi et al., 2017; Næsset and Økland, 2002; Niemi and Vauhkonen, 2016; Rahlf et al., 2015; White et al., 2016).

In the last several years, the development of different sensor platforms, instruments and techniques has increased the availability of 3D RS data. The sensor platforms can be deployed on satellites, airplanes, unmanned aerial vehicles (UAVs), ground-based vehicles, and by ground-based people (Talbot et al., 2016). The different platforms give the possibility of collecting data at different spatial and temporal resolutions (Table 1). In forestry, 3D RS data derived from different sensors (i.e. laser scanner, radar, and camera) and platforms (i.e. unmanned aerial vehicle (UAV), aircraft, and terrestrial) are considered useful for many applications such as forest inventories, soils displacement and erosion, and habitat characterization (Gobakken et al., 2015; Koreň et al., 2015; Lim et al., 2003; Pierzchała et al., 2014; Puliti et al., 2015; Zahawi et al., 2015)

Table 1: General characterization of sensor deployment platforms to spatial coverage and temporal resolution (adapted from Talbot et al., (2016)).

Sensor deployment	Coverage	Spatial resolution	Temporal resolution
Satellite	Global/National	Low	Medium to high
Airplane	Regional	Medium	Low
UAV	Local	High	High
Vehicle	Site	Ultra-high	High
Human	Site	Ultra-high	High

In the last several decades, active sensors – in particular those based on Light Detection and Ranging (LiDAR) –have been the most used in forestry applications (Liang et al., 2016; Maltamo et al., 2014; White et al., 2016). Liang et al. (2016) provide a classification of laser scanning based on different platforms used, distinguishing between Airborne Laser Scanning (ALS), Terrestrial Laser Scanning (TLS), Mobile Laser Scanners (MLS) and Personal Laser Scanning (PLS). Moreover, Bauwens et al. (2016) introduced definitions for Hand-Held Mobile Laser Scanning (HMLS).

ALS is the most-studied 3D remote sensing technology for forestry applications (Bottalico et al., 2017; Hansen et al., 2015; Hyyppä et al., 2008; Maltamo et al., 2014; McRoberts et al., 2013a; Næsset, 2002, 1997; Næsset et al., 2004). Its advantage in mapping forest variables is well documented, especially in the context of National Forest Inventory (NFI) (McRoberts et al., 2013b; Næsset, 2007; Næsset et al., 2004), local forest inventory (Bottalico et al., 2017), biodiversity monitoring (Corona et al., 2011; Lefsky et al., 2002; Lim et al., 2003; Mura et al., 2015; Valbuena et al., 2016, 2013; Wulder et al., 2008) and for the characterization of wildlife habitats

(Sallabanks et al., 2006; Vogeler et al., 2014). ALS has, in fact, the ability to collect and capture highly detailed data of large areas, giving information of ground elevation and detailed characterization of forests (Holopainen et al., 2014; Hyyppä et al., 2008). In operational wall-to-wall forest inventories, a two-stage procedure using ALS data and field plots, i.e. an area-based approach (ABA, Næsset, 2002), has become particularly common, and several countries (e.g. Norway, Sweden, and Finland) already use this technology in the operational implementations of NFIs.

New advantages for precision forestry are derived also by the development of terrestrial laser scanning technologies that are slowly modifying methods for the field assessment of forest attributes (Moskal and Zheng, 2011; Hyyppä, et al., 2012; Holopainen et al., 2013; Kankare et al., 2015) and soil measurements (Koreň et al., 2015). TLS, MLS, PLS, and HMLS appear to be suitable for measuring millimetre-level information (e.g. soils) (Koreň et al., 2015), stand level information (e.g. an NFI sample plot level of 200-500 m^2) and single trees (Bauwens et al., 2016; Kankare et al., 2015a, 2014; Liang et al., 2016; Maas et al., 2008; Ryding et al., 2015). However, TLS has not yet been accepted as an operational tool in forestry inventories mainly because of the difficulties in the automation of point cloud processing to automatically derive meaningful variables. Liang et al. (2016) underline "how up to now there is a lack of automatic and accurate methods to detect tree attributes (e.g. tree species and height) which need further studies". As of 2017, the main research issue needed for terrestrial laser scanner applications in forestry is to improve the work efficiency in sample plots, most usually of 200-500 m^2 in size. These instruments permit, in fact, the replacement of manually measured tree attributes with those retrieved by TLS data (Bauwens et al., 2016; Maas et al., 2008; Newnham et al., 2015; Ryding et al., 2015). TLS was tested in collecting basic tree

attributes in sample plots, such as diameter at breast height (DBH), tree position, and tree height (Bauwens et al., 2016; Fleck et al., 2011; Kankare et al., 2015b; Maas et al., 2008; Ryding et al., 2015). The accuracy of DBH estimates based on terrestrial laser scanner pulses was demonstrated to be acceptable for most countries and forest types, e.g., to be within 1–2 cm RMSE (Liang et al., 2016). However, larger RMSEs were obtained for tree heights, e.g. RMSE in the range of 0.8-6.5 m (Fleck et al., 2011; Huang et al., 2011a; Maas et al., 2008). As reported by Kankare et al. (2015), the forest structure has a major impact on the accuracy of forest attribute estimates from terrestrial laser scanning since tree tops are usually shadowed by other trees (Huang et al., 2011b; Liang and Hyyppä, 2013; Maas et al., 2008). As reported in the review by Liang et al., (2016) "finding tree tops from TLS data in dense sample plots remains a challenge".

Moreover, TLS is considered a valued instrument to measure and to quantify soil disturbances. From TLS point clouds, it is possible to generate high-resolution digital terrain models (DTMs) that provide an accurate representation of topographical surfaces (Haubrock et al., 2009; Heritage and Large, 2009). Multi-temporal TLS acquisitions allow for the accurate measurement of changes and deformation in terrain (Haubrock et al., 2009; Heritage and Large, 2009; Milan et al., 2011), thus providing a measure of volumetric changes (Koren et al., 2015) and facilitating the documentation of terrain conditions (e.g., the development of rills or roughness) (Nadal-Romero et al., 2015).

In the last several years the use of photogrammetry has received increasing attention in forestry mapping and monitoring thanks to new methods developed for photogrammetric applications, advances in computer vision, new image matching algorithms, and increased computing power (Baltsavias et al., 2008; Lisein et al., 2013; Puliti et al., 2015;

Remondino et al., 2014). These advantage permit the application of Structure from Motion (SfM) Photogrammetry (Remondino et al., 2014) from optical images for 3D image-based point clouds and Digital Surface Model (DSM) derivation. Photogrammetry can be classified on the base of platforms used to acquire data in digital aerial photogrammetry (DAP), when images are acquired by an aircraft, (Bohlin et al., 2015; Ginzler and Hobi, 2015; Gobakken et al., 2015; Järnstedt et al., 2012; Rahlf et al., 2014; Vastaranta et al., 2013); Unmanned Aerial vehicle photogrammetry (UAVP), when the images are acquired from a UAV (Chianucci et al., 2016; Dandois and Ellis, 2013; Nex and Remondino, 2014; Puliti et al., 2017a, 2015; Wallace et al., 2016); and close-range terrestrial photogrammetry (CRP), when images are acquired from the ground with little distance between camera and targets.

Several authors have already demonstrated that with photogrammetry point clouds, acquired from aircraft (i.e. DAP) and UAV (i.e. UAVP), normalized with high-resolution DTMs (i.e., by subtracting the terrain elevation from the photogrammetric point cloud elevation (Lisein et al., 2013)) it is possible to derive explanatory variables that can be used for ABA estimations (e.g. photogrammetry based estimation of variables such as volume, height, basal area, and number of trees) and produce results with accuracies that are comparable with those obtained with traditional ALS metrics (Dandois et al., 2015; Hobi and Ginzler, 2012; Järnstedt et al., 2012; Puliti et al., 2017a, 2017b; Rahlf et al., 2014; White et al., 2013; Whitehead et al., 2014; Zahawi et al., 2015). Moreover, Waser et al., (2015) have found that photogrammetric data are useful for wall-to-wall forest estimations. The attention to photogrammetric 3D data in forest inventory is increasing also because of the low cost of the acquisition of this data compared to ALS (Waser et al., 2015). However, several authors have

mentioned that 3D photogrammetric data in forestry are limited by the need for high-resolution DTMs (Bohlin et al., 2012; Järnstedt et al., 2012; Lisein et al., 2013; Ota et al., 2015; Vastaranta et al., 2013).

Photogrammetric data (i.e. image-based point cloud and DSM) are also considered useful for quantifying soil disturbances (e.g. soils displacement (Pierzchała et al., 2014) and soil erosion (Micheletti et al., 2015; Nadal-Romero et al., 2015). SfM photogrammetry techniques make it possible to generate digital surface models that accurately reproduce topographic (Nadal-Romero et al., 2015; Pierzchała et al., 2014; Vericat et al., 2014). The use of close-range photogrammetry in mapping soil surface structure was demonstrated more than 20 years ago (Warner, 1995), while the advent of structure-from-motion (SfM) photogrammetry (James and Robson, 2012) has generated an improvement in topographic methods, due to its better accessibility to a wider variety of users, low cost, and the increased automation of routines and workflow (Fonstad et al., 2013; Nadal-Romero et al., 2015). The advantages introduced by SfM in the geosciences were demonstrated by James and Robson (2012), and the reconstruction of high-resolution surface models (Turner et al., 2012) has opened new possibilities in the applications of geoscience analysis (Castillo et al., 2015), forestry (Pierzchała et al., 2014; Talbot et al., 2016) and agriculture (Nouwakpo and Huang, 2012).

3D photogrammetric data, ALS, TLS, PLS and HMLS all have the ability to automatically measure the surrounding 3D space using millions to billions 3D points. The new 3D RS techniques overcome traditional forest measuration techniques using simple tools, such as callipers, measuring tape, and clinometers, thus improving the work efficiency in forest measuration, inventory, and monitoring (lower costs and time) (Henning and Radtke, 2008; Liang et al., 2016).

2. Background motivation and aims

The increasing availability of 3D RS data has inspired the research work of this thesis. This research work addresses the synergetic integration of 3D RS data and forest field surveying to develop tools and procedures useful for precision forestry. The present thesis is aimed at contributing to the gap in research between advances in 3D RS technologies and precision forestry application as, for example, (i) exceeding the use of high resolution DTMs to estimate forest variables using UAVP; (ii) increasing the accuracy of single-trees estimations derived from 3D RS data from different laser scanner clouds acquired by different platforms; (iii) and testing the utility of 3D RS technologies in measuring soil displacement caused by forest operations. In particular, attention was focused on developing new tools and procedures (i) for operational forest inventories using HMLS, TLS, UAVP, and ALS; and (ii) for estimation soil disturbances caused by logging operations using PLS and CRP. For this reason, the papers included in the thesis are divided into two main categories: (i) forest inventory and (ii) soil disturbance.

The specific objectives of the forest inventory papers are:

- to assess and compare the precision and accuracy of PLS and TLS with and without the integration of ALS to measure single trees variables (Paper I);
- to develop and to assess a new set of explanatory variables derived by UAVP data (i.e. DTM-independent explanatory variables) without relaying of any DTM for ABA estimation of inventory variables (Paper II);
- to assess the use of DTM-independent explanatory variables to predict forest structure indices (Paper III).

- The specific objectives of the soils displacement paper are:
- to assess soil compaction, and to determine the extent of logging-induced rutting by way of multi-temporal high-resolution DTM generated by PLS (Paper IV) and CRP data (Paper V).

Forest inventory applications

Paper I - Integrating terrestrial and airborne laser scanning for the assessment of single tree attributes in Mediterranean forest stands

"In this study, our main objective was to assess and compare the precision and accuracy of ZEB1 HMLS and FARO® FOCUS 3D TLS to measure single tree attributes within a complex mixed Mediterranean forest. In particular, we considered the following attributes: tree position (TP), stem diameter at breast height (DBH), tree height (TH), crown base height (CBH), and the radii of the crown projection area (CPAR). Using conventional field survey as a benchmark, the main aim was to compare tree level attributes obtained by the automatic elaboration of four different point clouds: (i) HMLS; (ii) TLS; (iii) integration of HMLS and ALS ($HMLS_{ALS}$); (iv) integration of TLS and ALS (TLS_{ALS}). The accuracy of the estimates was evaluated on the basis of bias and Root Mean Square Error (RMSE) calculated comparing tree level estimations with field reference data."

(Giannetti et al., 2017b)

Paper II - Development and assessment of DTM-independent variables for prediction of forest biophysical properties using UAV photogrammetric data.

"The overall objective of this study was to develop a set of DTM-independent explanatory variables and assess their usefulness when modeling the following forest biophysical forest properties: growing stock

volume (V; m^3 ha^{-1}), basal area (G; m^2 ha^{-1}), number of stems per hectare (N; ha^{-1}), Lorey's height (H_{Lor}; m), and dominant height (H_{dom}; m). The DTM-independent variables were assessed against two more traditional sets of variables: (1) height and density variables from UAV photogrammetric data normalized using an ALS DTM (denoted Image-DTM_{ALS} variables) and (2) height and density variables extracted from normalized ALS data (denoted ALS variables). Moreover, to gain further insights in the applicability of the approach across different regions and for different forest types, the assessment of the DTM-independent variables was performed across two different study sites, namely a temperate mixed forest in Italy and a boreal forest in Norway".

(Giannetti et al., 2017d)

Paper III - UAV photogrammetric DTM-independent variables can be used to predict forest structural indices? A case of study in mixed temperate forests.

"In this contribution we present the area-based (Nasset,2002) spatial estimation of the following forest structure complexity indices: basal area (G; m^2ha^{-1}); mean DBH (DBH_{mean}; cm); standard deviation of DBH (DBH_{σ}; cm); DBH Gini coefficient (Gini); standard deviation of H ($H_{\sigma\ h}$; m); dominant height (H_{dom}) and Lory's height (H_l) and stem volume (V m^3 ha^{-1}). Predictors are DTM-independent variables (Giannetti et al., 2017d) from 3D UAV photogrammetric imagery. The accuracy of the DTM-independent approach was assessed against a more traditional approach based on ALS data in two forest districts in Italy".

(Giannetti et al., 2017c)

Soil disturbance applications

Paper IV - Assessment of soil disturbance caused by forest operations by means of Portable Laser Scanner and soil physical parameters.

"The objectives of this study were to: (i) assess soil compaction, and (ii) determine the extent of logging-induced rutting by way of multi-temporal high-resolution DTM generated by PLS data.

The effects of mechanized logging on soil compaction and rutting were investigated along two skid trails, in the Apennine Mountains of central Italy. Traditional soil sampling methods, integrated with laser scanning data from PLS, taken both before and after logging, were used for this investigation.

The results of this analysis and subsequent discussion account for the fact that the number of machine passes and slope differ among the two study trails".

(Francesca Giannetti et al., 2017a)

Paper V - Estimating soil impact in logging skid trails via close-range photogrammetry and soil parameters: a case study in central Italy

"This study was carried out to investigate the use of SfM photogrammetry in association with traditional methods for assessing soil disturbance in forest operations. The effects of forest operations on soil were considered for two forest machines, forwarders and skidders. The specific objectives of the study were:

(1) to assess soil compaction with traditional techniques; and (2) to evaluate multitemporal analysis based on the use of image-based high-resolution ground surface models generated through the use of SfM photogrammetry workflow as an instrument to determine rutting and bulges caused by forest operations along all trail surfaces."

(Cambi et al., 2017)

References

Arabatzis, G., 2010. Development of Greek forestry in the framework of the European Union policies. Journal of Environmental Protection and Ecology 11, 682–692.

Baltsavias, E., Gruen, a., Eisenbeiss, H., Zhang, L., Waser, L.T., 2008. High-quality image matching and automated generation of 3D tree models. International Journal of Remote Sensing 29, 1243–1259. doi:10.1080/01431160701736513

Barneveld, R.J., Seeger, M., Maalen-Johansen, I., 2013. Assessment of terrestrial laser scanning technology for obtaining high-resolution DEMs of soils. Earth Surface Processes and Landforms 38, 90–94. doi:10.1002/esp.3344

Bauwens, S., Bartholomeus, H., Calders, K., Lejeune, P., 2016. Forest inventory with terrestrial LiDAR: A comparison of static and hand-held mobile laser scanning. Forests 7 (127). doi:10.3390/f7060127

Bohlin, J., Wallerman, J., Fransson, J.E.S., 2012. Forest variable estimation using photogrammetric matching of digital aerial images in combination with a high-resolution DEM. Scandinavian Journal of Forest Research 27, 692–699. doi:10.1080/02827581.2012.686625

Bohlin, J., Wllerman, J., Fransson, J.E.S., 2015. Deciduous forest mapping using change detection of multi-temporal canopy height models from aerial images acquired at leaf-on and leaf-off conditions. Scandin 7, 8–9. doi:10.1016/j.dcn.2015.01.008

Bottalico, F., Chirici, G., Giannini, R., Mele, S., Mura, M., Puxeddu, M., McRoberts, R.E., Valbuena, R., Travaglini, D., 2017. Modeling Mediterranean forest structure using airborne laser scanning data. International Journal of Applied Earth Observation and Geoinformation 57, 145–153. doi:10.1016/j.jag.2016.12.013

Cambi, M., Giannetti, F., Bottalico, F., Travaglini, D., Nordfjell, T., Chirici, G., Marchi, E., 2017. Estimating machine impact on strip roads via close-range photogrammetry and soil parameters: a case study in central Italy. submitted.

Castillo, C., James, M.R., Redel-Macías, M.D., Pérez, R., Gómez, J. a., 2015. SF3M software: 3-D photo-reconstruction for non-expert users and its application to a gully network. Soil 1, 583–594. doi:10.5194/soil-1-583-2015

Chianucci, F., Disperati, L., Guzzi, D., Bianchini, D., Nardino, V., Lastri, C., Rindinella, A., Corona, P., 2016. Estimation of canopy attributes in beech forests using true colour digital images from a small fixed-wing UAV. International Journal of Applied Earth Observation and Geoinformation 47, 60–68. doi:10.1016/j.jag.2015.12.005

Chirici, G., McRoberts, R.E., Winter, S., Bertini, R., Bröändli, U.-B., Asensio, I.A., Bastrup-Birk, A., Rondeux, J., Barsoum, N., Marchetti, M., 2012. National forest inventory contributions to forest biodiversity monitoring. Forest Science 58, 257–268. doi:10.5849/forsci.12-003

Corona, P., Chianucci, F., Quatrini, V., Civitarese, V., Clementel, F., Costa, C., Floris, A., Menesatti, P., Puletti, N., Sperandio, G., Verani, S., Turco, R., Bernardini, V., Plutino, M., Scrinzi, G., 2017. Precision forestry: concepts, tools and perspectives in Italy. Forest@ - Rivista di Selvicoltura ed Ecologia Forestale 14, 1–12. doi:10.3832/efor2285-014

Corona, P., Chirici, G., McRoberts, R.E., Winter, S., Barbati, A., 2011. Contribution of large-scale forest inventories to biodiversity assessment and monitoring. Forest Ecology and Management 262, 2061–2069. doi:10.1016/j.foreco.2011.08.044

Corona, P., Fattorini, L., 2008. Area-based lidar-assisted estimation of forest standing volume. Canadian Journal of Forest Research 38, 2911–2916. doi:10.1139/X08-122

Dandois, J.P., Ellis, E.C., 2013. High spatial resolution three-dimensional mapping of vegetation spectral dynamics using computer vision. Remote Sensing of Environment 136, 259–276. doi:10.1016/j.rse.2013.04.005

Dandois, J.P., Ellis, E.C., 2010. Remote sensing of vegetation structure using computer vision. Remote Sensing 2, 1157–1176. doi:10.3390/rs2041157

Dandois, J.P., Olano, M., Ellis, E.C., 2015. Optimal altitude, overlap, and weather conditions for computer vision uav estimates of forest structure. Remote Sensing 7, 13895–13920. doi:10.3390/rs71013895

Dash, J.P., Watt, M.S., Bhandari, S., Watt, P., 2016. Characterising forest structure using combinations of airborne laser scanning data, RapidEye satellite imagery and environmental variables. Forestry 89, 159–169. doi:10.1093/forestry/cpv048

Dinerstein, E., Olson, D.M., Graham, D.J., Webster, A.L., Primm, S.A., Bookbinder, M.P., Ledec, G., 1995. Conservation Assessment of the Terrestrial Ecoregions of Latin America and the Caribbean. The World Bannk Washington (DC).

Dyck, B., 2003. Precision Forestry - the path to increased profitability. In: Procee, 3–8.

Fardusi, M.J., Chianucci, F., Barbati, A., 2017. Concept to Practices of Geospatial Information Tools to Assist Forest Management and Planning under Precision Forestry Framework : a review 41, 3–14.

Fleck, S., Mölder, I., Jacob, M., Gebauer, T., Jungkunst, H.F., Leuschner, C., 2011. Comparison of conventional eight-point crown projections with

LIDAR-based virtual crown projections in a temperate old-growth forest. Annals of Forest Science 68, 1173–1185. doi:10.1007/s13595-011-0067-1

Fonstad, M.A., Dietrich, J.T., Courville, B.C., Jensen, J.L., Carbonneau, P.E., 2013. Topographic structure from motion: A new development in photogrammetric measurement. Earth Surface Processes and Landforms 38, 421–430. doi:10.1002/esp.3366

FOREST EUROPE, 2015. State of Europe's Forests 2015., Ministerial Conference on the Protection of Forests in Europe, FOREST EUROPE Liaison Unit Madrid.

Fotakis, D.G., Sidiropoulos, E., Myronidis, D., Ioannou, K., 2012. Spatial genetic algorithm for multi-objective forest planning. Forest Policy and Economics 21, 12–19. doi:10.1016/j.forpol.2012.04.002

Giannetti, F., Chirici, G., Travaglini, D., Bottalico, F., Marchi, E., Cambi, M., 2017a. Assessment of Soil Disturbance Caused by Forest Operations by Means of Portable Laser Scanner and Soil Physical Parameters. Soil Science Society of America Journal 1–23. doi:10.2136/sssaj2017.02.0051

Giannetti, F., Puletti, N., Quatrini, V., Travaglini, D., Bottalico, F., Corona, P., Chirici, G., 2017b. Integrating terrestrial and airborne laser scanning for the assessment of single tree attributes in Mediterranean forest stands. submitted.

Giannetti, F., Puletti, N., Puliti, S.,Travaglini, D., Chirici, G., 2017c. UAV photogrammetric DTM-independent variables can be used to predict forest structural indices? A case of study in mixed temperate forests. Manuscript.

Giannetti, F., Chirici, G., Gobakken, T., Næsset, E., Travaglini, D., Puliti, S., 2017d. Development and assessment of DTM-independent variables for prediction of forest biophysical properties using UAV photogrammetric data. submitted.

Ginzler, C., Hobi, M., 2015. Countrywide Stereo-Image Matching for Updating Digital Surface Models in the Framework of the Swiss National Forest Inventory. Remote Sensing 7, 4343–4370. doi:10.3390/rs70404343

Gobakken, T., Bollandsås, O.M., Næsset, E., 2015. Comparing biophysical forest characteristics estimated from photogrammetric matching of aerial images and airborne laser scanning data. Scandinavian Journal of Forest Research 30, 73–86. doi:10.1080/02827581.2014.961954

Hansen, E.H., Gobakken, T., Bollandsås, O.M., Zahabu, E., Næsset, E., 2015. Modeling aboveground biomass in dense tropical submontane rainforest using airborne laser scanner data. Remote Sensing 7, 788–807. doi:10.3390/rs70100788

Henning, J.G., Radtke, P.J., 2008. Multiview range-image registration for forested scenes using explicitly-matched tie points estimated from natural surfaces. ISPRS Journal of Photogrammetry and Remote Sensing 63, 68–83. doi:10.1016/j.isprsjprs.2007.07.006

Hobi, M.L., Ginzler, C., 2012. Accuracy assessment of digital surface models based on WorldView-2 and ADS80 stereo remote sensing data. Sensors (Basel, Switzerland) 12, 6347–68. doi:10.3390/s120506347

Holopainen, M., Vastaranta, M., Hyyppä, J., 2014. Outlook for the next generation's precision forestry in Finland. Forests 5, 1682–1694. doi:10.3390/f5071682

Huang, H., Li, Z., Gong, P., Cheng, X., Clinton, N., Cao, C., Ni, W., Wang, L., 2011a. Automated methods for measuring DBH and tree heights with a commercial scanning lidar. Photogrammetric Engineering and Remote Sensing 77, 219–227. doi:10.14358/PERS.77.3.219

Huang, H., Li, Z., Gong, P., Cheng, X., Clinton, N., Cao, C., Ni, W., Wang, L., 2011b. Automated methods for measuring DBH and tree heights with a commercial scanning lidar. Photogrammetric Engineering and Remote Sensing 77, 219–227. doi:10.14358/PERS.77.3.219

Hyyppä, J., Hyyppä, H., Leckie, D., Gougeon, F., Yu, X., Maltamo, M., 2008. Review of methods of small footprint airborne laser scanning for extracting forest inventory data in boreal forests. International Journal of Remote Sensing 29, 1339–1366. doi:10.1080/01431160701736489

IUFRO, 2015. Collection of definition or related elements Precision Forestry. SILVAOC Terminology Prokect.

IUFRO, 2014. Precision Forestry: The anchor of your value chain. In: First Announcement, Precision Forestry Sym- posium. Stellenbosch, South Africa.

James, M.R., Robson, S., 2012. Straightforward reconstruction of 3D surfaces and topography with a camera: Accuracy and geoscience application. Journal of Geophysical Research: Earth Surface 117, 1–17. doi:10.1029/2011JF002289

Järnstedt, J., Pekkarinen, A., Tuominen, S., Ginzler, C., Holopainen, M., Viitala, R., 2012. Forest variable estimation using a high-resolution digital surface model. ISPRS Journal of Photogrammetry and Remote Sensing 74, 78–84. doi:10.1016/j.isprsjprs.2012.08.006

Joint Research Centre, 2014. Precision agricolture: an opportunity for EU-farmers- potential support with the CAP 2014-2020. Policy Department B, European Union 56 p.

Kamphorst, E.C., Jetten, V., Guerif, J., Pitkanen, J., Iversen, B. V, Douglas, J.T., Paz, A., 2000. Predicting Depressional Storage from Soil Surface Roughness. Soil Sci Soc Am J 64, 1749–1758.

doi:10.2136/sssaj2000.6451749x
Kankare, V., Joensuu, M., Vauhkonen, J., Holopainen, M., Tanhuanpää, T., Vastaranta, M., Hyyppä, J., Hyyppä, H., Alho, P., Rikala, J., Sipi, M., 2014. Estimation of the timber quality of scots pine with terrestrial laser scanning. Forests 5, 1879–1895. doi:10.3390/f5081879
Kankare, V., Liang, X., Vastaranta, M., Yu, X., Holopainen, M., Hyyppä, J., 2015a. Diameter distribution estimation with laser scanning based multisource single tree inventory. ISPRS Journal of Photogrammetry and Remote Sensing 108, 161–171. doi:10.1016/j.isprsjprs.2015.07.007
Kankare, V., Liang, X., Vastaranta, M., Yu, X., Holopainen, M., Hyyppä, J., 2015b. Diameter distribution estimation with laser scanning based multisource single tree inventory. ISPRS Journal of Photogrammetry and Remote Sensing 108, 161–171. doi:10.1016/j.isprsjprs.2015.07.007
Koreň, M., Slančík, M., Suchomel, J., Dubina, J., 2015. Use of terrestrial laser scanning to evaluate the spatial distribution of soil disturbance by skidding operations. IForest 8, 386–393. doi:10.3832/ifor1165-007
Kovácsová, P., Antalová, M., 2010. Precision Forestry – Definition and Technologies. Šumarski List 143, 603–611.
Kurttila, M., 2001. The spatial structure of forests in the optimization calculations of forest planning - A landscape ecological perspective. Forest Ecology and Management 142, 129–142. doi:10.1016/S0378-1127(00)00343-1
Lefsky, M., Cohen, W.B., Parker, G.G., Harding, D.J., 2002. Lidar Remote Sensing for Ecosystem Studies. Bioscience 52, 19–30. doi:10.1641/0006-3568(2002)052[0019:LRSFES]2.0.CO;2
Liang, X., Hyyppä, J., 2013. Automatic stem mapping by merging several terrestrial laser scans at the feature and decision levels. Sensors (Switzerland) 13, 1614–1634. doi:10.3390/s130201614
Liang, X., Kankare, V., Hyyppä, J., Wang, Y., Kukko, A., Haggrén, H., Yu, X., Kaartinen, H., Jaakkola, A., Guan, F., Holopainen, M., Vastaranta, M., 2016. Terrestrial laser scanning in forest inventories. ISPRS Journal of Photogrammetry and Remote Sensing 115, 63–77. doi:10.1016/j.isprsjprs.2016.01.006
Lim, K.P.., Treitz, P.., Wulder, M.A.., St-Onge, B.A.., Flood, M., 2003. LiDAR remote sensing of forest structure. Progress in Physical Geography 27, 88–106.
Lisein, J., Pierrot-Deseilligny, M., Bonnet, S., Lejeune, P., 2013. A photogrammetric workflow for the creation of a forest canopy height model from small unmanned aerial system imagery. Forests 4, 922–944. doi:10.3390/f4040922

Maack, J., Katternborn, T., Fassnacht, F.E., Enßle, F., Hernández, J., Corvalá, P., Koch, B., 2015. Modeling forest biomass using Very-High-Resolution data - Combining textural, spectral and photogrammetric predictors derived from spaceborne stereo images. European Journal of Remote Sensing 6, 1–26. doi:10.5721/EuJRS20154814

Maas, H.-G., Bienert, A., Scheller, S., Keane, E., 2008. Automatic forest inventory parameter determination from terrestrial laser scanner data. International Journal of Remote Sensing 29, 1579–1593. doi:10.1080/01431160701736406

Maltamo, M., Næsset, E., Vauhkonen, J., 2014. Forestry Applications of Airborne Laser Scanning: Concepts and Case Studies, Forestry Applications of Airborne Laser Scanning: Concepts and Case Studies. doi:10.1007/978-94-017-8663-8

McRoberts, R.E., Næsset, E., Gobakken, T., 2013a. Inference for lidar-assisted estimation of forest growing stock volume. Remote Sensing of Environment 128, 268–275. doi:10.1016/j.rse.2012.10.007

McRoberts, R.E., Næsset, E., Gobakken, T., 2013b. Inference for lidar-assisted estimation of forest growing stock volume. Remote Sensing of Environment 128, 268–275. doi:10.1016/j.rse.2012.10.007

Micheletti, N., Chandler, J.H., Lane, S.N., 2015. Investigating the geomorphological potential of freely available and accessible structure-from-motion photogrammetry using a smartphone. Earth Surface Processes and Landforms 40, 473–486. doi:10.1002/esp.3648

Mura, M., McRoberts, R.E., Chirici, G., Marchetti, M., 2015. Estimating and mapping forest structural diversity using airborne laser scanning data. Remote Sensing of Environment 170, 133–142. doi:10.1016/j.rse.2015.09.016

Nadal-Romero, E., Revuelto, J., Errea, P., López-Moreno, J.I., 2015. The application of terrestrial laser scanner and photogrammetry in measuring erosion and deposition processes in humid badlands in the Central Spanish Pyrenees. SOIL Discussions 2, 337–369. doi:10.5194/soild-2-337-2015

Næsset, E., 2007. Airborne laser scanning as a method in operational forest inventory: Status of accuracy assessments accomplished in Scandinavia. Scandinavian Journal of Forest Research 22, 433–422.

Næsset, E., 2002. Predicting forest stand characteristics with airborne scanning laser using a practical two-stage procedure and field data. Remote Sensing of Environment 80, 88–99. doi:10.1016/S0034-4257(01)00290-5

Næsset, E., 1997. Estimating timber volume of forest stands using airborne laser scanner data. Remote Sensing of Environment 61, 246–253.

doi:10.1016/S0034-4257(97)00041-2
Næsset, E., Gobakken, T., Holmgren, J., Hyyppä, H., Hyyppä, J., Maltamo, M., Nilsson, M., Olsson, H., Persson, Å., Söderman, U., 2004. Laser scanning of forest resources: the nordic experience. Scandinavian Journal of Forest Research 19, 482–499. doi:10.1080/02827580410019553
Næsset, E., Økland, T., 2002. Estimating tree height and tree crown properties using airborne scanning laser in a boreal nature reserve. Remote Sensing of Environment 79, 105–115. doi:10.1016/S0034-4257(01)00243-7
Newnham, G.J., Armston, J.D., Calders, K., Disney, M.I., Lovell, J.L., Schaaf, C.B., Strahler, A.H., Danson, F.M., 2015. Terrestrial Laser Scanning for Plot-Scale Forest Measurement. Current Forestry Reports 1, 239–251. doi:10.1007/s40725-015-0025-5
Nex, F., Remondino, F., 2014. UAV for 3D mapping applications: A review. Applied Geomatics 6, 1–15. doi:10.1007/s12518-013-0120-x
Niemi, M., Vauhkonen, J., 2016. Extracting Canopy Surface Texture from Airborne Laser Scanning Data for the Supervised and Unsupervised Prediction of Area-Based Forest Characteristics. Remote Sensing 8, 582. doi:10.3390/rs8070582
Nouwakpo, S.K., Huang, C., 2012. A Simplified Close-Range Photogrammetric Technique for Soil Erosion Assessment. Soil Science Society of America Journal 76, 70. doi:10.2136/sssaj2011.0148
O'Farrell, P.J., Anderson, P.M.L., 2010. Sustainable multifunctional landscapes: A review to implementation. Current Opinion in Environmental Sustainability 2, 59–65. doi:10.1016/j.cosust.2010.02.005
Ota, T., Ogawa, M., Shimizu, K., Kajisa, T., Mizoue, N., Yoshida, S., Takao, G., Hirata, Y., Furuya, N., Sano, T., Sokh, H., Ma, V., Ito, E., Toriyama, J., Monda, Y., Saito, H., Kiyono, Y., Chann, S., Ket, N., 2015. Aboveground biomass estimation using structure from motion approach with aerial photographs in a seasonal tropical forest. Forests 6, 3882–3898. doi:10.3390/f6113882
Ozdemir, I., 2008. Estimating stem volume by tree crown area and tree shadow area extracted from pansharpened Quickbird imagery in open Crimean juniper forests. International Journal of Remote Sensing 29, 5643–5655. doi:10.1080/01431160802082155
Pierzchała, M., Talbot, B., Astrup, R., 2014. Estimating soil displacement from timber extraction trails in steep terrain: Application of an unmanned aircraft for 3D modelling. Forests 5, 1212–1223. doi:10.3390/f5061212
Puliti, S., Ene, L.T., Gobakken, T., Næsset, E., 2017a. Use of partial-coverage

UAV data in sampling for large scale forest inventories. Remote Sensing of Environment 194, 115–126. doi:10.1016/j.rse.2017.03.019

Puliti, S., Gobakken, T., Ørka, H.O., Næsset, E., 2017b. Assessing 3D point clouds from aerial photographs for species-specific forest inventories. Scandinavian Journal of Forest Research 32:1, 68–79. doi:10.1080/02827581.2016.1186727

Puliti, S., Olerka, H., Gobakken, T., Næsset, E., 2015. Inventory of Small Forest Areas Using an Unmanned Aerial System. Remote Sensing 7, 9632–9654. doi:10.3390/rs70809632

Rahlf, J., Breidenbach, J., Solberg, S., Astrup, R., 2015. Forest parameter prediction using an image-based point cloud: A comparison of semi-ITC with ABA. Forests 6, 4059–4071. doi:10.3390/f6114059

Rahlf, J., Breidenbach, J., Solberg, S., Næsset, E., Astrup, R., 2014. Comparison of four types of 3D data for timber volume estimation. Remote Sensing of Environment 155, 325–333. doi:10.1016/j.rse.2014.08.036

Remondino, F., Spera, M.G., Nocerino, E., Menna, F., Nex, F., 2014. State of the art in high density image matching. The Photogrammetric Record 29, 144–166. doi:10.1111/phor.12063

Ryding, J., Williams, E., Smith, M.J., Eichhorn, M.P., 2015. Assessing handheld mobile laser scanners for forest surveys. Remote Sensing 7, 1095–1111. doi:10.3390/rs70101095

Sallabanks, R., Haufler, J., Mehl, C., 2006. Influence of Forest Vegetation Structure on Avian Community Composition in West-Central Idaho. Wildlife Society Bulletin 34, 1079–1093.

Talbot, B., Pierzchała, M., Astrup, R., 2016. Applications of Remote and Proximal Sensing for Improved Precision in Forest Operations 327–336.

Taylor, S.E., McDonald, T.P., Veal, M.W., Corley, F.W., Grift, T.E., 2002. Precision Forestry: Operational tactics for today and tomorrow. 25th Annual Meeting of the Council of Forest Engineers 6.

Tran, D.., Nguyen, N.V., 2006. The concept and implementation of precision farming and reice integrated crop management systems for sustainable production in the twenty-first century. International Rice Commission Newsletter 55, 103–113.

Turner, D., Lucieer, A., Watson, C., 2012. An automated technique for generating georectified mosaics from ultra-high resolution Unmanned Aerial Vehicle (UAV) imagery, based on Structure from Motion (SFM) point clouds. Remote Sensing 4, 1392–1410. doi:10.3390/rs4051392

Valbuena, R., Eerik??inen, K., Packalen, P., Maltamo, M., 2016. Gini

coefficient predictions from airborne lidar remote sensing display the effect of management intensity on forest structure. Ecological Indicators 60, 574–585. doi:10.1016/j.ecolind.2015.08.001

Valbuena, R., Packalen, P., Mehtätalo, L., García-Abril, A., Maltamo, M., 2013. Characterizing forest structural types and shelterwood dynamics from Lorenz-based indicators predicted by airborne laser scanning. Canadian Journal of Forest Research 43, 1063–1074. doi:10.1139/cjfr-2013-0147

Vastaranta, M., Wulder, M.A., White, J.C., Pekkarinen, A., Tuominen, S., Ginzler, C., Kankare, V., Holopainen, M., Hyyppä, J., Hyyppä, H., 2013. Airborne laser scanning and digital stereo imagery measures of forest structure: comparative results and implications to forest mapping and inventory update. Canadian Journal of Remote Sensing 39, 382–395. doi:10.5589/m13-046

Vericat, D., Smith, M.W., Brasington, J., 2014. Patterns of topographic change in sub-humid badlands determined by high resolution multi-temporal topographic surveys. Catena 120, 164–176. doi:10.1016/j.catena.2014.04.012

Vogeler, J.C., Hudak, A.T., Vierling, L.A., Evans, J., Green, P., Vierling, K.T., 2014. Terrain and vegetation structural influences on local avian species richness in two mixed-conifer forests. Remote Sensing of Environment 147, 13–22. doi:10.1016/j.rse.2014.02.006

Wallace, L., Lucieer, A., Malenovský, Z., Turner, D., Vopěnka, P., 2016. Assessment of forest structure using two UAV techniques: A comparison of airborne laser scanning and structure from motion (SfM) point clouds. Forests 7, 1–16. doi:10.3390/f7030062

Warner, W.S., 1995. Mapping a three-dimensional soil surface with hand-held 35 Mm photography. Soil and Tillage Research 34, 187–197.

Waser, L.T., Fischer, C., Wang, Z., Ginzler, C., 2015. Wall-to-wall forest mapping based on digital surface models from image-based point clouds and a NFI forest definition. Forests 6, 4510–4528. doi:10.3390/f6124386

White, J.C., Coops, N.C., Wulder, M.A., Vastaranta, M., Hilker, T., Tompalski, P., 2016. Remote Sensing Technologies for Enhancing Forest Inventories: A Review. Canadian Journal of Remote Sensing 42, 619–641. doi:10.1080/07038992.2016.1207484

White, J.C., Wulder, M.A., Vastaranta, M., Coops, N.C., Pitt, D., Woods, M., 2013. The utility of image-based point clouds for forest inventory: A comparison with airborne laser scanning. Forests 4, 518–536. doi:10.3390/f4030518

Whitehead, K., Hugenholtz, C.H., Myshak, S., Brown, O., LeClair, A., Tamminga, A., Barchyn, T.E., Moorman, B., Eaton, B., 2014. Remote

sensing of the environment with small unmanned aircraft systems (UASs), part 1: a review of progress and challenges. Journal of Unmanned Vehicle Systems 2, 86–102. doi:10.1139/juvs-2014-0007

Wulder, M.A., Bater, C.W., Coops, N.C., Hilker, T., White, J.., 2008. The role of LiDAR in sustainable forest management. The Forestry Chronicle 84, 807–826.

Zahawi, R.A., Dandois, J.P., Holl, K.D., Nadwodny, D., Reid, J.L., Ellis, E.C., 2015. Using lightweight unmanned aerial vehicles to monitor tropical forest recovery. Biological Conservation 186, 287–295. doi:10.1016/j.biocon.2015.03.031

Paper

Forest inventory applications

Paper I - Integrating terrestrial and airborne laser scanning for the assessment of single tree attributes in Mediterranean forest stands

Francesca Giannetti[a], Nicola Puletti[b], Valerio Quatrini[c], Davide Travaglini[a]; Francesca Bottalico[a], Piermaria Corona[c], Gherardo Chirici[a]*

[a] Università degli Studi di Firenze, Department of Agricultural, Food and Forestry Systems, Via San Bonaventura, 13-50145, Firenze, Italy.

[b] Consiglio per la ricerca in agricoltura e l'analisi dell'economia agraria (CREA), Research Centre for Forestry and Wood, Piazza Nicolini 6, 38123 Trento, Italy.

[c] Consiglio per la ricerca in agricoltura e l'analisi dell'economia agraria (CREA), Research Centre for Forestry and Wood, Viale Santa Margherita 80 52100 Arezzo, Italy.

[*]corresponding author *francesca.giannetti@unifi.it*

Submitted

Abstract

The development of laser scanning technologies has gradually modified methods for forest mensuration and inventory. Airborne laser scanning (ALS) has demonstrated to be an unprecedented source of information for estimating forest attributes. Terrestrial laser scanning has the potential of additionally improving work efficiency in collecting forest information in the field, replacing manually measured tree attributes with more automatic procedures. The main objective of this study is to assess the potential of integrating ALS and terrestrial laser scanning data in a complex mixed Mediterranean forest for assessing a set of five single tree attributes: tree position (TP), stem diameter at breast height (DBH), tree height (TH), crown base height (CBH), and crown projection area radii

(CPAR). Four different point clouds were used: from ZEB1, a hand-held mobile terrestrial laser scanner (HMLS), and from FARO FOCUS 3D, a static terrestrial laser scanner (TLS), both alone or in combination with ALS. The precision of single tree predictions, in terms of bias and Root Mean Square Error (RMSE), was evaluated against data recorded manually in the field with traditional instruments. We found that: i) TLS and HMLS have excellent comparable performances for the estimation of TP, DBH and CPAR; ii) TH was correctly assessed by TLS, while the accuracy by HMLS was lower; iii) CBH was the most difficult attribute to be reliably assessed; iv) the integration with ALS increased the performance of the assessment of TH and CPAR with both HMLS and TLS. Our results show that the integration of both TLS and HMLS with ALS is useful for assessing single tree attributes that are related with the top of the forest canopy, while the use of TLS or HMLS alone provides accurate estimates for the undercanopy attributes (like TP and DBH) in forests with complex structure.

Keywords: remote sensing, proximal sensing, LiDAR, forest inventories, forest structure, precision forestry

1. Introduction

Over the last several decades airborne laser scanning (ALS) demonstrated to be useful in providing accurate estimations of tree heights and forest attributes related to tree spatial arrangement (Hyyppä, et al., 2012). However, ALS data alone may not completely capture the information on the vertical distribution of the canopy because of the attenuation of the laser impulses, particularly in complex multi-layered and dense forests (Lim et al., 2003). ALS-based estimations rely on the acquisition of information in the field from a sample extracted from the investigated forest area, usually in circular plots selected in the framework of a statistical sampling design (Corona, 2016; Chirici et al., 2016).

Conventional forest mensuration in sampling plots is based on tree measurements carried out by mechanical or optical instruments, such as callipers, hypsometers, compass and measuring tapes. The development of laser scanning technologies is gradually modifying methods for assessing forest attributes in the field (Moskal and Zheng, 2011; Holopainen et al., 2013; Kankare et al., 2015). These technologies can improve work efficiency in forest inventory, potentially replacing manually measured tree attributes with more automatic procedures (Henning and Radtke, 2006; Liang et al., 2016). Hence, static and mobile terrestrial laser scanners are acquiring increasing relevance in forestry (Liang et al., 2016a). Forest stand structure, especially the vertical distribution of forest vegetation, can be detected with high detail by laser scanners, providing single tree estimations better than those obtained by remote sensing or traditional field measurements (Loudermilk et al., 2009). Furthermore, terrestrial laser scanning data can be used to assess single tree attributes which can be hardly measured with other methods, such as tree architecture or detailed tree assortments (Dassot et al., 2011).

The use of terrestrial laser scanning for forest and tree

mensuration can be classified according to the requested level of complexity of the attributes to be produced (Liang et al., 2016). From basic attributes such as the stem diameter at breast height (DBH), tree height, tree position, and three-dimensional (3D) models of the main stem, up to the provisioning of additional structural parameters such as crown width, crown projection area, crown height, crown surface area, secondary branches, and leaves.

Static terrestrial laser scanning (TLS) is suitable to measure millimetre-level information from a sample plot level to a single tree (Maas et al., 2008; Liang et al., 2012, 2014; Lindberg et al., 2012; Kankare et al., 2013; Kankare et al., 2014). The penetration of the laser pulse through the canopy is one of the main cause of measurements uncertainties. For instance, tree height underestimation occurs when LiDAR (Light Detection and Ranging) point density in the upper canopy is reduced due to the occlusion caused by the lower portion of tree canopy and understory vegetation (Maas et al., 2008). TLS point density is in fact negatively correlated with tree height (Van der Zande et al., 2006). Furthermore, TLS accuracy is influenced by other factors such as tree distance from the scanner, number of scans, and DBH extraction method (Liang et al., 2016; Srinivasan et al., 2014). The hardware costs are still rather high (albeit even more decreasing) and the mobility of instruments is relatively low.

The disadvantages of TLS are partially reduced by mobile laser scanning technology, which allows a significant increase in productivity (e.g. area covered per hour of survey) and thus in capability of collecting inventory data over large areas (Ryding et al., 2015). Distinctively, hand-held mobile laser scanner (HMLS) has lower hardware costs compared to TLS and, using Simultaneous Localization and Mapping (SLAM) methods, the reliance on satellite positioning is no more needed (Ryding et al., 2015). At

the same time, HMLS is less precise providing less accurate estimation of tree position and structure, in particular for smaller trees, than TLS. However, when trees with DBH<10 cm are not considered, even better results by HMLS, at least in DBH estimations, can be achieved (Bauwens et al., 2016; Ryding et al., 2015).

The integration of TLS and HMLS scans with ALS provides a further possible solution to enhance characterization of forest stand overstory and understory. In this case, accurate tree heights are measured using ALS returns and the tree positions and structure mainly on the basis of TLS or HMLS returns, so that integrating terrestrial scans and ALS data results in an improvement of measurement accuracy.

Few studies have focused on the analysis of the benefits resulting from TLS and HMLS merging with ALS (e.g. Paris et al., 2015; Yang et al., 2015; Hauglin et al., 2014), and no studies were carried out under complex Mediterranean environments, at least to our knowledge. In this study, our main objective was to assess and compare the precision and accuracy of ZEB1 HMLS and FARO® FOCUS 3D TLS to measure single tree attributes within a complex mixed Mediterranean forest. In particular, we considered the following attributes: tree position (TP), stem diameter at breast height (DBH), tree height (TH), crown base height (CBH), and the radii of the crown projection area (CPAR). Using conventional field survey as a benchmark, the main aim was to compare tree level attributes obtained by the automatic elaboration of four different point clouds: (i) HMLS; (ii) TLS; (iii) integration of HMLS and ALS ($HMLS_{ALS}$); (iv) integration of TLS and ALS (TLS_{ALS}). The accuracy of the estimates was evaluated on the basis of bias and Root Mean Square Error (RMSE) calculated comparing tree level estimations with field reference data.

This research note is organized as follows. First, the study area,

field reference data and HMLS TLS, and ALS data are presented. Then, a concise description of the approach applied to align the different point clouds and the automatic procedure to derive single tree attributes are reported. Finally, the results are discussed to highlight pros and cons of mobile (HMLS) and statitc (TLS) laser scanning techniques, as well as their potential integration with ALS for single tree attributes estimation.

2. Material

2.1 Study area and field reference data

The study area is located in a Mediterranean dense and multi-layered forest stand close to Firenze (Central Italy), dominated by coniferous (*Cupressus sempervirens* L. and *Pinus pinaster* Aiton) and evergreen broadleaves (*Quercus ilex* L.), that can be ascribed to the type 9.1 of the European Forest Types (Barbati et al., 2014).

The field data were acquired on March the 18th 2016 within one circular plot having a radius of 13 m (531 m^2). The latitude and longitude of the centre of the plot were recorded by a GNSS receiver Trimble Geo 7X, that lasted for approximately 1 hour with a 2-sec logging rate. The post-processed centre coordinates revealed standard deviations for x, y and z of 0.8 cm, 0.6 cm and 1.8 cm, respectively.

For all living and dead trees with DBH > 2.5 cm, the following attributes were collected: horizontal distance and azimuth from the plot centre to compute tree position (TP); tree species, DBH, total tree height (TH), and crown base height (CBH). In addition, crown projection area (CPA) was calculated using the four crown radii (CPAR) measured in the field at each cardinal directions (north, east, south and west). DBH was measured with a calliper, TH, CBH, CPAR and horizontal distances were measured with a Vertex IV Hypsometer, while the azimuth was collected with a Suunto KB-14/360 R compass. A total of 56 stems (i.e. 52 living trees and 4 standing

dead trees) and 224 CPAR were measured (Figure 1).

The measured stems had an average DBH of 20.8 cm (standard deviation (SD) of 9.6 cm), an average height of 12.5 m (SD of 3.92 m), an average CBH of 4.76 m (SD of 3.06 m), and an average CPAR of 1.66 m (SD of 1.30 m) (Figure 2).

These measures, collected by traditional instruments, are here assumed as error free and used as reference field data for evaluating the estimates produced on the basis of the different laser scans.

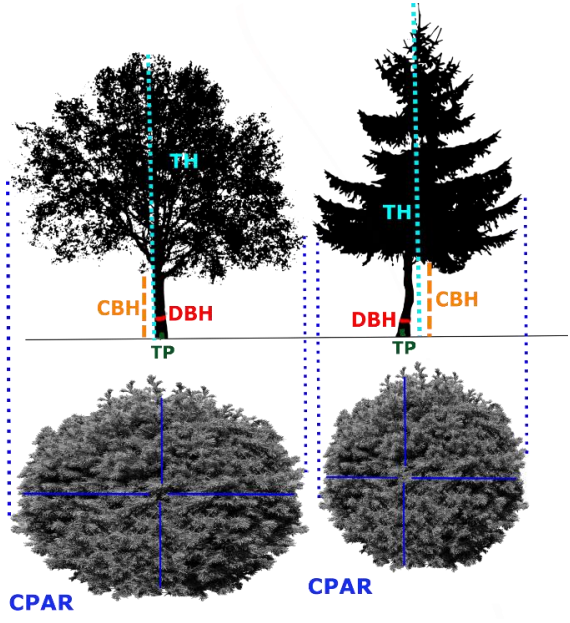

Figure 1: Graphical scheme of single tree attributes measured in the field.

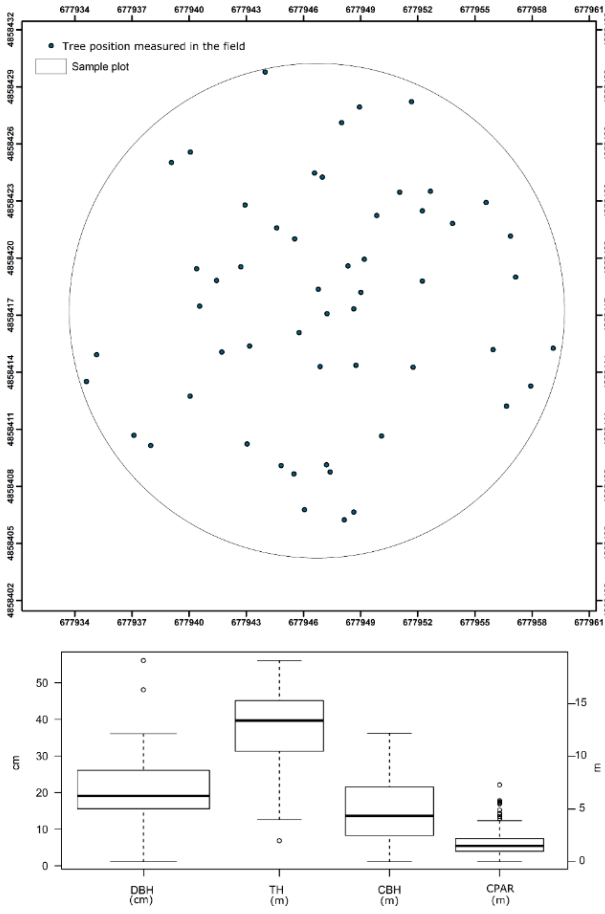

Figure 2: Summary of the reference field data measured with traditional instruments. Above the single tree position, below the boxplot of resulting values for DBH, TH, CBH, and CPAR.

2.2 Laser Scanner data collection and pre-processing

2.2.1. Hand-held Mobile Laser Scanning

As HMLS we used the ZEB 1, which is a personal laser scanner instrument combined with an inertial measurement unit (IMU). The reported operative laser range outdoors is 15-20 m around the instrument (Bosse et al., 2012). Data acquisition is conducted by a person walking with

the instrument through the plot (Bauwens et al., 2016; Ryding et al., 2015). Only one walking scan was needed to acquire the field plot. A complete description of the instrument can be found in Giannetti et al., (2017), Bauwens et al. (2016) and in Ryding et al. (2015).

Data acquisition was carried out on March the 22th 2016. Six spherical targets (each with a diameter of 14 cm) were fixed on the ground in different cardinal positions and at different distances from the centre to georeference the point cloud in post-processing (Figure 2). The spherical targets were measured starting from the plot centre. The azimuth was measured using a compass and the horizontal distance to the centre of the plot was determined with a VERTEX IV instrument.

According to Bauwens et al. (2016), a walking fixed path was followed by the ZEB1 user to avoid shadow zones; the start and final points of the walking scan acquisition were coincident and fixed in the centre of the plot to ensure a close loop, as requested when the SLAM algorithm is used. In the field, for the operator it was not easy to follow the desired theoretical path for the presence of obstacle on the ground. As a consequence the real walking path resulted not coincident with the fixed one (Figure 3).

The raw ZEB1 data were processed with the in-house procedure GeoSLAM, which uses the SLAM algorithm to locate the scanner in an unknown environment position/location and to register the whole 3D point clouds using IMU data and feature detection algorithms (Bauwens et al., 2016).

The 3D point cloud we obtained was rotated and translated using the six spherical targets from the local coordinate system to a geographic coordinate system (i.e. WGS84 UTM32N).

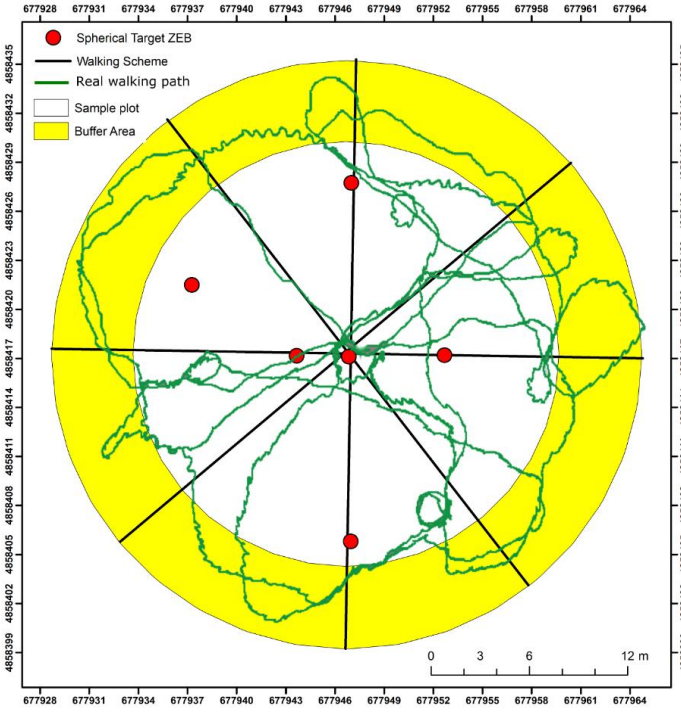

Figure 3: The HMLS (ZEB1) walking scheme acquisition.

The six spherical targets were automatically detected in the cloud using Cloud Compare software (Compare Cloud, 2017) and with the *align point pairs picking tools* implemented in this software the reference coordinate system has been assigned. The final RMSE of roto-translation was 3.83 cm.

2.2.2. Static Terrestrial Laser Scanning

As the TLS we used the FARO FOCUS 3D instrument that acquires data from eight fixed points through a scan angle of 360°. The instrument uses a phase-shift-based technology with a maximum range of 120 m. It is

able to record and measure the x, y, z coordinates and the intensity of laser returns. A complete description of the instrument can be found in Bauwens et al. (2016) and Ryding et al. (2015).

According to results reported by Trochta et al. (2013), several scans are needed in a forest field plot to acquire 50% of the DBH cross-section and to detect 90% of the trees. Data acquisition was carried out on March the 25th 2016. Given the complexity of the forest, eight static scans were acquired to avoid shadow zones. We used 12 spherical targets mounted on poles to co-register the different scans. One spherical target was fixed on the plot centre and the remaining were distributed within the plot to ensure the larger scans visibility; in order to obtain a good post-processing co-registration, scan positions were chosen to ensure as much as possible the higher inter-visibility of one scan to each other and the larger number of spherical targets (Figure 4).

The FARO scan system was set to obtain black and white scans (no RGB) with an intermediate resolution (i.e. distance between two points at 10 m equal to 9 mm).

The different scans were co-registered using Trimble RealWorks software (Trimble, 2017) through the automatic detection of the spherical targets. All the spherical targets were recognized and the different scans were merged together in one point cloud.

2.2.3. Airborne Laser Scanning

The ALS survey was carried out in May 2015 with an Eurocopter AS350 B3 equipped with a LiDAR RIEGL LMS-Q680i sensor. The flight height was 1,100 m a.t.l. Full-waveform LiDAR data was registered and discretized to a point density

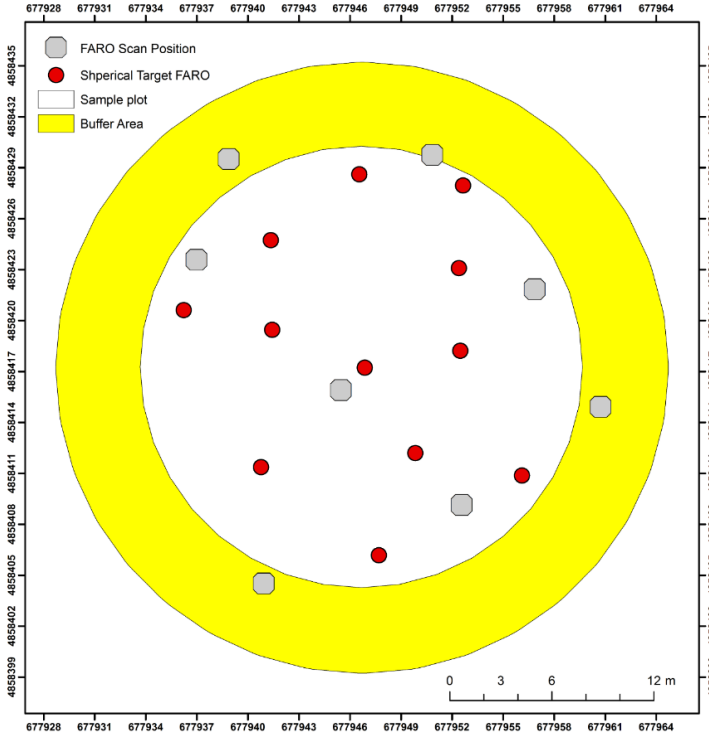

Figure 4: TLS (FARO) scheme acquisition and the location of the twelve spherical targets used to align the scans.

of 10 point m^{-2} georeferenced in WGS84 UTM32N. Common procedures for pre-processing ALS data (e.g. outliers and noise cleaning, classification of ground/non-ground points and computation of height) were done using LAStools software. For more information on this ALS acquisition and the pre-processing techniques we refer to Chirici et al. (2017).

2.3 Co-registration of point clouds

To allow the comparison of the two different point clouds (i.e. TLS and HMLS) and ease the analysis at single tree level, the TLS point cloud was

coregistered to the georeferenced HMLS cloud following the procedure described in Bauwens et al. (2016). A rough alignment in Cloud Compare (http://cloudcompare.org) software with the *align* function (Compare Cloud, 2017) was done using as corresponding points the trees in the plot identified by visual interpretation. The accuracy of the rough alignment calculated on the corresponding points was 5 cm. To obtain the best overall fit of the two point clouds and to improve the alignment accuracy a Hybrid Multi-Station Adjustment (RIEGL LMS, 2017) was also carried out using a Digital Terrain Model (DTM) extracted and automatically aligned from the point clouds themselves. The achieved accuracy was 2 cm.

In addition, the two point clouds (i.e. TLS and HMLS) were merged with ALS using the reference coordinate system (WGS84 UTM 32 N). The accuracy of the merging process was calculated on the basis of differences between terrain heights from the DTM based on ALS and the DTM obtained by TLS and HMLS with a spatial resolution of 0.5 m. The RMSE between all the pixels revealed a mean difference of 2 and 3 cm for TLS and HMLS, respectively. As a result of this procedure we obtained four georeferenced point clouds, namely TLS, HMLS, TLS_{ALS} and $HMLS_{ALS}$, which were used in the following analysis.

3. Methods

3.1 Extraction of single tree attributes

The Computree software (http://computree.onf.fr) was used to automatically extract the five considered single tree attributes (TP, DBH, TH, CBH, CPAR) from the four point clouds. This approach allows the automatic extraction of all the attributes by the algorithms implemented in several tools. Simple trees tools (Hackenberg et al., 2015) were used to segment the plot point clouds into single trees point clouds, and to extract the single

tree attributes related to height (TH and CBH), DBH and TP. The ONF-ENSAM tools (Othmani et al., 2011) were used to determine the CPA for each single tree. The 4 radii (CPAR) of the CPA were derived from the crown projection area in a GIS environment. Figure 5 shows the workflow used to process the four point clouds.

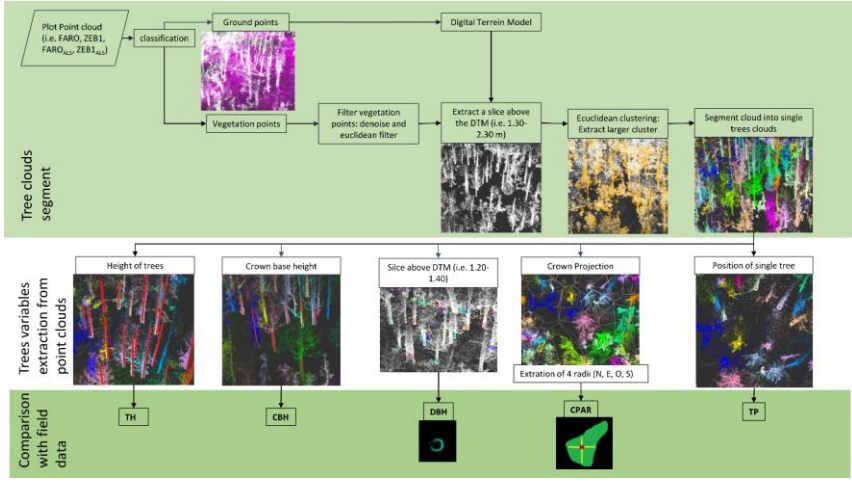

Figure 5: procedure used to automatically extract the single tree attribute from TLS (FARO) and HMLS (ZEB1) point clouds.

3.2 Accuracy assessment

For each considered single tree attribute we compared the estimation obtained by point clouds with the traditional manual field measures. To assess the accuracy of the tree level estimations we calculated the coefficient of determination (R^2). A paired *t-test* was used (95% critical significant level, α=0.05) to test statistical differences. In addition, we calculated the RMSE and bias as follows:

$$RMSE = \sqrt{\frac{\sum_{i=1}^{n}(X_{oi} - X_{Si})^2}{n}}$$

$$bias = \frac{\sum_{i=1}^{n}(X_{oi} - X_{Si})}{n}$$

where *n* is the number of trees measured in the field, X_o is the true value of the attribute measured in the field; X_S is the estimated value of the attribute for each *i*-th tree. We used the Euclidean distance from the plot centre as X_o and X_S to calculate the RMSE and bias for TP.

4. Results

The automatic procedure allowed the segmentation of all the target trees measured in the field using HMLS, TLS, $HMLS_{ALS}$ and TLS_{ALS} point clouds. The coefficient of determination (R^2*=0.98* for X coordinate and R^2*=0.99* for Y coordinate) and *t-test* (*p>0.9*) revealed a good fit between the tree position extracted from the four point clouds and the corresponding field reference measures (Figure 6). For TP, bias and RMSE were approximately 2.0 cm and 9.3 cm, respectively, independently of the cloud used (Table 1). A *t-test* confirmed that no significant differences (*p>0.90*) exist among the different clouds.

For the DBH estimations, the coefficient of determination revealed a good fit between DBH estimated by HLMS (*p>0.90;* R^2*=0.99*) and TLS (*p>0.80;* R^2*=0.99*) and the field reference measures (Figure 7). Comparable results in terms of bias and RMSE were observed between the two instruments. As for TP, the merging of ALS cloud did not increased the accuracy of DBH estimations. The results provided by TLS_{ALS} and $HMLS_{ALS}$ were equal with those obtained by TLS and HMLS (R^2*=1*) (Table 1). However, using TLS and TLS_{ALS} clouds was possible to detect 55 DBHs (DBH>2.5 cm) of the 56 trees measured in the field with conventional instruments while with HMLS and $HMLS_{ALS}$ only 53 DBHs (DBH> 5 cm) were detected

Table 1: Summary statistics of single tree attributes detected by each point clouds. The * indicate significant differences between the results obtained by the point cloud analysis and the measures in the field (t-test, $p<0.05$).

Attributes	Point cloud	RMSE	bias
Tree position (cm)	HMLS	9.31	2.06
	$HMLS_{ALS}$	9.31	2.06
	TLS	9.32	2.07
	TLS_{ALS}	9.32	2.07
Stem diameter at breast height (cm)	HMLS	1.28	-0.38
	$HMLS_{ALS}$	1.28	-0.38
	TLS	1.13	-0.41
	TLS_{ALS}	1.13	-0.41
Tree height (m)	HMLS	2.15	-4.61*
	$HMLS_{ALS}$	0.94	-0.30
	TLS	0.88	-0.61
	TLS_{ALS}	0.43	-0.19
Crown base height (m)	HMLS	1.91	1.67*
	$HMLS_{ALS}$	1.91	1.67*
	TLS	1.95	1.82*
	TLS_{ALS}	1.95	1.82*
Crown projection area radii (m)	HMLS	0.59	0.25*
	$HMLS_{ALS}$	0.44	0.20
	TLS	0.49	0.24
	TLS_{ALS}	0.24	0.18

TH estimated by HMLS registered a large bias (Table 1 and Figure 8) and significant differences with reference field measures ($p<0.05$ and $R^2= 0.94$), while TLS produced more accurate results ($p>0.5$; $R^2=0.98$) both in terms of bias and RMSE (Table 1 and Figure 8).

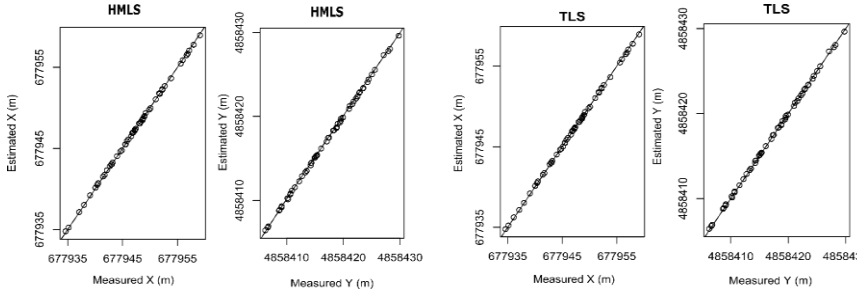

Figure 6: performance of tree position assessment on the basis of HMLS (ZEB1) and TLS (FARO) point clouds. Values in meters. The black line is the 1:1 line.

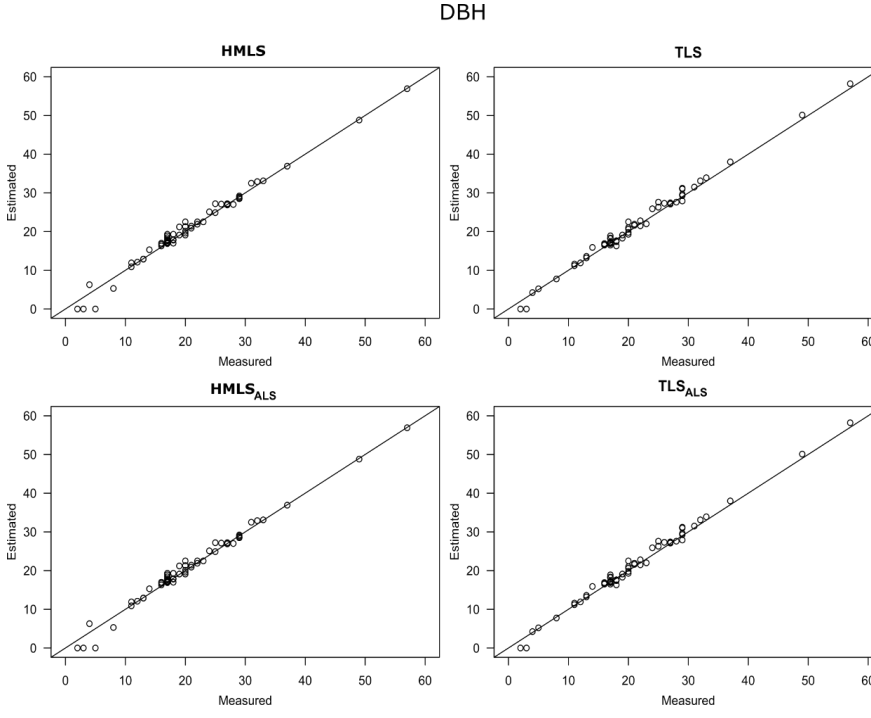

Figure 7: performance of DBH assessment on the basis of HMLS (ZEB1)

RMSE of TH estimation was on average 17.2% (2.15 m) of the truth

values when calculated on the basis of the HMLS cloud alone, and 7 % (0.88 m) when based on the TLS cloud. As expected, the inclusion of the ALS cloud contributed in obtaining better results in the estimation of TH, especially for $HMLS_{ALS}$ for which a consistent decreasing of bias and RMSE (7.4% of the truth values) was observed. Concurrently, the coefficient of determination (R^2*=0.97)* and *t-test* (*p>0.7*) revealed a good fit between TH estimated by $HMLS_{ALS}$ and the field measures. The same positive effect by ALS integration was observed using TLS_{ALS} in terms of bias and RMSE (Table 1), which moved to 3.4% of the truth value (*p>0.8;* R^2*=0.99*) (Figure 8).

We were able to estimate the CBH of all the segmented trees, both on the basis of HMLS and TLS clouds, but independently of the considered cloud or of the inclusion

of ALS data, we registered always low accuracies, with R^2 equal to 0.85, consistent bias and relatively high RMSE (Table1). The *t-test* between the CBH values estimated by clouds revealed a significant difference with the ones measured in the field (*p<0.05*), with RMSE equal, on average, to 40% (1.91 m) and 41% (1.95 m) of the reference values, for HMLS and TLS respectively (Table 1). However, no significant differences were found (*p>0.9,* R^2*=0.99*) between the results obtained by HMLS and TLS (Figure 9) with a constant underestimation especially for stems with larger CBH.

The CPAR estimation using HMLS and TLS alone showed significant differences with reference field measures (*p<0.05;* HMLS: R^2*=0.91*; TLS: R^2*=0.93*) showing large bias with RMSE values equal, on average, to 36% (0.59 m) and 29% (0.88 m) of the reference values, for HMLS and TLS respectively (Figure 10). As reported for TH, the inclusion of the ALS cloud contributed in obtaining better CPAR estimations (*p<0.05;* $HMLS_{ALS}$: R^2*=0.95;* TLS_{ALS}: R^2*=0.95*) showing a decreasing trend of RMSE, equal to 27% and 23%, for $HMLS_{ALS}$ and TLS_{ALS}, respectively, and no significant differences

with reference values (*p>0.5*) (Table 1). The ALS integration contributes to obtain a decrease of bias equal to 0.05 m and 0.06 m, for HMLS and TLS respectively.

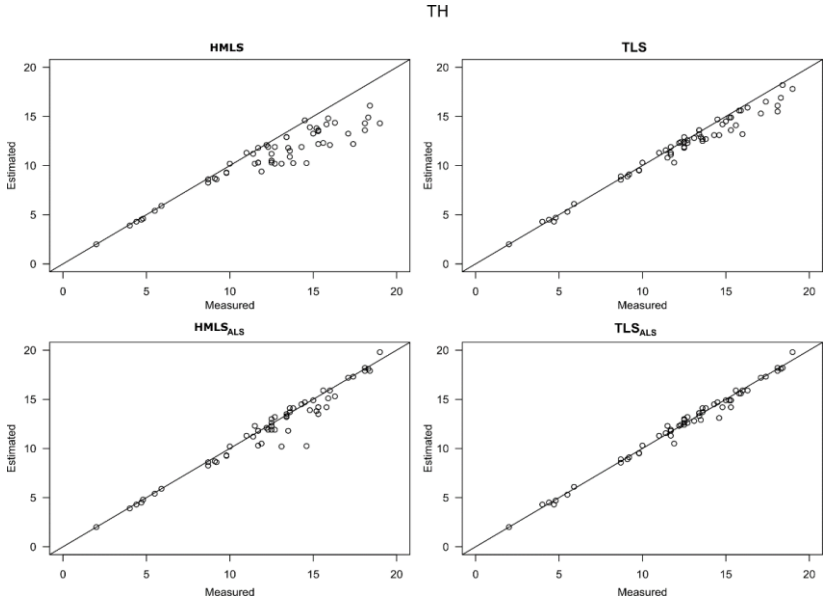

Figure 8: performance of tree height assessment on the basis of HMLS (ZEB1) and TLS (FARO) point clouds, both alone and integrated with ALS. Values in m. The black line is the 1:1 line.

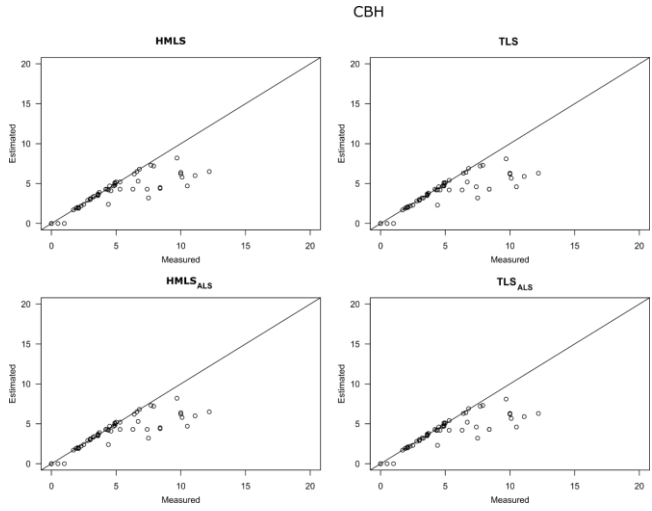

Figure 9: performance of crown base height assessment on the basis of HMLS (ZEB1) and TLS (FARO) point clouds, both alone and integrated with ALS. Values in m. The black line is the 1:1 line.

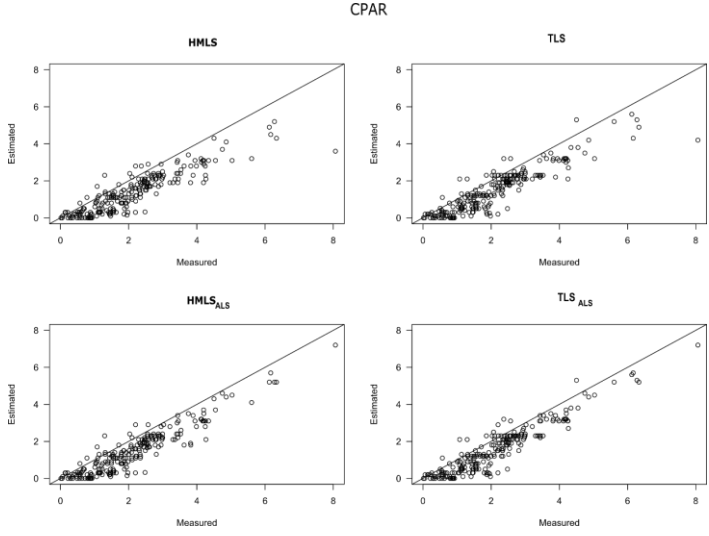

Figure 10: performance of crown projection area radii estimation on the basis of the HMLS (ZEB1) and TLS (FARO) point clouds, both alone and integrated with ALS. Values in m. The black line is the 1:1 line.

5. Discussion

We tested the potential of assessing single tree attributes in a complex mixed Mediterranean forest addressing two main issues: i) to assess and compare the results achieved on the basis of a FARO FOCUS 3D vs. a ZEB1 instrument, ii) and to investigate the influence of ALS integration on estimation accuracies. The assessment of tree position and DBH was satisfying, independently of the instrument used and independently of the additional use of ALS data. Using eight FARO TLS scans for DBH estimation, we obtained a bias of -0.41 cm and a RMSE of 1.13 cm, very similar to the ones reported by Bauwens et al. (2016) using five FARO scans (bias=-0.17 and RMSE=1.3 cm), while with the ZEB1 HMLS we obtained a bias of -0.38 cm and a RMSE of 1.28 cm for DBH estimation, similar to what reported by Ryding et al. (2015) (bias=0.30 cm and RMSE=2.9 cm), and by Bauwens et al. (2016) (bias= -0.08 cm and RMSE=1.11 cm). More in general, our DBH estimations by HMLS and TLS point clouds are in the range between 1.5 cm and 3.3 cm in terms of RMSE and in the range between -1.5 cm and 1.3 cm in terms of bias, confirming previous studies based on different TLS systems (Oveland et al., 2017; Hopkinson et al., 2004; Maas et al., 2008; Thies et al., 2004; Tansey et al., 2009). Differences between the two instruments were instead noted in terms of the minimum DBH recorded. On the basis of ZEB1 HMLS cloud we were not able to segment trees smaller than 10 cm in DBH, while with FARO TLS we found a minimum DBH of 2.5 cm (Figure 7). Thus confirming the results from Bauwens et al. (2016) and Ryding et al. (2015) who extracted single tree DBH and TP from trees with DBH>10 cm.

As reported from previous studies, terrestrial laser scanning has objective limitations for the direct measure of TH especially when the laser range similar to tree heights and/or when several vegetation layers occlude the laser path (Paris et al., 2015; Kankare et al., 2013; Krooks et al., 2014; Liang and Hyyppä, 2013; Maas et al., 2008). In our case study, we were able

to obtain good precision using the FARO TLS point cloud (RMSE of 0.88 m and bias of -0.61 m, see Table 1), better than the precision of 4.55 m in terms of RMSE obtained with Riegl LMS Z420i and FARO LS 800 HE80 reported by Maas et al. (2008). The results obtained by ZEB1 HMLS were less precise because of the limited range of the laser (15-20 m outdoor for the manufacturer). Under this point of view the procedure we propose for merging the ALS point cloud with the ZEB1 data was successful: RMSE moved from 2.15 to 0.94 m (Figure 8) and the bias moved from -4.61 m to -0.30 m, in line with the results achieved by Paris et al. (2015), who reported a change in RMSE due to ALS inclusion from 3.71 to 1.50 m.

Estimation of CBH by HMLS and TLS showed a consistent bias with high values of relative RMSE (40% for HMLS and 41% for TLS), mainly due to the impossibility of recognizing dead branches on the basis of both HMLS and TLS clouds.

As observed for TH, merging HMLS or TLS clouds with ALS data contributed to obtain more accurate results for CPAR estimation. In fact, on average the RMSE calculated on the base of the reference values decreased from 36% to 27% for HMLS and from 29% to 23% for TLS, and bias decreased from 0.25 to 0.20 for HMLS and from 0.24 to 0.18 for TLS. The positive effects of ALS inclusion were observed especially for larger crown radii (Figure 11). Usually the larger crown radii are those of dominant trees and we can suppose that both HMLS and TLS cannot accurately detect these trees because of the occlusion derived by the presence of dominated trees. Similar results are reported by Paris et al. (2015).

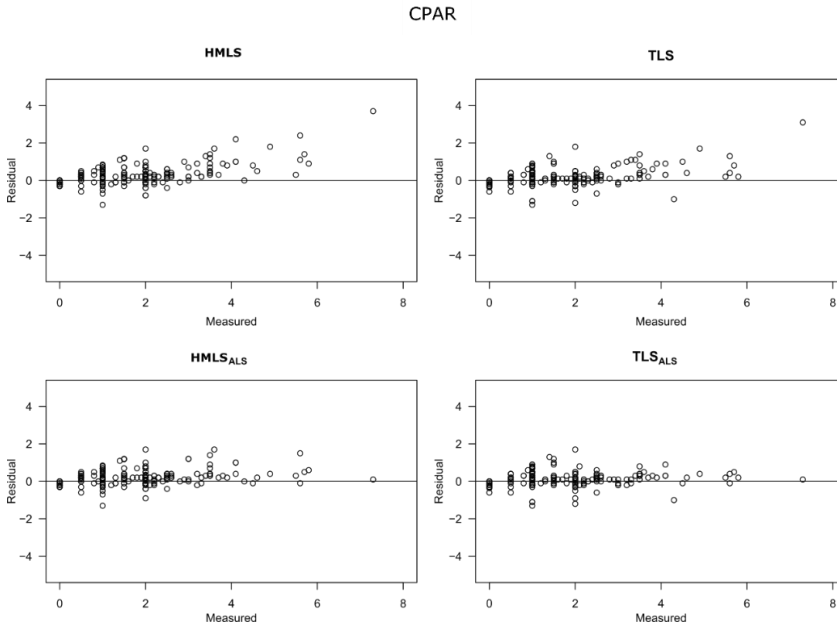

Figure 11: performance of crown projection area radii assessment on the basis of HMLS (ZEB1) and TLS (FARO) point clouds, both alone and integrated with ALS. Residuals were calculate subtracting from the measured value the one esteemed from the cloud. Values in m. The black line is the 0:0 line.

In terms of workload, the acquisition of field data with conventional manual measurements required a total of 12 man-hours. The eight FARO scans were done in one hour, more than the time reported by other studies, such as the 30 minutes in ash and elm woodland reported in Ryding et al. (2015). The time needed for the ZEB1 acquisition was only 7 minutes, which is in line with the results for a mixed forest in Belgium (Bauwens et al., 2016) and an ash and elm woodland in the UK (Ryding et al., 2015). The workload for coding and optimization of the procedures for point clouds segmentation and single tree attributes extraction was instead

around 50 man-days. The main problems in this phase were related to the high level of intersection between tree crowns and the complexity of the vertical structure (dominated trees under dominant trees).

6. Conclusions

Any rational decision related to the maintenance and enhancement of the multiple functions provided by forests needs to be based on objective, reliable information (Corona et al., 2002): as such, forest monitoring and assessment are rapidly evolving as new information needs arise and new techniques and tools become available. However, the exploitation of the latter, as well as their implementation within operative forest management processes, should be evidence-based (Corona, 2014). Under this perspective, the results obtained by this study highlight the following main issues:

- The FARO 3D FOCUS instrument with eight scans in a plot of 13 m radius was able to produce an excellent point cloud for a complete and detailed single tree segmentation. The estimations for the four attributes produced on the basis of this point cloud had errors in line or smaller than those reported in literature, even if the Mediterranean vegetation was dense and multi-layered. Under this point of view, this study confirms that TLS technique is promising also in such complex forest types.
- Even if the ZEB1 instrument has a limited scanning range, in only 7 minute of walking scan we were able to produce a point cloud for good estimations of tree positioning and DBH, obtaining the same accuracy provided by the FARO scans in one hour acquisition.

- The integration of ALS and HMLS or TLS data did not determined a significant improvement on tree position and DBH estimation.
- The inclusion of ALS data determined a strong increase in the accuracy of tree height and crown projection assessment, especially with respect to ZEB1.

These findings cast a promising light on the use of HMLS such as the ZEB1, especially in those areas where recent ALS or photogrammetry point clouds are available. To increase the accuracy of the estimation based on HMLS ways to optimise the walking scan line should be devised, since it is rather difficult to understand during the path in the field which areas have been already scanned. Especially in complex forest or orographic conditions.

Future research need also to be focused on standardize HMLS and TLS clouds segmentations to improve the utility of these instruments in complex forests: the complexity of forest stand structure influences a lot the time required to automatically analyze the data. For this reason, similar experiments should be carried out in different forest conditions.

Acknowledgments

The work was partially carried out in the framework of the FRESh LIFE project "Demonstrating Remote Sensing integration in sustainable forest management" (LIFE14/IT000414).

We wish to thank Franco Piemontese for the participation in the fieldwork.

References

Barbati A., Marchetti M., Chirici G., Corona P., 2014. European Forest Types and Forest Europe SFM indicators: Tools for monitoring progress on forest biodiversity conservation. Forest Ecology and Management 321: 145-157. doi: 10.1016/j.foreco.2013.07.004.

Bauwens, S., Bartholomeus, H., Calders, K., Lejeune, P., 2016. Forest inventory with terrestrial LiDAR: A comparison of static and hand-held mobile laser scanning. Forests 7 (127). doi:10.3390/f7060127.

Bosse, M., Zlot, R., and Flick, P. Zebedee: Design of a spring-mounted 3-d range sensor with application to mobile mapping. IEEE Trans. Robot. 2012, 28, 1104–1119.

Chirici G., McRoberts R.E., Fattorini L., Mura M., Marchetti M. Comparing echo-based and canopy height model-based metrics for enhancing estimation of forest aboveground biomass in a model-assisted framework. Remote Sensing of Environment 2016, 174, 1-9.

Chirici G., Bottalico F., Giannetti F., Del Perugia B., Travaglini D., Nocentini S., Kutchartt E., Marchi E., Foderi C., Fioravanti M., Fattorini L., Bottai L., McRoberts R.E., Næsset E., Corona P., Gozzini B. Assessing forest windthrow damage using single date, post-event airborne laser scanning data. Forestry: An International Journal of Forest Research, 2017 https://doi.org/10.1093/forestry/cpx029

Corona, P. (2016) Consolidating new paradigms in large-scale monitoring and assessment of forest ecosystems. Environmental Research 144: 8-14.

Corona. P., Chirici, G., Marchetti, M. (2002) Forest ecosystem inventory and monitoring as a framework for terrestrial natural renewable resource survey programmes. Plant Biosystems 136: 69-82.

Corona P. (2014) Forestry research to support the transition towards a bio-based economy. Annals of Silvicultural Research 38: 37-38.

Dassot, M., Constant, T., and Fournier, M. The use of terrestrial LiDAR technology in forest science: Application fields, benefits and challenges. Ann. For. Sci. 2011, 68, 959–974.

Giannetti, F., Chirici, G., Travaglini, D., Bottalico, F., Marchi, E., Cambi, M. Assessment of Soil Disturbance Caused by Forest Operations by Means of Portable Laser Scanner and Soil Physical Parameters. Soil Sci. Soc. Am. J, 2017 doi:10.2136/sssaj2017.02.0051

Hackenberg, J., Spiecker, H., Calders, K., Disney, M., and Raumonen, P. SimpleTree – An efficient Open Source Tool to build Tree Models from TLS Clouds. Forests. 2015, 6, 4245-4294.

Henning, J.G., and Radtke, P.J. Detailed stem measurements of standing trees from ground-based scanning lidar. For. Sci. 2006, 52, 67–80.

Hyyppä, J., Holopainen, M., and Olsson. H. Laser scanning in forests. Remote

Sens. 2012, 4, 2919–2922.
Hilker, T., van Leeuwen M., Coops, N., Wulder, M.A., Newnham, G., Jupp, D., and Culvenor, D. Comparing canopy metrics derived from terrestrial and airborne laser scanning in a Douglas-fir dominated forest stand. Trees. 2010, 24, 819–832.
Holopainen, M., Kankare, V., Vastaranta, M., Liang, X., Lin, Y., Vaaja, M., and Kukko, A. Tree mapping using airborne, terrestrial and mobile laser scanning – A case study in a heterogeneous urban forest. Urban forestry & urban greening. 2013, 12(4), 546-553.
Hopkinson, C., Chasmer, L., Young-Pow, C., and Treitz, P. Assessing forest metrics with a ground-based scanning LiDAR. Canadian Journal of Remote Sensing. 34, 573–583.
Hauglin, M., Lien, V., Næsset, E., and Gobakken, T. Geo-referencing forest field plots by co-registration of terrestrial and airborne laser scanning data. Int. J. Remote Sens. 2014, 35(9), 3135-3149
Kankare, V., Liang, X., Vastaranta, M., Yu, X., Holopainen, M., and Hyyppä, J. Diameter distribution estimation with laser scanning based multisource single tree inventory. ISPRS Journal of Photogrammetry and Remote Sensing. 2015, 108, 161-171.
Kankare, V., Joensuu, M., Vauhkonen, J., Holopainen, M., Tanhuanpää, T., Vastaranta, M., Hyyppä, J., Hyyppä, H., Alho, P., Rikala, J., and Sipi, M. Estimation of the timber quality of scots pine with terrestrial laser scanning. Forests. 2014, 5, 1879–1895. http://dx.doi.org/10.3390/f5081879.
Kankare, V., Holopainen, M., Vastaranta, M., Puttonen, E., Yu, X., Hyyppä, J., Vaaja, M., Hyyppä, H., and Alho, P. Individual tree biomass estimation using terrestrial laser scanning. ISPRS J. Photogramm. Remote Sens., 2013 75, 64–75. http://dx.doi.org/10.1016/j.isprsjprs.2012.10.003.
Krooks, A., Kaasalainen, S., Kankare, V., Joensuu, M., Raumonen, P., and Kaasalainen, M. Tree structure vs. height from terrestrial laser scanning and quantitative structure models. Silva Fenn. 2014, 48, 1–11. doi:10.14214/sf.1125
Liang, X., Kankare, V., Hyyppä, J., Wang, Y., Kukko, A., Haggrén, H., and Holopainen, M. Terrestrial laser scanning in forest inventories. ISPRS Journal of Photogrammetry and Remote Sensing. 2016, 115, 63-77.
Liang, X., and Hyyppä, J. Automatic stem mapping by merging several terrestrial laser scans at the feature and decision levels. Sensors (Switzerland). 2013, 13, 1614–1634. doi:10.3390/s130201614
Liang, X., Kankare, V., Yu, X., Hyyppa, J., and Holopainen, M. Automated stem curve measurement using terrestrial laser scanning. IEEE Trans. Geosci. Remote Sens. 2014, 52, 1739–1748. http://dx.doi.org/10.1109/TGRS.2013.2253783.

Liang, X., Hyyppä, J., Kaartinen, H., Holopainen, M., and Melkas, T. Detecting changes in forest structure over time with bi-temporal terrestrial laser scanning data. ISPRS Int. J. Geo-Inform. , 2012, 1, 242–255. http://dx.doi.org/10.3390/ijgi1030242.

Lindberg, E., Holmgren, J., Olofsson, K., and Olsson, H. Estimation of stem attributes using a combination of terrestrial and airborne laser scanning. Eur. J. Forest Res. 2012, 131, 1917–1931.

Lim, K., Treitz, P., Wulder, M., St-Onge, B., and Flood, M. LiDAR remote sensing of forest structure. Prog. Phys. Geogr. 2003, 27, 88-106.

Loudermilk, E.L., Hiers, J.K., O'Brien, J.J., Mitchell, R.J., Singhania, A., Fernandez, J.C., Cropper, W.P., Jr., and Slatton, K.C. Ground-based LIDAR: A novel approach to quantify fine-scale fuelbed characteristics. Int. J. Wildland Fire. 2009, 18, 676–685.

Maas, H.G., Bienert, A., Scheller, S., and Keane, E. Automatic forest inventory parameter determination from terrestrial laser scanner data. Int. J. Remote Sens. 2008, 29, 1579–1593. http://dx.doi.org/10.1080/01431160701736406.

Moskal, L.M., and Zheng, G. Retrieving forest inventory variables with terrestrial laser scanning (TLS) in urban heterogeneous forest. Remote Sens. 2011, 4, 1–20.

Othmani, A.; Piboule, A.; Krebs, M.; Stolz, C.; and Voon, L.L.Y. Towards Automated and Operational Forest Inventories with T-Lidar. 2011. Available online: https://hal.archives-ouvertes.fr/hal-00646403/document (accessed on 30 April 2017)

Paris, C., Kelbe, D., van Aardt, J., and Bruzzone, L. A precise estimation of the 3D structure of the forest based on the fusion of airborne and terrestrial lidar data. In Geoscience and Remote Sensing Symposium (IGARSS), 2015 IEEE International (pp. 49-52). IEEE.

Ryding, J., Williams, E., Smith, M.J., and Eichhorn, M.P. Assessing handheld mobile laser scanners for forest surveys. Remote Sensing. 2015, 7(1), 1095-1111.

Srinivasan, S., Popescu, S.C., Eriksson, M., Sheridan, R.D., and Ku, N.W. Terrestrial laser scanning as an effective tool to retrieve tree level height, crown width, and stem diameter. Remote Sensing. 2015, 7(2), 1877-1896.

Tansey, K., Selmes, N., Anstee, A., Tate, N.J., and Denniss, A. Estimating tree and stand variables in a Corsican Pine woodland from terrestrial laser scanner data. International Journal of Remote Sensing. 2009, 30, 5195–5209.

Thies, M., Pfeifer, N., Winterhalder, D., and Gorte, B.G.H. Three-dimensional reconstruction of stems for assessment of taper, sweep, and lean based on laser scanning of standing trees. Scandinavian

Journal of Forest Research. 2004, 19, 571–581.
Trochta, J. Král, K. Janík, D. and Adam, D. Arrangement of terrestrial laser scanner positions for area-wide stem mapping of natural forests. Can. J. For. Res. 2013, 43, 355–363.
Van der Zande, D., Hoet, W., Jonckheere, I., van Aardt, J., Coppin, P. Influence of measurement set-up of ground-based LiDAR for derivation of tree structure. Agric. For. Meteorol. 2006, 141, 147–160.
White, J.C., Coops, N.C., Wulder, M.A., Vastaranta, M., Hilker, T., and Tompalski, P. Remote Sensing Technologies for Enhancing Forest Inventories: A Review. Can. J. Remote Sens. 2016, 42, 619–641. doi:10.1080/07038992.2016.1207484.
Yang, B., Zang, Y., Dong, Z., and Huang, R. An automated method to register airborne and terrestrial laser scanning point clouds. ISPRS Journal of Photogrammetry and Remote Sensing. 2015, 109, 62-76.

Paper II - Development and assessment of DTM-independent variables for prediction of forest biophysical properties using UAV photogrammetric data.

Francesca Giannetti[a], Gherardo Chirici[a], Terje Gobakken[b], Erik Næsset[b], Davide Travaglini[a], Stefano Puliti[b]*

* Corresponding author francesca.giannetti@unifi.it

[a] Dipartimento di Gestione dei Sistemi Agrari, Alimentari e Forestali, Università degli Studi di Firenze, Italy

[b] Faculty of Environmental Sciences and Natural Resource Management, Norwegian University of Life Sciences, P.O. Box 5003, NO-1432 Ås, Norway

Submitted

Abstract

We present a novel approach for extraction of explanatory variables from unmanned aerial vehicle (UAV) photogrammetric data for prediction of forest biophysical properties without relying on a digital terrain model. This DTM-independent approach was developed to avoid the need of a detailed DTM which is required when UAV photogrammetric data are normalized to obtain relative heights above the terrain, hence increasing the potential areas of application of UAVs in forest inventory. The approach was tested in two different forest types, namely boreal forests and temperate mixed forests. The following five response variables were studied: growing stock volume (m^3 ha^{-1}), basal area (m^2 ha^{-1}), stem number (ha^{-1}), Lorey's height (m), and dominant height (m).

We compared the predictive accuracy of models using DTM-independent variables with that of models using two more traditional sets of variables, namely (i) height and density variables from UAV photogrammetric data normalized using a DTM acquired using airborne laser scanning (ALS) (Image-DTM_{ALS} variables) and (ii) height and density variables extracted from normalized ALS data (ALS variables). Root mean square error as percentage of the mean ($RMSE_{\%}$) was used as measure of

accuracy in the comparison. Overall, the average $RMSE_{\%}$ across all of the studied response variables was smaller (19.6%) for the DTM-independent variables compared to Image-DTM_{ALS} variables (19.7%) and ALS variables (21.6%). Interestingly, the DTM-independent variables yielded more accurate predictions ($RMSE_{\%}$ = 19.1%) compared to ALS variables ($RMSE_{\%}$ = 23.2%) in the study site characterized by larger complexity in terms of forest structure and terrain. The generality of the results was confirmed by consistency of the results across the two study sites with $RMSE_{\%}$ for the DTM-independent models in the range 15.9% - 19.2%, 12.8% - 15.9%, 37.3% - 40.7%, 14.6% - 15.9%, and 10.7% - 13.5% for growing stock volume, basal area, stem number, Lorey's height, and dominant height, respectively.

Our results demonstrated that UAV photogrammetric data can be used effectively for estimating forest variables even when high-resolution DTMs are not available.

Keywords: unmanned aerial vehicle, photogrammetry, digital terrain model, airborne laser scanning, forest inventory.

Highlights:

- A new set of DTM-independent explanatory variables were developed
- DTM-independent explanatory variables were derived from UAV photogrammetry data.
- The DTM-independent variables were regressed with forest inventory variables.
- The results obtained were compared with traditional variables: Image-DTMALS and ALS.
- The accuracy of the predictions between the three set of variables was similar.

1. Introduction

During the last two decades, three-dimensional (3D) remotely sensed (RS) data have become a fundamental source of information for estimating and mapping forest biophysical properties (Maltamo et al., 2014; Næsset et al., 2004). Among the multiple techniques to acquire 3D RS data, modern digital photogrammetric has received increasing attention in recent years. Because of the lower acquisition costs and similar performances compared to alternative 3D RS data (e.g. laser scanning data), there is an increasing use of photogrammetric data for modeling, prediction, mapping, and estimation of forest biophysical properties. More recently, great interest in the use of photogrammetric data for forest inventory was triggered by the advent of versatile imaging platforms such as UAVs and the development of advanced structure from motion (SfM) photogrammetry algorithms (Remondino et al., 2014).

Several studies have demonstrated that photogrammetric data generated from UAV imagery are a viable data source for forest inventories (Dandois and Ellis, 2013; Lisein et al., 2013; Puliti et al., 2017a, 2015a; Wallace et al., 2016). However, limited availability of detailed digital terrain models (DTMs) in large parts of the world has been a severe limitation to the use of photogrammetric data. A detailed DTM would be needed to obtain relative heights above ground by normalization, i.e., by subtracting the terrain elevation from the photogrammetric point cloud elevation (Lisein et al., 2013). The normalized point clouds are typically used to compute explanatory variables to predict forest biophysical properties. Because of the difficulty in generating detailed DTMs from photogrammetric data in vegetated areas, most studies based on photogrammetric data have employed pre-existing DTMs constructed from airborne laser scanning (ALS) data. However, ALS data are available only for small portions of the world's forests. The use of photogrammetric data for

forest inventory purposes has therefore been limited to mainly managed forest in the western world.

Some studies have attempted to use alternative sources of DTMs. Examples include DTMs obtained from UAV photogrammetric data (Dandois and Ellis, 2013; Kachamba et al., 2016; Miller et al., 2017; Wallace et al., 2016) or from space observations (Kachamba et al., 2016). Dandois & Ellis (2013) and Wallace et al. (2016) reported a mean difference (MD) between DTMs derived from ALS data and UAV in the range between 0.09 m and 4.9 m. In addition to the potentially large MD of the DTMs, and especially in areas with dense canopy cover, both studies were conducted in very small areas (0.15 – 6.25 ha) and the reported findings can therefore hardly be generalized to a wider range of forest types. A major limitation in the use of DTMs generated from UAV photogrammetric data is the large variability of the quality of the DTM depending on canopy cover, leading potentially to small precision and also large systematic errors in the estimation of forest biophysical properties.

It is important to note though that even ALS DTMs are affected by errors, especially in steep terrain combined with dense forest cover (Hodgson et al., 2003; Hodgson and Bresnahan, 2004; Hollaus et al., 2006; Hyyppä et al., 2005). For example, Hodgson and Bresnahan (2004) found that the observed errors between ground reference elevation and ALS derived elevation on 25° slopes may be about twice of those on relatively smaller slopes (e.g. 1.5°). Hyyppä et al. (2005) reported a standard deviation of up to 0.25 m for slopes <30° and up to 0.45 m for slopes greater than 30° while Hollaus et al. (2006) observed a standard error >0.5 m for slopes >60°. Furthermore, Hodgson et al. (2003) reported a mean absolute elevation error of ALS DTM ranging between 0.58 m and 0.96 m in slopes ranging between 0° and 8° in deciduous and mixed forests. As shown by Dandois

and Ellis (2013) and Wallace et al. (2016), errors in the DTM propagate into errors in the modeled relationships between variables derived from the point clouds and the forest biophysical properties.

A conceptually different approach for the extraction of explanatory variables from photogrammetric point clouds, which to the very best of the authors' knowledge is yet unexplored, could be to eliminate the need of a DTM by adopting a set of explanatory variables (DTM-independent variables) from the raw, non-normalized photogrammetric point cloud. Such an approach could potentially increase the area of application of UAV photogrammetric data to all forests around the world, hence release the full potential of this technology. Furthermore, these variables could eliminate the negative effects deriving from erroneously classified DTMs on the explanatory variables. The DTM-independent variables proposed in this study extend beyond the traditionally used height and density variables by extracting information not only on the vertical structure but also on the horizontal structure and spectral properties of the forest canopy. The main hypothesis is that by extracting DTM-independent explanatory variables it can be possible to provide explanatory power as by using height and density variables from normalized point clouds.

1.1. Objective

The overall objective of this study was to develop a set of DTM-independent explanatory variables and assess their usefulness when modeling the following forest biophysical forest properties: growing stock volume (V; m^3 ha^{-1}), basal area (G; m^2 ha^{-1}), number of stems per hectare (N; ha^{-1}), Lorey's height (H_{Lor}; m), and dominant height (H_{dom}; m). The DTM-independent variables were assessed against two more traditional sets of variables: (1) height and density variables from UAV photogrammetric data normalized using an ALS DTM (denoted Image-DTM_{ALS} variables) and (2)

height and density variables extracted from normalized ALS data (denoted ALS variables). Moreover, to gain further insights in the applicability of the approach across different regions and for different forest types, the assessment of the DTM-independent variables was performed across two different study sites, namely a temperate mixed forest in Italy and a boreal forest in Norway.

2. Materials

2.1 Study areas

The study was conducted in two areas, one in central Italy (43°43'N, 11°34'E) and one in southeastern Norway (59°30'N, 10°55'E) (Figure 1).

The Italian study area is located in the Biogenetic reserve of Vallombrosa, municipality of Reggello (Florence Province) and has an area of 115 ha. The area is characterized by steep slopes (mean slope = 37%) and large altitude differences (1042 – 1434 m above sea level). The forest is a mixed temperate forest dominated by European beech (*Fagus sylvatica* L.) and Silver fir (*Abies alba* M.). Other tree species include Common ash (*Fraxinus excelsior* L.), Turkey oak (*Quercus cerris* L.), Downy oak (*Quercus pubescens* L.), European hop-hornbeam (*Ostrya carpinifolia* Scop.), and Douglas fir (*Pseudotsuga menziesii (Mirb.) Franco*).

The Norwegian study area is located in Våler municipality and has an area of 194 ha. The forest is a boreal forest dominated by Norway spruce (*Picea abies* (L.) Karst.), Scots pine (*Pinus sylvestris* L.), and deciduous trees dominated by birch (*Betula pubescens* Ehrh.). The forest area in Norway is characterized by a gentler terrain, with mean slope = 6% and smaller differences in altitude (70–129 m above sea level) compared to the Italian site.

2.2 Field data

In Italy field measurements consisted in a total of 30 circular fixed-area sample plots (530 m^2) measured in June 2015. The plots were located on the basis of a tessellation stratified sampling scheme (Barabesi and Franceschi, 2011) based on a hexagonal grid with 1 ha hexagons.

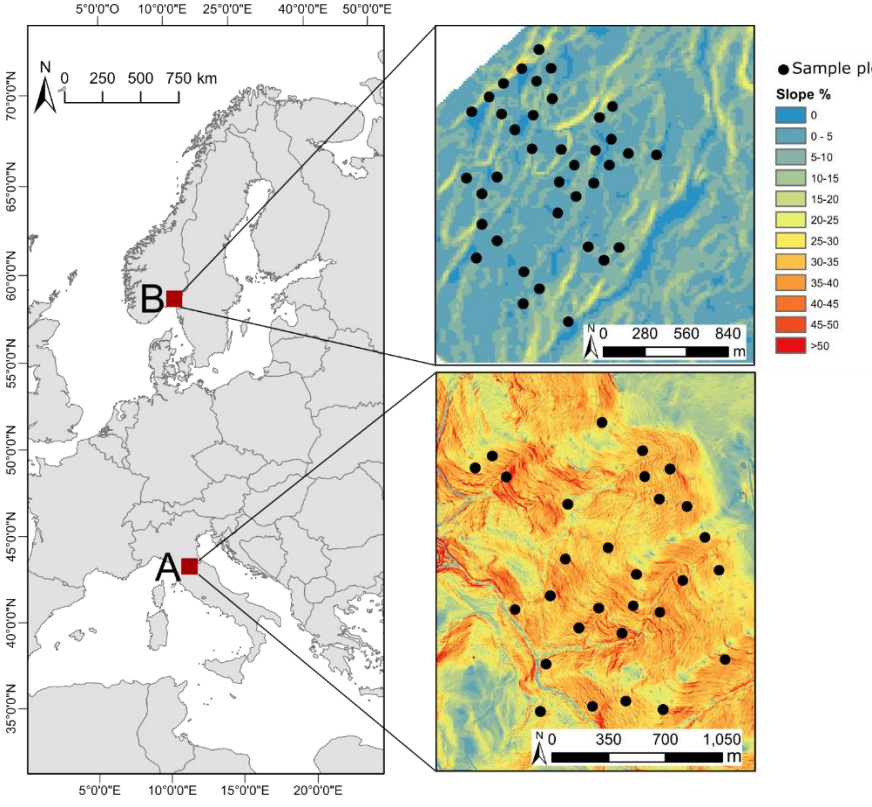

Figure 1: on the left, map of Europe with the location of the two study areas: (A) mixed temperate forest (Italy) and (B) boreal forest (Norway). On the right, the two forest sites are shown; black dots correspond to field plots. Slope maps are displayed in the background.

The plot data were collected by measuring the DBH of all trees with a DBH ≥4 cm. All callipered trees were measured for height using a Vertex

hypsometer in both areas. The errors that can be expected in the height measurements are in the order of 2%–5% of the tree height (Daamen, 1980; Eriksson, 1970). The volume of each tree was predicted using the models developed in the framework of the 2nd Italian National Forest Inventory that predict the growing stock volume of a tree using tree DBH and tree height as independent variables (Tabacchi et al., 2011). In table 1, the field reference values of the analyzed biophysical proprieties are summarized.

The center point positions of the sample plots were measured using global navigation satellite system (GNSS) receivers. A Trimble Juno 3 B Handheld receiver observing the pseudorange of both Global Positioning System (GPS) and Global Navigation Satellite System (GLONASS) was used. Data collection for each plot lasted for approximately 50 minutes with a 2-sec logging rate. The post-processed center coordinates revealed standard deviations for northing and easting ranging between 1.5 m and 3 m.

In Norway, field measurements consisted in a total of 38 circular fixed-area sample plots (400 m^2). The plot data were collected by measuring the DBH all trees with a DBH ≥4 cm. Sample trees for height measurements were selected based on a probability proportional to stem basal area. The sample trees height were measured using a Vertex hypsometer. The heights were predicted for the trees without height measurements using the height-DBH models devised by Fitje and Vestjordet (1977) and Vestjordet (1968). Heights were predicted for all trees using models dependent on DBH (Fitj and Vestjordet, 1977; Vestjordet, 1968), so that a volume could be obtained for each tree using species-specific volume models dependent on DBH and height (Braastad, 1966; Brantseg, 1967; Vestjordet, 1967). For height sample trees, volume estimates were also obtained using the observed height and DBH and the same volume models as indicated above. For each height sample tree, a ratio between volume estimate obtained

using observed height and volume estimate obtained using predicted height was then calculated. Plot- and species-specific mean ratios were used to correct the volume estimates to obtain single-tree volume estimates on each plot. The center point positions of the sample plots were measured using GNSS receivers. A Topcon Legacy-E+ 40 channel dual-frequency receiver observing the pseudorange and carrier phase of both GPS and GLONASS was used. Data collection lasted for approximately 40-50 min for each point with a 2-sec logging rate. Back in the office, the recorded GNSS data were post-processed with correction data from a base station into submeter precision.

In table 1, the field reference values of the analyzed biophysical proprieties are summarized.

Table 1: summary of the field data.

Biophysical forest properties	Study Area	Range	Mean
V (m^3 ha^{-1})	Italy	154.2–1013.2	602.8
	Norway	136.6–580.9	256.1
G (m^2 ha^{-1})	Italy	13.0–99.0	58.9
	Norway	19.6–43.8	29.2
N (ha^{-1})	Italy	546–3449	1257
	Norway	350–3625	1372
H_{Lor} (m)	Italy	9.2–27.3	19.6
	Norway	6.7–17.1	11.4
H_{dom} (m)	Italy	11.2–39.0	24.8
	Norway	13.1–28.4	19.8

2.3 Remotely sensed data

2.3.1 UAV photogrammetric data

In the present study, two SenseFly eBee Ag fixed-wing UAV were used for the image acquisition in both study areas. Prior to the UAV acquisition, 12 ground control points (GCPs) were marked in each area using 50 × 50 cm targets. The GCPs were measured using GNSS

measurements performed using a Trimble Geo 7X receiver in Italy and a Topcon Legacy-E+ 40 channel receiver in Norway. Data collection lasted for approximately 15 min for each GCP with a 2-sec logging rate. The post-processed GCP coordinates revealed standard deviations for northing, easting, and height of 0.8 cm, 0.6 cm, and 1.8 cm, respectively, in Italy and 0.7 cm, 0.5 cm, and 1.4 cm in Norway. The GCPs were later used to ensure accurate geometry and positioning of the photogrammetric point clouds.

UAV images in Italy were collected in June 2015 under good conditions with sunny weather and wind speeds <1 m/s. The flight altitude was set to 150 m above ground level and the images were acquired using a Canon ELPH 110 HS RGB camera (16.1 MP). The overlap was set to 85% longitudinal and 75% lateral. The quality of images acquired in Italy were good without any problems related to light and atmospheric conditions, saturation, or blurriness.

UAV images in Norway were collected between November and December 2014. The flight altitude was set to 120 m above ground level and the images were acquired by Canon S110 near infra-red (NIR) camera (12 MP). The overlap was set to 90% longitudinal, 80% lateral, and in addition perpendicular flight lines were flown. In this area, several factors affected the image quality, such as different light and atmospheric conditions in different flights, saturation, blurriness, the presence of snow on part of the canopy, and presence of snowflakes and/or fog in parts of the images. Table 2 summarizes the flight and image parameters.

Table 2: parameters used during the UAV image acquisitions in the two study areas.

	Italy	Norway
Study area	115 ha	194 ha

Area covered by flight	198 ha	242 ha
Number of flights	2	15
Flight altitude above ground level	150 m	120 m
Camera	Canon S110 RGB	Canon S110 NIR
R	660 nm	625 nm
G	520 nm	550 nm
B	450 nm	-
NIR	-	850 nm
Forward overlap	80%	90%
Side overlap	75%	85%
Number of images acquired	228	3250
Focal length	4 mm	5 mm
ISO Sensibility	ISO-1000	ISO-1600
Shutter speed	1/2000 sec	1/2000 sec
Image dimension	4608 x 3456	4000 x 3000
Field of view	200 x 150 m	168 × 126 m
Estimated ground sampling distance	0.050 m	0.042 m

The UAV images were processed using the Agisoft PhotoScan (Agisoft LLC, 2017) to create a 3D point cloud. Agisoft Photoscan combines SfM and photogrammetric stereo-matching algorithms for 3D reconstruction from unordered but overlapping imagery. This software was chosen because it was previously found to be suitable for forest inventory applications (Dandois and Ellis, 2013; Kachamba et al., 2016; Puliti et al., 2017a, 2017b, 2015a). For a detailed description of the different processing steps and parameters used to generate photogrammetric point clouds from UAV imagery, we refer to Puliti et al. (2015).

The output point clouds had a point density of 44.3 points/m^2 in Italy and 72.5 points/m^2 in Norway. In addition to *x*, *y*, and *z* coordinates for each point, *intensity* (see figure 2), Red (*R*), Green (*G*), Blue (*B*) (in Italy), and *G, R* and Near Infrared *(NIR)* (in Norway) values were recorded. The *intensity* values were calculated based on proprietary image-matching algorithms

implemented in Agisoft Photoscan. According to personal communication with Photoscan support (Pasumansky, 2017)) the *intensity* value is calculate according the equation:

$$intensity = 0.2 \times B1 + 0.72 \times B2 + 0.07 \times B3 \quad (1)$$

where *B1*, *B2* and *B3* are the color channels used to generate the point, in our case, *R*, *G*, *B* in Italy and *G*, *R*, *NIR* in Norway, respectively.

2.3.2 Airborne laser scanning data

The ALS data in Italy were derived from a leaf-on acquisition (10 points m^{-2}). ALS data were acquired in May 2015 using a RIEGL LMS-Q680i sensor. In Norway, the ALS data were acquired from a leaf-on acquisition (2 points m^{-2}) in November 2015 using a Leica ALS70 HM sensor.

The ALS data were pre-processed and classified in ground/non-ground echoes by the contractors GeoCart spa and Terratec As in Italy and Norway, respectively.

In addition, a triangulated irregular network (TIN) surface was created by linear interpolation from the ground-classified points (Axelsson, 2000) to construct high resolution ALS DTMs (DTM_{ALS}).

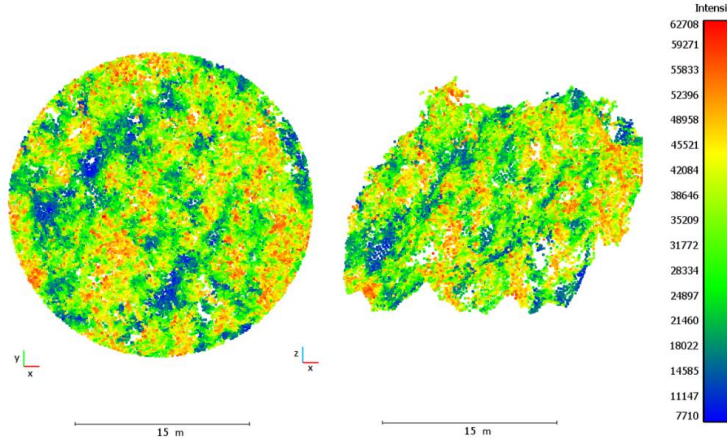

Figure 2: example of point cloud with intensity values clipped with a field plot in the Italian study area. On the right it is show the planimetric view and on the left the vertical view of the plot point cloud.

3. Methods

3.1 Extraction of explanatory variables

Three different sets of explanatory variables were extracted from the point clouds associated with each field plot, namely DTM-independent, Image-DTM_{ALS}, and ALS variables. While the first one was extracted from non-normalized point clouds, the latter two were extracted from normalized point clouds using a DTM_{ALS} as ground elevation reference and were used as benchmark. In the following sections, a detailed description of the three sets of variables is provided with particular detail on the innovative DTM-independent variables.

3.1.1 DTM-independent variables

A total of 163 DTM-independent explanatory variables were computed either directly from the point cloud (n= 148) or at pixel level using a rasterized digital surface model (DSM) (n= 15).

The point cloud DTM-independent variables were computed directly from the points' *z*, *intensity*, *R*, *G*, *B*, *NIR* values. These included variables related to the *z* and *intensity* distributions and combinations of the two. Some variables related to *z* were computed on the basis of standardized *z* (z_{st}) values. The z_{st} was computed for each point as:

$$z_{st} = \frac{z_i - \bar{z}_p}{\sigma\, z_p} \qquad (2)$$

where z_i is the *z* coordinate of the point, $\bar{z}_p$ is the average value of *z* in the plot and $\sigma\, z_p$ is the standard deviation of *z* in the plot.

Furthermore, spectral variables from the bands available in the UAV imagery were extracted as mean and standard deviation for the values of each individual band. The description of the point cloud DTM-independent variables is provided in table 3.

Table 3: summary of the point cloud DTM-independent explanatory variables.

Explanatory variables	Description
sd_z	*z* standard deviation
kur_z	*z* kurtosis (Davies and Goldsmith, 1984; McGaughey, 2014)
ske_z	*z* skewness (Davies and Goldsmith, 1984; McGaughey, 2014)
AAD_z	*z* median absolute deviation (McGaughey, 2014)
range_z	Difference between maximum and minimum *z* values
entropy	*z* normalized Shannon diversity index (*entropy*) (Pretzsch, 2009; Shannon, 1948)
z_d1, z_d2,..., z_d9, z_d10	*z* density variables defined as tenths of the distance between the 100th percentile and the lowest *z* value.
z_{st}*_sum*	Sum of z_{st} values
z_p1, z_p2, ..., z_ p95, z_p100	Percentile of 10, 20, 30, 50, 60, 70, 80, 90, 95, 100 z_{st} distribution
max_i	*Intensity* maximum value

min_i	*Intensity* minimum value
Explanatory variables	**Description**
avg_i	*Intensity* average value
sd_i	*Intensity* standard deviation
kur_i	*Intensity* kurtosis (Davies and Goldsmith, 1984; McGaughey, 2014)
ske_i	*Intensity* skewness (Davies and Goldsmith, 1984; McGaughey, 2014)
AAD_i	*Intensity* median absolute deviation (McGaughey, 2014)
range_i	Difference between maximum and minimum *Intensity* values
entropy_i	*Intensity* normalized Shannon diversity index (*entropy*) (Pretzsch, 2009; Shannon, 1948)
i_quart_1; i_quart_2; i_quart_3;i_quart_4	Quartile of 25, 50, 75, 100 intensity distribution
i_d1, i_d2, i_d3, i_d4	*Intensity* density calculated for equally intensity layers, defined as quarters of the distance between the 100th percentile and the lowest intensity value.
i_1q_p1,……, i_1q_p100	*z* percentiles of 1st intensity quartiles
i_1_p50/p25	Ratio between *i_1q_p50/i_1q_p25*
i_2q_p1,……, i_2q_p100	*z* percentiles of 2nd intensity quartiles
i_2_p50/p25	Ratio between *i_2q_p50/i_2q_p25*
i_3q_p1,……, i_3q_p100	*z* percentiles of 3rd intensity quartiles
i_3_p50/p25	Ratio between *i_3q_p50/i_3q_p25*
i_4q_p1,……, i_4q_p100	*z* percentiles of 4th intensity quartiles
i_4_p50/p25	Ratio between *i_4q_p50/i_4q_p25*
i_1q_d1,……, i_1q_d10	*z* density variables of 1st intensity quartiles
i_2q_d1,……, i_2q_d10	*z* density variables of 2nd intensity quartiles
i_3q_d1,…, i_3q_d10	*z* density variables of 3rd intensity quartiles
i_4q_d1,…, i_4q_d10	*z* density variables of 4th intensity quartiles
mean_R, mean_G, mean_B, mean_NIR	Mean value of *R*, *G*, *B* and *NIR* bands
min_R, min_G, min_B, min_NIR	Minimum value of *R*, *G*, *B* and *NIR* bands
max_R, max_G, max_B, max_NIR	Maximum value of *R*, *G*, *B* and *NIR* bands
sd_R, sd_G, sd_B, sd_NIR	Standard deviation of *R*, *G*, *B* and *NIR* bands

Furthermore, raster DTM-independent variables were extracted from the rasterized DSM. Given the bi-dimensionality of raster data, these variables were used to describe horizontal properties of the forest canopy. In a first step of the calculation of these variables the photogrammetric point cloud was rasterized. In order to avoid data gaps (i.e., pixels where no photogrammetric points were available) and in accordance with previous

findings by Niemi and Vauhkonen (2016) the resolution of the raster was set to 0.5 m x 0.5 m. The height value assigned to these pixels were calculated as the maximum *z* value of the points within the pixel area. Additionally, a gaussian smoothing filter of 1 m was applied to the DSM to further reduce no-data gaps (Pyysalo and Hyyppä, 2002) and noise in the data.

The raster DTM-independent explanatory variables were subdivided into (i) textural variables (Haralick et al., 1973) and (ii) local maxima count. Textural variables were computed using the GLCM package in R (Zvoleff, 2015) using a window size of 3 pixels × 3 pixels and in all directions. The algorithm examines image textures by calculating how often pairs of pixels with specific values and in a specified spatial relationship occur in an image (Lu and Batistella, 2005). From the GLCM package seven raster maps (see figure 3) were produced for each field plot describing the following textural variables: *mean*, *variance*, *homogeneity, contrast*, *dissimilarity*, *entropy,* and *second moment* (Haralick et al., 1973). These raster values were then used to compute plot level *average* and the *standard deviation* (table 4), resulting in a total of 14 textural variables.

The number of local maxima (*num_max*) was computed with a search window size of 3 pixels × 3 pixels and the number of local maxima was used as a variable (see figure 3). Such a variable was derived to describe the number of dominant trees in the plot. The use of local maxima counting has been widely documented in single-tree detection approaches (Solberg et al., 2006) however its use in the area-based approach is a novelty of the current study. A summary of the DTM-independent image explanatory variables is provided in table 4, while figure 3 shows the raster DTM-independent explanatory variables calculate for a single plot in the Italian study area.

Table 4: summary of the raster DTM-independent explanatory variables.

Explanatory variables	Description
AVG_mean	Average of GLCM *mean* textural (Haralick et al., 1973)
SD_mean	Standard deviation of GLCM *mean* textural (Haralick et al., 1973)
AVG_variance	Average of GLCM *variance* textural (Haralick et al., 1973)
SD_variance	Standard deviation of GLCM *variance* textural (Haralick et al., 1973)
AVG_ homogeneity	Average of GLCM *homogeneity* textural (Haralick et al., 1973)
SD_ homogeneity	Standard deviation of GLCM *homogeneity* textural (Haralick et al., 1973)
AVG_ contrast	Average of GLCM *contrast* textural (Haralick et al., 1973)
SD_ contrast	Standard deviation of GLCM *contrast* textural (Haralick et al., 1973)
AVG_ dissimilarity	Average of GLCM *dissimilarity* textural (Haralick et al., 1973)
SD_ dissimilarity	Standard deviation of GLCM *dissimilarity* textural (Haralick et al., 1973)
AVG_ entropy	Average of GLCM *entropy* textural (Haralick et al., 1973)
SD_ entropy	Standard deviation of GLCM *entropy* textural (Haralick et al., 1973)
AVG_ second moment	Average of GLCM *second moment* textural (Haralick et al., 1973)
SD_ second moment	Standard deviation of GLCM *second moment* textural (Haralick et al., 1973)
num_max	Number of local maxima

3.1.2 Image-DTMALS and ALS variables

Explanatory variables were extracted from the normalized UAV photogrammetric point cloud using the DTM_{ALS} (Image-DTM_{ALS} variables) and from the normalized ALS data (ALS variables). Identical variables were derived for the UAV photogrammetric point clouds and the ALS point clouds. For each plot, we calculated 28 point cloud variables (Table 5) typically used in forest inventories. These included base statistical variables (Laes et al., 2011; McGaughey, 2014), height, density variables (Næsset et al., 2004). The base statistical variables are: total number of points (*tot*),

sum of the heights (*sum*), mean height (*avg*), height standard deviation (*sd*), skewness of height (*sk*), kurtosis of height (*kur*), and average square height (*qav*)(Laes et al., 2011; McGaughey, 2014). The

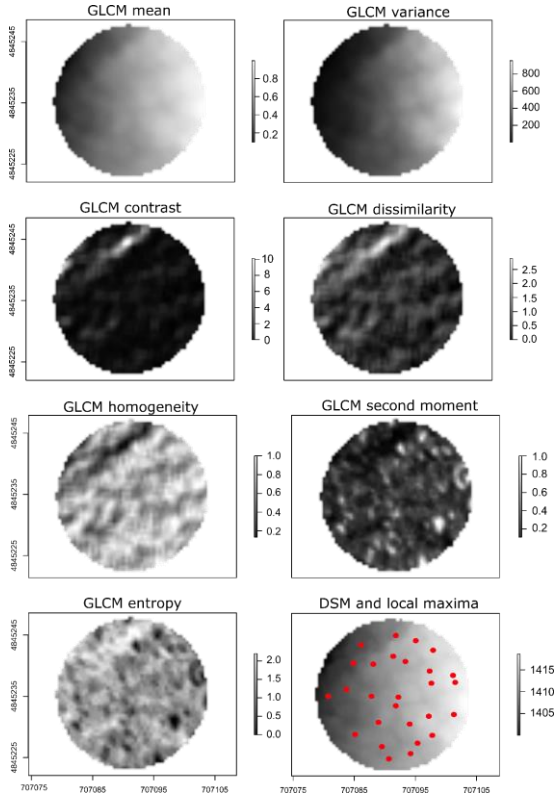

Figure 3: example of raster DTM-independent explanatory variables calculated for a field plot in the Italian study area.

height variables are: height percentiles (*p10, …, p100*) calculate between the 100th percentile and a minimum threshold of 1.3 m.The density variables were calculated for equally spaced vertical layers, defined as tenths of the distance between the 95th percentile and the lowest canopy height (i.e. 1.3 m). The densities were computed as the proportion of points

above the 1st,…,9th (d0,…,d9) spaced vertical layer to the total number of points.

Table 5: Image-DTM_{ALS} and ALS explanatory variables

Explanatory variable	Description
tot	Total number of points
sum	Sum of height
avg	Average height
sd	Height standard deviation
sk	Skewness of height (Davies and Goldsmith, 1984; McGaughey, 2014)
kur	Kurtosis of height (Davies and Goldsmith, 1984; McGaughey, 2014)
qav	Average of the square height (McGaughey, 2014)
p1, p2, …, p95, p100	Percentile of 10, 20, 30, 50, 60, 70, 80, 90, 95, 100 of height distribution
d0, d1,….,d8,d9	Proportion of points above 1.3 m and the 1st,…,9th spaced vertical layer to the total number of points

3.2 Regression models

Multivariate linear regression models were fitted using the forest biophysical properties of interest as response variables and separately the three different sets of remote sensed variables as explanatory variables, namely (i) DTM-independent variables, (ii) Image-DTM_{ALS} variables, and (iii) ALS variables.

A stepwise algorithm was used for variable selection. To avoid poor performance of stepwise variable selection when explanatory variables are highly correlated (Harrell, 2001; p. 64–65), correlation analyses were performed using Pearson's product moment correlation (r) matrix. In case of two variables with $r > 0.85$, only the ones with the lower correlation with other variables were considered as candidate variables in the subsequent modeling. The stepwise algorithm was set to find models with one to five

explenatory variables that produced the greatest *Adj. R^2* by searching for the best combination among the variables that were not mutually correlated. The sum of squared errors of the models with one to five predictor variables were compared using an F-test to keep the most statistically significant model with the fewest number of predictor variables. The explanatory variables with a significance value of partial F statistic >0.05 (Næsset, 2002) were removed.

Furthermore, the assumptions of linearity, homoscedasticity, and independence of the residuals of the models were assessed by a Kolmogorov-Smirnof test (George, 1983), a Breusch-Pagan test (Breusch and Pagan, 1979), and Durbin-Watson test (Durbin and Watson, 1950), respectively.

3.3 Accuracy assessment

The performance of the different sets of explanatory variables (i.e., DTM-independent, Image-DTM_{ALS}, and ALS) in the two different study sites (i.e., Italy and Norway) was evaluated using leave-one-out cross validation (LOOCV) by means of adjusted R^2 (*Adj. R^2*), mean difference (*MD*), root mean square error (*RMSE*), relative mean difference ($MD_{\%}$), and relative root mean square error ($RMSE_{\%}$),The *MD and RMSE* were calculated as:

$$MD = \frac{\sum_{i=1}^{n}(\hat{y}_i - y_i)}{n} \quad (3)$$

$$RMSE = \sqrt{\frac{\sum_{i=1}^{n}(\hat{y}_i - y_i)^2}{n}} \quad (4)$$

where $\hat{y}_i$ and y_i are the predicted and ground reference values for the *i-th s*ample plot, and *n* is the number of plots. The $MD_{\%}$ and relative $RMSE_{\%}$ were calculated as the percentage of the average ground reference value of the modeled forest biophysical proprieties.

Furthermore, for the sake of comparison between the three different sets of variables, the average $RMSE_{\%}$ ($\overline{RMSE_{\%}}$) was computed as the average between the $RMSE_{\%}$ obtained for all of the studied forest biophysical properties in both study areas.

4. Results

4.1 Variable selection

4.1.1 DTM-independent

The results of the variable selection for the DTM-independent variables are reported in table 6. The number of explanatory variables selected with the stepwise algorithm ranged between three and four and the absolute value of the Pearson correlation coefficient ranged between 0.01 and 0.71 with an average of 0.3 (Table 6).

When considering both study areas and all models, the point cloud variables were selected 74% of the times while the raster variables were selected 26% of the times. When analyzing the different sub-categories of variables, the *intensity* variables were the most selected (21 % of the times) followed by the *intensity-z* variables (19% of the times), the *R, G, B* and *NIR* variables (17% of the times), the *z* variables (14% of the times), the textural variables (14% of the times), the local maxima variable (12% of the times), and the *z_st* variables (2% of the times).

When looking at single variables, the most frequently selected variable was *num_max* (five times) as it was selected in both study areas for the *G* model and for the *V,* H_{Lor} *, and* H_{dom} models in Italy. The textural *AVG_homogeneity* was the second most selected variable (four times) and was used to model *V*, *G*, and H_{dom} in Italy and *N* in Norway.

With respect to each individual study area, the raster variables were the most frequently selected in Italy (52% of the times) while the point cloud variables were most frequently selected in Norway (86% of the times). In Italy, the most selected variables were *num_max* (21% of the

times) and *AVG_homogeneity* (16% of the times), followed by the sub-category of *intensity* variables (21% of the times). In Norway, the most selected variables were *R*, *G*, *B*, and *NIR* (26% of the times), follow by the sub-category of *z* and *intensity* variables (both selected 23% of the times).

In Italy, the combination of *num_max* and *AVG_homogeneity* was used to model three different forest biophysical variables, i.e., *V*, *G*, and H_{dom}, and in addition, also *i_4q_p95* was selected in the models for *V* and H_{dom}. In Norway, the combination of *i_min* and *max_G* was selected to model both the height forest variables (H_{Lor} and H_{dom}).

4.1.2 Image-DTM$_{ALS}$ and ALS variables

The results of the variable selection for the Image-DTM$_{ALS}$ variables and ALS variables are reported in tables 7 and 8, respectively. The number of explanatory variables selected with the stepwise algorithm ranged between one and three for the Image-DTM$_{ALS}$ and one and two for ALS. The absolute values of the Pearson correlation coefficients were in the ranges 0.02–0.95 (average = 0.47) and 0.02–0.90 (average = 0.63) for Image-DTM$_{ALS}$ and ALS, respectively (Table 7 and Table 8).

When Image-DTM$_{ALS}$ variables were used to model forest biophysical properties, the base statistical variables were selected 61% of the times followed by height percentiles (22% of the times) and densities variables (16% of the times). The most selected variable was *avg*, selected four times, to model *G* in both study areas and in Norway also for *N* and H_{Lor}. The density variables were selected only in Italy while the percentiles were selected three times in Italy and two times in Norway.

The most selected ALS variables were the percentiles (selected 66% of the times) followed by base statistical variables (33% of the times) while the densities variables were never selected. The most selected variable was *p50*, which was selected two times in Italy to model *V* and H_{dom} and one time in Norway to model *G*.

Table 6: summary of the variables selected by the stepwise algorithm from the models using DTM-independent variables. The Pearson correlation coefficient between the biophysical variables and the selected DTM-explanatory variables (point cloud and DSM) is reported. Results of the LOOCV are reported in terms RMSE.

			Biophysical forest proprieties									
			V (m^3ha^{-1})		*G* (m^2ha^{-1})		*N* (ha^{-1})		H_{Lor} (m)		H_{Dom} (m)	
DTM-independent variables			ITA	NOR	ITA	NOR	ITA	NOR	ITA	NOR	ITA	NOR
Point cloud	*z*	*entropy_z*										-0.23
		z_sd			0.19			-0.57				
		z_d4								-0.10		
		z_d9		0.13								
		z_d6				-0.01						
		z_d7										
	z_{st}	z_{st}_*sum*					-0.42					
	intensity	*i_min*				-0.59				-0.57		-0.71
		i_ske							0.41			
		i_renge										
		i_quart_1	-0.18				0.52					
		i_quart_2								-0.49		
		i_quart_4						0.42				
		i_d2					-0.31					
	intensity-z	*i_1_p50/p25*								0.42		
		i_1q_d5		-0.06								
		i_2q_d7		-0.30								
		i_4q_p95	-0.30								-0.29	
		i_1q_d5				-0.19						
		i_1q_d8										
		i_2q_d10							-0.15			
		i_4q_d10			-0.40							
	R, G, B, NIR	*max_G*								-0.39		0.14
		mean_G		-0.57								
		min_B							0.15			
		max_NIR		0.40								-0.32
		sd_NIR				0.63						
DSM	*Local Max*	*num_max*	-0.46		-0.31	0.25			-0.35		0.36	
	Textural metrics	*AVG_homogeneity*	-0.10					-0.07	-0.20		-0.20	
		AVG_dissimilarity										0.07
		SD_dissimilarity									-0.18	
Results		*RMSE*	96.2	49.3	7.6	4.6	469	559	3.1	1.6	3.4	2.1

Table 7: summary of the variables selected by the stepwise algorithm from the models using Image-DTM_{ALS} variables. The Pearson correlation coefficient between the biophysical variables and the selected DTM-explanatory variables (point cloud and DSM) is reported. Results of the LOOCV are reported in terms RMSE

		Biophysical forest proprieties									
		V (m^3ha^{-1})		*G* (m^2ha^{-1})		*N* (ha^{-1})		H_{Lor} (*m*)		H_{dom} (*m*)	
Image-DTM_{ALS} variables		ITA	NOR	ITA	NOR	ITA	NOR	ITA	NOR	ITA	NOR
Base											
statistical	*avg*			-0.16	0.71		-0.33		0.73		
	sum					-0.50					
	sd			-0.24						0.21	
	ske	-0.16						-0.25			
	qav		0.91								
Percentiles	*p10*								-0.02		
	p40			0.64							
	p50										
	p60							0.85			
	p90										0.95
	p95	0.84									
	p100									0.67	
Densities	*d5*					0.13					
	d7									0.36	
	d10	-0.26									
Results	*RMSE*	94.2	41.8	6.4	4.8	547	653	2.8	1.7	3.1	1.0

Table 8: summary of the variables selected by the stepwise algorithm from the models using ALS variables. The Pearson correlation coefficient between the biophysical variables and the selected DTM-explanatory variables (point cloud and DSM) is reported. Results of the LOOCV are reported in terms RMSE

		Biophysical forest proprieties									
		V (m^3ha^{-1})		*G* (m^2ha^{-1})		*N* (ha^{-1})		H_{Lor} (*m*)		H_{dom} (*m*)	
ALS variables		ITA	NOR	ITA	NOR	ITA	NOR	ITA	NOR	ITA	NOR
Base											
statistical	*avg*						-0.46		0.82		
	kur									0.23	
	qav		0.74								
Percentiles	*p10*			0.74			-0.02				
	p25										
	p50	0.90			0.70					0.81	
	p75							0.86			
	p90										0.77
	p95					-0.51					
Results	*RMSE*	101.0	46.0	9.4	4.48	679	628	3.01	1.52	3.5	1.0

4.2 Accuracy assessment

The fitted models using DTM-independent variables showed a rather good fit with an *Adj.* R^2 ranging between 0.51 and 0.79. Similar ranges in *Adj.* R^2 were found for models using Image-DTM_{ALS} (0.31–0.91) or ALS variables (0.24–0.91) (Figure 4). Among the three sets of variables, the DTM-independent variables resulted in consistently larger *Adj.* R^2 for *G*

(Italy = 0.76; Norway = 0.57) and *N* (Italy = 0.60; Norway = 0.51) across study sites (see figure 4). For the other studied forest biophysical properties, Image-DTM_{ALS} and ALS models yielded similar or better model fit compared to DTM-independent variables.

The LOOCV of the selected models revealed that the differences in predictive accuracy in terms of $RMSE_{\%}$ (see Figure 4) between DTM-independent and ALS models considering both study areas were limited to -0.7% – 1.3%, -3.6% – -0.7%, and 0.56% – 1.2% for *V*, *G*, and H_{Lor}, respectively. A similar trend was observed when comparing the predictive accuracy of models using DTM-independent against Image-DTM_{ALS} for *V*, *G*, and H_{Lor}. Furthermore, the results showed that when DTM-independent variables were used rather Image-DTM_{ALS} and ALS, *N* was predicted with smaller $RMSE_{\%}$ consistently across study sites with reductions in $RMSE_{\%}$ compared to ALS in the range of 5.1% – 16.8%. For H_{dom}, the results were not consistent between study sites as the $RMSE_{\%}$ found for DTM-independent models was similar to what found for ALS in Italy, while it was 5.5% larger than ALS in Norway. The $\overline{RMSE}_{\%}$ found using DTM-independent variables, was slightly smaller (19.6%) compared to the ones found when using Image-DTM_{ALS} (19.7%) and ALS (21.6%). In Italy, the DTM-independent ($\overline{RMSE}_{\%}$ = 19.1%) and Image-DTM_{ALS} ($\overline{RMSE}_{\%}$ = 19.4%) revealed a slight increase in predictive accuracy compared to ALS ($\overline{RMSE}_{\%}$ = 23.2%), while in Norway, ALS variables resulted in the slightly smaller $\overline{RMSE}_{\%}$ (19.8%) compared to DTM-independent (20.2%) and Image-DTM_{ALS} variables (20.7%).

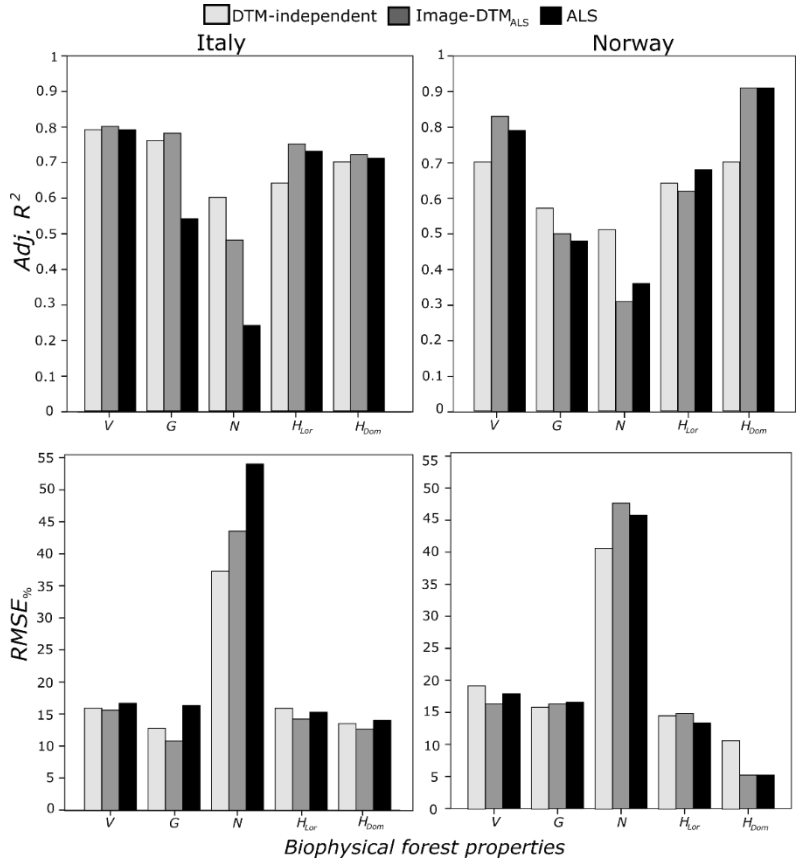

Figure 4: Bar plots of *Adj.* R^2 and $RMSE_{\%}$ for the two different study areas, for each of the forest biophysical properties, and the different sets of variables.

The LOOCV of all the selected models revealed small MD values, which in all cases had an absolute value ≤ 1.5% of the mean field reference value. Furthermore, the MD values were never statistically significant with *p-values* for the two-sided *t-test* always ≥ 0.90.

The analysis of the residuals revealed no violation of the assumptions of linearity, normality of the residuals, homoscedasticity, and independence for any of the models. The NCV test, the Kolmogorov-

Smirnov and the Durbin-Watson test always resulted in *p-values* > 0.05. The visual analysis of the scatterplot of the field reference against the LOOCV predicted values (see Figure 5) confirmed the results of the previously mentioned tests. Furthermore, it was possible to observe that the effect of under-prediction of large values was reduced when adopting DTM-independent variables, especially in the case of *V* and *N*.

5. Discussion

The current study introduced a new set of DTM-independent explanatory variables computed from raw, non-normalized UAV photogrammetric data and assessed their use in modeling of biophysical forest properties across two different forest types, namely mixed temperate forests in Italy and boreal forests in Norway. The novelty of these DTM-independent variables is that they allow the use of UAV photogrammetric data without the need of any terrain information. To the authors' knowledge, the present study is the first to utilize raw photogrammetric data to model forest biophysical properties without relying on any DTM for normalization. Thus, the current discussion is mainly focused on the assessing the proposed DTM-independent variables in relation to benchmark methods that are already widely applied (i.e., Image-DTM_{ALS} and ALS).

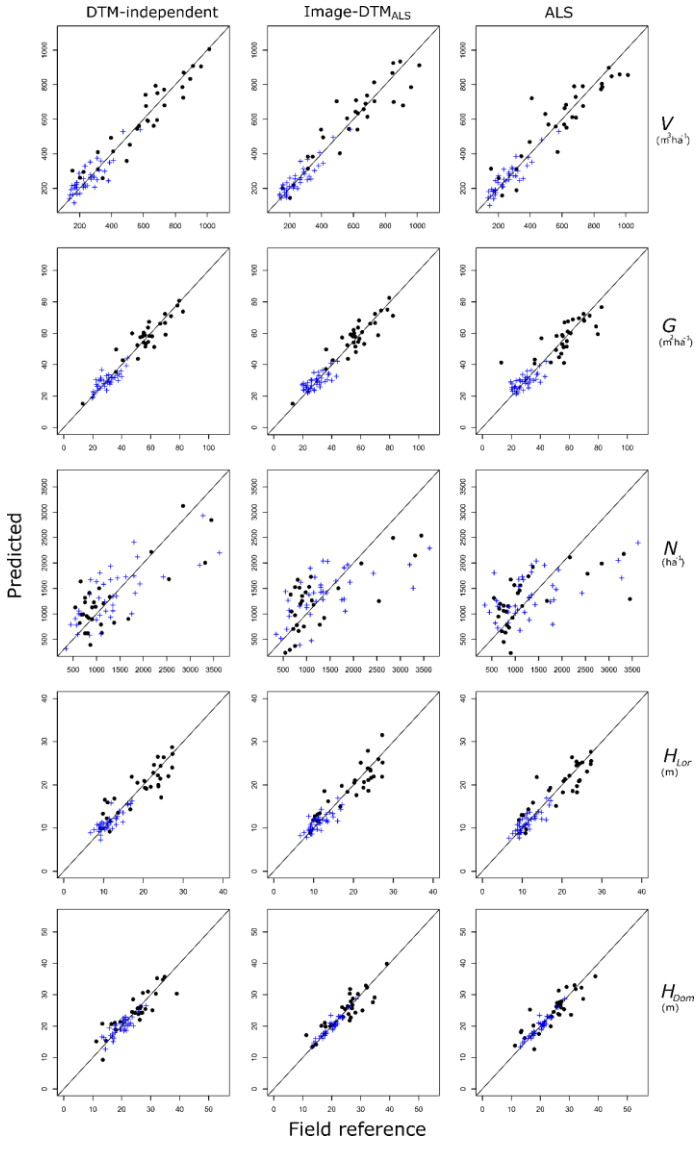

Figure 5: Scatterplot of field reference versus predicted values from the LOOCV for the models with different types of explanatory variables: DTM-independent, Image-DTMALS, and ALS. Black dots represent the observations from the Italian area while the blue crosses represent the Norwegian observations. The black line is the 1:1 line.

5.1. DTM-independent variables

A large number of DTM-independent explanatory variables were extracted from the raw UAV photogrammetric data. The number of DTM-independent variables selected in the models was generally larger (3–5) than for Image-DTM_{ALS} (1–3) and ALS (1–2). As shown by the smaller average Pearson's correlation coefficient found between DTM-independent variables (0.30) compared to Image-DTM_{ALS} (0.47) and ALS (0.63), DTM-independent variables were individually less correlated with the studied biophysical forest properties. Nevertheless, the multiple sources of information (z, intensity, spectral, textural, and local maxima) used for the extraction of the DTM-independent resulted in less inter-correlated explanatory variables compared to solely using height percentiles and density variables. In addition to the description of the vertical structure of the canopy provided by height and density variables, DTM-independent variables include also information regarding the horizontal structure and spectral properties of the forest. Thus, the extraction of a large number (i.e., 163) of fairly uncorrelated DTM-independent variables enabled an explanatory power (average *Adj.* R^2 = 0.65) compared to traditional explanatory variables from Image-DTM_{ALS} (average *Adj.* R^2 = 0.67) and ALS (average *Adj.* R^2 = 0.62).

The analysis of the single DTM-independent variables selected in the models demonstrated the relevance of *intensity* and *intensity-z* variables. These variables were the most frequently selected in the models using DTM-independent variables across the study sites and they made a significant contributions to the models' predictive ability ($p<0.01$). To the authors' knowledge, this study is the first to use the *intensity* values from photogrammetric point clouds and to highlight its importance in modelling forest biophysical properties. It is however important to note that the

intensity values are limited to data processed by SfM photogrammetry software that incorporate intensity pattern matching algorithms such as Agisoft Photoscan (Agisoft LLC, 2017) or SURE (Rothermel and Wenzel, 2012). Furthermore, the computation of *intensity* values may vary substantially between different software packages. Due to the lack of empirical experience in the use of *intensity* data further studies should investigate the signal obtained from these data more in depth.

The *R*, *G*, *B* and *NIR* variables were selected one time in Italy to predict H_{Lor} and six times in Norway for all forest biophysical variables except for *N*. These spectral variables improved the predictive accuracy of the models ($p<0.01$) especially in boreal forest site, for which large correlations with the studied biophysical proprieties were observed ($-0.57 \leq r \leq -0.32$ and $0.25 \leq r \leq 0.63$).

The present study confirms the findings by Bohlin et al. (2012) and Niemi and Vauhkonen (2016) by demonstrating that textural variables extracted from 3D remote sensing data are useful in modelling forest biophysical properties ($p<0.01$) even when calculated from a raster DSM and not from a CHM. The texture variables were selected at least one times for all the biophysical forest proprieties consistently across the two study sites, except for *G*. This result is in line with what Niemi and Vauhkonen (2016) reported. They observed a smaller $RMSE_{\%}$ for *V* when using CHM textures and ALS variables (32.6%) compared to only using ALS variables (44.4%). As pointed out by Gómez et al. (2011) and Ozdemir (2008), the resolution of the raster data from which textural information is extracted has a crucial role on the scale of the observed textural variable. In regard to the raster resolution suitable for providing valuable textural information for modelling forest biophysical properties, Niemi and Vauhkonen (2016) demonstrated a loss of textural information when increasing the resolution

beyond 0.5–1 m. Given these requirements in resolution of the 3D data input for extracting textural variables, UAV photogrammetric data is very well suited to provide fine-scale textural information due to the very high resolution of the achievable point clouds (approximately 44–72 points m^{-2} in the current study).

Furthermore, the number of local maxima, which this study pioneered as an explanatory variable in an area-based approach, emerged as the most correlated variable with the studied biophysical parameters in mixed temperate forest ($0.24 \leq r \leq -0.46$), except for *N*. In both forest types, *num_max* was selected to model *G* and in both cases the correlation was of similar magnitude (Italy: $r = -0.30$; Norway: $r = 0.25$).

The new explanatory variables are quite easy to compute also in large areas, with number of local maxima as an exception. At large scales, the derivation of this latter is computational demanding due to the high DSM resolution (0.5 m), the proposed window size (3 pixels x 3 pixels), and algorithm complexity.

5.2. Accuracy of DTM-independent models

The models fitted using the DTM-independent variables showed similar model fit and predictive accuracy compared to Image-DTM_{ALS} and ALS in both forest areas and for the variables *V*, *G*, H_{Lor} and H_{dom}. With respect to *V*, the present study showed smaller RMSE% values for the Italian study site when using ALS variables (16.0%) compared to previous study using ALS in Italy using field plots ranging in size between 314 and 1256 m^2 (Barbati et al., 2009; Bottalico et al., 2017; Corona and Fattorini, 2008; Tonolli et al., 2011), for which $RMSE_{\%}$ values typically have ranged between 16.7% and 30%. In Norway, the ALS $RMSE_{\%}$ value for *V* (17.9%) was in line with previous findings under boreal conditions in the Nordic countries

(Næsset, 2007) where values in the range 15.0-25.0% can be expected at plot level (Næsset, 2004). The models using DTM-independent revealed an $RMSE_{\%}$ value for *V* (19.2%) of similar magnitude compared to a previous study by Gobakken et al. (2014) using normalized digital aerial photogrammetry (DAP; photogrammetric data large format airborne photogrammetric cameras) (18.7%) but 4.7% larger than reported by Puliti et al. (2015) using the same data but a different approach in variables extraction and selection. The comparison of the predictive accuracy reported in the current study for *G* using DTM-independent models with previous experiences in Italian conditions revealed smaller $RMSE_{\%}$ (12.8%) compared to what Bottalico et al. (2017) reported by using ALS data (20.8%–27.6%). For Norway, the $RMSE_{\%}$ found in the current study for *G* (15.9%) was consistent with figures reported by Gobakken et al. (2014) and Puliti et al. (2015) in the same study area using either Image-DTM_{ALS} (15.38%), DAP (16.3%), or ALS data (13.1%). For the *N* model the DTM-independent variables resulted consistently in better performances in terms model fit and predictive accuracy compared to the alternative variables (i.e., Image-DTM_{ALS} and ALS). The reported $RMSE_{\%}$ values for *N* using DTM-independent variables were smaller (37.3%) compared to the ones obtained in mixed forests by Bottalico et al. (2017) using normalized ALS data (47.8%). The $RMSE_{\%}$ for *N* in the Norwegian site was in line (40.7%) with what Puliti et al. (2015) reported but larger than reported by Gobakken et al. (2015) who in similar conditions reported $RMSE_{\%}$ values of 37.5% and 31.0% using DAP and ALS, respectively. Furthermore, the present study revealed that the use of DTM-variables in boreal conditions resulted in an increase in $RMSE_{\%}$ of 5.4% compared to use of ALS variables to model height forest properties (H_{Lor} and H_{dom}). Such difference was somewhat expected as normalized ALS data directly describe tree height. On the other hand, it

was encouraging to see the small differences between the predictive accuracy for H_{Lor} and H_{dom} when using DTM-independent models against ALS variables in temperate mixed forests. The $RMSE_{\%}$ values for H_{Lor} when using DTM-independent variables in mixed temperate (15.9%) and boreal forests (14.6%) were larger than previous studies using ALS (7.0%-8.96%) (Bottalico et al., 2017; Gobakken et al., 2015; White et al., 2015), DAP (8.6%) (Gobakken et al., 2015), and UAV Image-DTM_{ALS} (8.5%) (Ullah et al., 2017). In regard to H_{dom} models using DTM-independent variables, this study found larger $RMSE_{\%}$ values than previously reported when using ALS (7.4%-8.2%) (Bottalico et al., 2017; Gobakken et al., 2015), DAP and Image-DTM_{ALS} (3.5%-8.5%) (Lisein et al., 2013; Puliti et al. 2015).

One important aspect worthwhile discussing was highlighted by the visual comparison of the LOOCV residuals for the *V* (see Figure 5), where the three largest field reference observations (i.e. V ranging between 850 and 1256 m^3 ha^{-1}) in the Italian study area were subject to under-prediction when using Image-DTM_{ALS} and ALS variables. Under-prediction of large values has often been reported in the literature (Hansen et al., 2015; Tonolli et al., 2011), especially in heterogeneous forests and forests with large timber volumes (Hansen et al., 2015). In the current study, we observed that the adoption of DTM-independent variables led to a decrease in the under-prediction of these large values (see Figure 5). It is relevant to mention that the plots corresponding to these extreme observations were characterized by dense crown cover (> 80%) and steep terrain. The combination of these two factors resulted in a reduced density of ALS ground returns (0.2 point m^2) compared to the rest of the plots (≥ 1 point m^2). As demonstrated in previous studies (Hodgson et al., 2003; Hodgson and Bresnahan, 2004; Hollaus et al., 2006; Hyyppä et al., 2005), significant errors in the DTM (i.e., up to 0.98 m) can be expected under such

conditions. In fact, explanatory variables, derived by point cloud normalized with DTM affected by small errors, can produce larger errors in the prediction of biophysical proprieties (Dandois and Ellis, 2013). In this regard, DTM-independent variables may contribute to circumvent some of the detrimental effects of DTM errors on the explanatory variables typically used to model biophysical forest properties. This finding may even indicate that extraction of DTM-independent variables may be beneficial also in cases where traditional Image-DTM_{ALS} or ALS forest inventories are carried out. This could in fact allow to benefit from the high correlation of the conventional height and density variables from normalized point clouds while possibly reducing the under-prediction of highly timbered forests by including DTM-independent variables free from DTM errors.

The DTM-independent variables produced, also, benefit for *N* models in both study area. In fact, the largest field reference observations (i.e. ranging between 2.200 and 3625 ha^{-1}) showed larger under-prediction using Image-DTM_{ALS} and ALS comparing to the use of DTM-independent variables (see Figure 5).

Overall, the comparison of our results with the available literature revealed that the results obtained by using the proposed DTM-independent approach were consistent with results for all the biophysical forest proprieties under study. What was most surprising was that the DTM-independent variables extracted from UAV photogrammetric data were able to perform as well as data from state-of-the-art technology such as ALS even under more complex forest structures like the highly timbered mixed forests in the Italian study area characterized by large canopy cover and on steep slopes. Further research should address the use of DTM variables in even more complex forest types such as tropical forest, where the use of

UAV photogrammetry can be most effective (Paneque-Gálvez et al., 2014; Puliti et al., 2017a).

5.3. General considerations

Several authors have mentioned the need for high-resolution DTMs as the main limitation of the use of 3D photogrammetric data in forest inventories (Bohlin et al., 2012; Järnstedt et al., 2012; Lisein et al., 2013; Nurminen et al., 2013; Ota et al., 2015; White et al., 2013). Nevertheless, the current study demonstrated that photogrammetric data may be used even in the absence of any terrain information.

One of the strengths of this study was the consistency of the results across two different forest types, slopes, imaging sensors, seasons, and specifications for UAV data acquisition. Despite the differences in image acquisition parameters (e.g. focal length, flying height, camera resolution, image overlap) which may have affected the results of this study, our results suggest that DTM-independent variables might be consistent also across UAV acquisition campaigns.

Furthermore, adoption of DTM-independent variables eliminates the processing steps required for DTM generation and point cloud normalization, hence increases the cost-efficiency of an inventory. On the other hand, some of the proposed variables (e.g. textural and local maxima) may be computationally intensive when applied on a large scale, thus reducing the cost-efficiency.

6. Conclusions

Overall, the results were encouraging for further research and three main conclusions can be drawn from the study:

(i) UAV photogrammetric data can be used to model forest biophysical properties even when no terrain information is available by adopting the proposed DTM-independent explanatory variables;

(ii) The prediction accuracy when using models based on DTM-independent variables was similar to that of Image-DTMALS and ALS;

(iii) The DTM-independent variables performed well even in complex forest structures such as the temperate mixed forest in Italy and under steep terrain conditions.

Acknowledgments

This research was funded in part by Accademia Italiana di Scienze Forestali in the framework of PhD Student Scholarship given to Francesca Giannetti and in part by the LIFE program in the framework of the project "FRESh LIFE—Demonstrating Remote Sensing integration in sustainable forest management" (LIFE14 ENV/IT/000414).

References

Agisoft LLC, 2017. Agisoft PhotoScan User Manual. Available online http://www.agisoft.com/pdf/photoscan-pro_1_3_en.pdf (accessed on 11 April 2017).

Arabatzis, G., 2010. Development of Greek forestry in the framework of the European Union policies. Journal of Environmental Protection and Ecology 11, 682–692.

Axelsson, P., 2000. DEM Generation from Laser Scanner Data Using adaptive TIN Models. International Archives of Photogrammetry and Remote Sensing 23, 110–117. doi:10.1016/j.isprsjprs.2005.10.005

Baltsavias, E., Gruen, a., Eisenbeiss, H., Zhang, L., Waser, L.T., 2008. High-quality image matching and automated generation of 3D tree models. International Journal of Remote Sensing 29, 1243–1259. doi:10.1080/01431160701736513

Barabesi, L., Franceschi, S., 2011. Sampling properties of spatial total estimators under tessellation stratified designs. Environmetrics 22, 271–278. doi:10.1002/env.1046

Barbati, A., Chirici, G., Corona, P., Montaghi, A., Travaglini, D., 2009. Area-based assessment of forest standing volume by field measurements and airborne laser scanner data. International Journal of Remote Sensing 30, 5177–5194. doi:10.1080/01431160903023017

Barneveld, R.J., Seeger, M., Maalen-Johansen, I., 2013. Assessment of terrestrial laser scanning technology for obtaining high-resolution DEMs of soils. Earth Surface Processes and Landforms 38, 90–94. doi:10.1002/esp.3344

Bauwens, S., Bartholomeus, H., Calders, K., Lejeune, P., 2016. Forest inventory with terrestrial LiDAR: A comparison of static and hand-held mobile laser scanning. Forests 7 (127). doi:10.3390/f7060127

Bohlin, J., Wallerman, J., Fransson, J.E.S., 2012. Forest variable estimation using photogrammetric matching of digital aerial images in combination with a high-resolution DEM. Scandinavian Journal of Forest Research 27, 692–699. doi:10.1080/02827581.2012.686625

Bohlin, J., Wllerman, J., Fransson, J.E.S., 2015. Deciduous forest mapping using change detection of multi-temporal canopy height models from aerial images acquired at leaf-on and leaf-off conditions. Scandin 7, 8–9. doi:10.1016/j.dcn.2015.01.008

Bottalico, F., Chirici, G., Giannini, R., Mele, S., Mura, M., Puxeddu, M., McRoberts, R.E., Valbuena, R., Travaglini, D., 2017. Modeling Mediterranean forest structure using airborne laser scanning data. International Journal of Applied Earth Observation and Geoinformation 57, 145–153. doi:10.1016/j.jag.2016.12.013

Braastad, H., 1966. Volume tables for birch. Meddelelser fra Det Norske Skogforsøksvesen. Norwegian with English summary 21, 23–78.

Brantseg, A., 1967. Volume functions and tables for Scots pine. South Norway. Meddelelser fra Det Norske Skogforsøksvesen. Norwegian with English summary. 22, 689–739.

Breusch, T.S., Pagan, A.R., 1979. A Simple Test for Heteroscedasticity and Random Coefficient Variation. Econometrica 47, 1287–1294.

Castillo, C., James, M.R., Redel-Macías, M.D., Pérez, R., Gómez, J. a., 2015. SF3M software: 3-D photo-reconstruction for non-expert users and its application to a gully network. Soil 1, 583–594. doi:10.5194/soil-1-583-2015

Chianucci, F., Disperati, L., Guzzi, D., Bianchini, D., Nardino, V., Lastri, C., Rindinella, A., Corona, P., 2016. Estimation of canopy attributes in beech forests using true colour digital images from a small fixed-wing UAV. International Journal of Applied Earth Observation and Geoinformation 47, 60–68. doi:10.1016/j.jag.2015.12.005

Chirici, G., Bottalico, F., Giannetti, F., Perugia, B. Del, Travaglini, D., Nocentini, S., Kutchartt, E., Marchi, E., Foderi, C., Fioravanti, M., Fattorini, L., Bottai, L., Mcroberts, R.E., Naesset, E., Corona, P., Gozzini, B., 2017. Assessing forest windthrow damage using single-date, post-event airborne laser scanning data. Forestry An International Journal of Forest Research 0, 1–11. doi:10.1093/forestry/cpx029

Chirici, G., McRoberts, R.E., Winter, S., Bertini, R., Bröändli, U.-B., Asensio, I.A., Bastrup-Birk, A., Rondeux, J., Barsoum, N., Marchetti, M., 2012. National forest inventory contributions to forest biodiversity monitoring. Forest Science 58, 257–268. doi:10.5849/forsci.12-003

Compare Cloud, 2017. version 2.8 -Available online: http://www.cloudcompare.org/ (accessed on 27 June 2017).

Corona, P., Chianucci, F., Quatrini, V., Civitarese, V., Clementel, F., Costa, C., Floris, A., Menesatti, P., Puletti, N., Sperandio, G., Verani, S., Turco, R., Bernardini, V., Plutino, M., Scrinzi, G., 2017. Precision forestry: concepts, tools and perspectives in Italy. Forest@ - Rivista di Selvicoltura ed Ecologia Forestale 14, 1–12. doi:10.3832/efor2285-014

Corona, P., Chirici, G., McRoberts, R.E., Winter, S., Barbati, A., 2011. Contribution of large-scale forest inventories to biodiversity assessment and monitoring. Forest Ecology and Management 262, 2061–2069. doi:10.1016/j.foreco.2011.08.044

Corona, P., Fattorini, L., 2008. Area-based lidar-assisted estimation of forest standing volume. Canadian Journal of Forest Research 38, 2911–2916. doi:10.1139/X08-122

Daamen, W., 1980. Results from a Check on Data Collection of the National Forest Survey in 1973–1977. Umeå: Institutionen för skogstaxering, Sveriges lantbruksuniversitet: Uppsala, Sweden. (in Swedish) 189.

Dandois, J.P., Ellis, E.C., 2013. High spatial resolution three-dimensional mapping of vegetation spectral dynamics using computer vision. Remote Sensing of Environment 136, 259–276. doi:10.1016/j.rse.2013.04.005

Dandois, J.P., Ellis, E.C., 2010. Remote sensing of vegetation structure using computer vision. Remote Sensing 2, 1157–1176. doi:10.3390/rs2041157

Dandois, J.P., Olano, M., Ellis, E.C., 2015. Optimal altitude, overlap, and weather conditions for computer vision uav estimates of forest structure. Remote Sensing 7, 13895–13920. doi:10.3390/rs71013895

Dash, J.P., Watt, M.S., Bhandari, S., Watt, P., 2016. Characterising forest structure using combinations of airborne laser scanning data, RapidEye satellite imagery and environmental variables. Forestry 89, 159–169. doi:10.1093/forestry/cpv048

Davies, O.L., Goldsmith, P.L., 1984. Statistical methods in research and production : with special reference to the Chemical Industry, Longman. ed. London.

Dinerstein, E., Olson, D.M., Graham, D.J., Webster, A.L., Primm, S.A., Bookbinder, M.P., Ledec, G., 1995. Conservation Assessment of the Terrestrial Ecoregions of Latin America and the Caribbean. The World Bannk Washington (DC).

Durbin, J., Watson, G.S., 1950. Testing for Serial Correlation in Least Squares Regression I. Biometrika 37, pp. 409–428, 1950. Biometrika 37, 409–428.

Dyck, B., 2003. Precision Forestry - the path to increased profitability. In: Procee, 3–8.

Eriksson, H., 1970. On Measuring Errors in Tree Height Determination with Different Altimeters. Stockholm Skogshögskolan, Institutionen för skogsproduktion: Stockholm, Sweden, (in Swedish).

Fardusi, M.J., Chianucci, F., Barbati, A., 2017. Concept to Practices of Geospatial Information Tools to Assist Forest Management and Planning under Precision Forestry Framework : a review 41, 3–14.

Fitj, A., Vestjordet, E., 1977. Stand height curves and new tariff tables for Norway spruce. Rep Norw For Res Inst. 34:23– 62. Norwegian with English summary.

Fitje, A., Vestjordet, E., 1977. Spruce, Stand height curves and new tariff tables for Norway. Commun. Nor. For. Res. Inst. 34, 23–62.

Fleck, S., Mölder, I., Jacob, M., Gebauer, T., Jungkunst, H.F., Leuschner, C., 2011. Comparison of conventional eight-point crown projections with

LIDAR-based virtual crown projections in a temperate old-growth forest. Annals of Forest Science 68, 1173–1185. doi:10.1007/s13595-011-0067-1

Fonstad, M.A., Dietrich, J.T., Courville, B.C., Jensen, J.L., Carbonneau, P.E., 2013. Topographic structure from motion: A new development in photogrammetric measurement. Earth Surface Processes and Landforms 38, 421–430. doi:10.1002/esp.3366

FOREST EUROPE, 2015. State of Europe's Forests 2015., Ministerial Conference on the Protection of Forests in Europe, FOREST EUROPE Liaison Unit Madrid.

Fotakis, D.G., Sidiropoulos, E., Myronidis, D., Ioannou, K., 2012. Spatial genetic algorithm for multi-objective forest planning. Forest Policy and Economics 21, 12–19. doi:10.1016/j.forpol.2012.04.002

George, M., 1983. Kendall, Maurice George 1938.

Giannetti, F., Chirici, G., Travaglini, D., Bottalico, F., Marchi, E., Cambi, M., 2017. Assessment of Soil Disturbance Caused by Forest Operations by Means of Portable Laser Scanner and Soil Physical Parameters 1–23. doi:10.2136/sssaj2017.02.0051

Ginzler, C., Hobi, M., 2015. Countrywide Stereo-Image Matching for Updating Digital Surface Models in the Framework of the Swiss National Forest Inventory. Remote Sensing 7, 4343–4370. doi:10.3390/rs70404343

Gobakken, T., Bollandsås, O.M., Næsset, E., 2015. Comparing biophysical forest characteristics estimated from photogrammetric matching of aerial images and airborne laser scanning data. Scandinavian Journal of Forest Research 30, 73–86. doi:10.1080/02827581.2014.961954

Gómez, C., Wulder, M.A., Montes, F., Delgado, J.A., 2011. Forest structural diversity characterization in Mediterranean pines of central Spain with quickbird-2 imagery and canonical correlation analysis. Canadian Journal of Remote Sensing 37, 628–642. doi:10.5589/m12-005

Hansen, E.H., Gobakken, T., Bollandsås, O.M., Zahabu, E., Næsset, E., 2015. Modeling aboveground biomass in dense tropical submontane rainforest using airborne laser scanner data. Remote Sensing 7, 788–807. doi:10.3390/rs70100788

Haralick, R.M., Shanmugam, K., Dinstein, I., 1973. Textural Features for Image Classification.

Harrell, F.E., 2001. Regression Modeling Strategies with Applications to Linear Models, Logistic Regression, and Survival Analysis.

Henning, J.G., Radtke, P.J., 2008. Multiview range-image registration for forested scenes using explicitly-matched tie points estimated from natural surfaces. ISPRS Journal of Photogrammetry and Remote Sensing 63, 68–83. doi:10.1016/j.isprsjprs.2007.07.006

Hobi, M.L., Ginzler, C., 2012. Accuracy assessment of digital surface models based on WorldView-2 and ADS80 stereo remote sensing data. Sensors (Basel, Switzerland) 12, 6347–68. doi:10.3390/s120506347

Hodgson, M.E., Bresnahan, P., 2004. Accuracy of Airborne Lidar-Derived Elevation. Photogrammetric Engineering & Remote Sensing 70.

Hodgson, M.E., Jensen, J.R., Schmidt, L., Schill, S., Davis, B., 2003. An evaluation of LIDAR- and IFSAR-derived digital elevation models in leaf-on conditions with USGS Level 1 and Level 2 DEMs. Remote Sensing of Environment 84, 295–308. doi:10.1016/S0034-4257(02)00114-1

Hollaus, M., Wagner, W., Eberhöfer, C., Karel, W., 2006. Accuracy of large-scale canopy heights derived from LiDAR data under operational constraints in a complex alpine environment. ISPRS Journal of Photogrammetry and Remote Sensing 60, 323–338. doi:10.1016/j.isprsjprs.2006.05.002

Holopainen, M., Vastaranta, M., Hyyppä, J., 2014. Outlook for the next generation's precision forestry in Finland. Forests 5, 1682–1694. doi:10.3390/f5071682

Huang, H., Li, Z., Gong, P., Cheng, X., Clinton, N., Cao, C., Ni, W., Wang, L., 2011a. Automated methods for measuring DBH and tree heights with a commercial scanning lidar. Photogrammetric Engineering and Remote Sensing 77, 219–227. doi:10.14358/PERS.77.3.219

Huang, H., Li, Z., Gong, P., Cheng, X., Clinton, N., Cao, C., Ni, W., Wang, L., 2011b. Automated methods for measuring DBH and tree heights with a commercial scanning lidar. Photogrammetric Engineering and Remote Sensing 77, 219–227. doi:10.14358/PERS.77.3.219

Hyyppä, H., Yu, X., Hyyppä, J., Kaartinen, H., Kaasalainen, S., Honkavaara, E., Rönnholm, P., 2005. Factors affecting the quality of DTM generation in forested areas. International Archives of Photogrammetry, Remote Sensing and Spatial Information Sciences 36 (Part 3, 97–102. doi:10.3390/s120506347

Hyyppä, J., Hyyppä, H., Leckie, D., Gougeon, F., Yu, X., Maltamo, M., 2008. Review of methods of small footprint airborne laser scanning for extracting forest inventory data in boreal forests. International Journal of Remote Sensing 29, 1339–1366. doi:10.1080/01431160701736489

IUFRO, 2015. Collection of definition or related elements Precision Forestry. SILVAOC Terminology Prokect.

IUFRO, 2014. Precision Forestry: The anchor of your value chain. In: First Announcement, Precision Forestry Sym- posium. Stellenbosch, South Africa.

James, M.R., Robson, S., 2012. Straightforward reconstruction of 3D

surfaces and topography with a camera: Accuracy and geoscience application. Journal of Geophysical Research: Earth Surface 117, 1–17. doi:10.1029/2011JF002289

Järnstedt, J., Pekkarinen, A., Tuominen, S., Ginzler, C., Holopainen, M., Viitala, R., 2012. Forest variable estimation using a high-resolution digital surface model. ISPRS Journal of Photogrammetry and Remote Sensing 74, 78–84. doi:10.1016/j.isprsjprs.2012.08.006

Joint Research Centre, 2014. Precision agricolture: an opportunity for EU-farmers- potential support with the CAP 2014-2020. Policy Department B, European Union 56 p.

Kachamba, D., Ørka, H., Gobakken, T., Eid, T., Mwase, W., 2016. Biomass Estimation Using 3D Data from Unmanned Aerial Vehicle Imagery in a Tropical Woodland. Remote Sensing 2016, Vol. 8, Page 968 8, 968. doi:10.3390/RS8110968

Kamphorst, E.C., Jetten, V., Guerif, J., Pitkanen, J., Iversen, B. V, Douglas, J.T., Paz, A., 2000. Predicting Depressional Storage from Soil Surface Roughness. Soil Sci Soc Am J 64, 1749–1758. doi:10.2136/sssaj2000.6451749x

Kankare, V., Holopainen, M., Vastaranta, M., Puttonen, E., Yu, X., Hyyppä, J., Vaaja, M., Hyyppä, H., Alho, P., 2013. Individual tree biomass estimation using terrestrial laser scanning. ISPRS Journal of Photogrammetry and Remote Sensing 75, 64–75. doi:10.1016/j.isprsjprs.2012.10.003

Kankare, V., Joensuu, M., Vauhkonen, J., Holopainen, M., Tanhuanpää, T., Vastaranta, M., Hyyppä, J., Hyyppä, H., Alho, P., Rikala, J., Sipi, M., 2014. Estimation of the timber quality of scots pine with terrestrial laser scanning. Forests 5, 1879–1895. doi:10.3390/f5081879

Kankare, V., Liang, X., Vastaranta, M., Yu, X., Holopainen, M., Hyyppä, J., 2015a. Diameter distribution estimation with laser scanning based multisource single tree inventory. ISPRS Journal of Photogrammetry and Remote Sensing 108, 161–171. doi:10.1016/j.isprsjprs.2015.07.007

Kankare, V., Liang, X., Vastaranta, M., Yu, X., Holopainen, M., Hyyppä, J., 2015b. Diameter distribution estimation with laser scanning based multisource single tree inventory. ISPRS Journal of Photogrammetry and Remote Sensing 108, 161–171. doi:10.1016/j.isprsjprs.2015.07.007

Koreň, M., Slančík, M., Suchomel, J., Dubina, J., 2015. Use of terrestrial laser scanning to evaluate the spatial distribution of soil disturbance by skidding operations. IForest 8, 386–393. doi:10.3832/ifor1165-007

Kovácsová, P., Antalová, M., 2010. Precision Forestry – Definition and Technologies. Šumarski List 143, 603–611.

Krooks, A., Kaasalainen, S., Kankare, V., Joensuu, M., Raumonen, P., Kaasalainen, M., 2014. Tree structure vs. height from terrestrial laser scanning and quantitative structure models. Silva Fennica 48, 1–11. doi:10.14214/sf.1125

Kurttila, M., 2001. The spatial structure of forests in the optimization calculations of forest planning - A landscape ecological perspective. Forest Ecology and Management 142, 129–142. doi:10.1016/S0378-1127(00)00343-1

Laes, C.D., Reutebuch, S.E., Mcgaughey, R.J., Mitchell, B., 2011. Guidelines to estimate forest inventory parameters from lidar and field plot data 1–22.

Lefsky, M., Cohen, W.B., Parker, G.G., Harding, D.J., 2002. Lidar Remote Sensing for Ecosystem Studies. Bioscience 52, 19–30. doi:10.1641/0006-3568(2002)052[0019:LRSFES]2.0.CO;2

Liang, X., Hyyppä, J., 2013. Automatic stem mapping by merging several terrestrial laser scans at the feature and decision levels. Sensors (Switzerland) 13, 1614–1634. doi:10.3390/s130201614

Liang, X., Kankare, V., Hyyppä, J., Wang, Y., Kukko, A., Haggrén, H., Yu, X., Kaartinen, H., Jaakkola, A., Guan, F., Holopainen, M., Vastaranta, M., 2016a. Terrestrial laser scanning in forest inventories. ISPRS Journal of Photogrammetry and Remote Sensing 115, 63–77. doi:10.1016/j.isprsjprs.2016.01.006

Liang, X., Kankare, V., Hyyppä, J., Wang, Y., Kukko, A., Haggrén, H., Yu, X., Kaartinen, H., Jaakkola, A., Guan, F., Holopainen, M., Vastaranta, M., 2016b. Terrestrial laser scanning in forest inventories. ISPRS Journal of Photogrammetry and Remote Sensing 115, 63–77. doi:10.1016/j.isprsjprs.2016.01.006

Liang, X., Wang, Y., Jaakkola, A., Kukko, A., Kaartinen, H., Hyyppä, J., Honkavaara, E., Liu, J., 2015. Forest data collection using terrestrial image-based point clouds from a handheld camera compared to terrestrial and personal laser scanning. IEEE Transactions on Geoscience and Remote Sensing 53, 5117–5132. doi:10.1109/TGRS.2015.2417316

Lim, K.P.., Treitz, P.., Wulder, M.A.., St-Onge, B.A.., Flood, M., 2003. LiDAR remote sensing of forest structure. Progress in Physical Geography 27, 88–106.

Lisein, J., Pierrot-Deseilligny, M., Bonnet, S., Lejeune, P., 2013. A photogrammetric workflow for the creation of a forest canopy height model from small unmanned aerial system imagery. Forests 4, 922–944. doi:10.3390/f4040922

Lu, D., Batistella, M., 2005. Exploring TM image texture and its relationships with biomass estimation in Rondônia, Brazilian Amazon. Acta

Amazonica 35, 249–257. doi:10.1590/S0044-59672005000200015
Maas, H.-G., Bienert, A., Scheller, S., Keane, E., 2008. Automatic forest inventory parameter determination from terrestrial laser scanner data. International Journal of Remote Sensing 29, 1579–1593. doi:10.1080/01431160701736406
Maltamo, M., Næsset, E., Vauhkonen, J., 2014. Forestry Applications of Airborne Laser Scanning: Concepts and Case Studies, Forestry Applications of Airborne Laser Scanning: Concepts and Case Studies. doi:10.1007/978-94-017-8663-8
McGaughey, R.J., 2014. FUSION/LDV: Software for LIDAR Data Analysis and Visualization 154.
McRoberts, R.E., Næsset, E., Gobakken, T., 2013a. Inference for lidar-assisted estimation of forest growing stock volume. Remote Sensing of Environment 128, 268–275. doi:10.1016/j.rse.2012.10.007
McRoberts, R.E., Næsset, E., Gobakken, T., 2013b. Inference for lidar-assisted estimation of forest growing stock volume. Remote Sensing of Environment 128, 268–275. doi:10.1016/j.rse.2012.10.007
Micheletti, N., Chandler, J.H., Lane, S.N., 2015. Investigating the geomorphological potential of freely available and accessible structure-from-motion photogrammetry using a smartphone. Earth Surface Processes and Landforms 40, 473–486. doi:10.1002/esp.3648
Miller, E., Dandois, J., Detto, M., Hall, J., 2017. Drones as a Tool for Monoculture Plantation Assessment in the Steepland Tropics. Forests 8, 168. doi:10.3390/f8050168
Mura, M., McRoberts, R.E., Chirici, G., Marchetti, M., 2015. Estimating and mapping forest structural diversity using airborne laser scanning data. Remote Sensing of Environment 170, 133–142. doi:10.1016/j.rse.2015.09.016
Nadal-Romero, E., Revuelto, J., Errea, P., López-Moreno, J.I., 2015. The application of terrestrial laser scanner and photogrammetry in measuring erosion and deposition processes in humid badlands in the Central Spanish Pyrenees. SOIL Discussions 2, 337–369. doi:10.5194/soild-2-337-2015
Næsset, E., 2007. Airborne laser scanning as a method in operational forest inventory: Status of accuracy assessments accomplished in Scandinavia. Scandinavian Journal of Forest Research 22, 433–422.
Næsset, E., 2004. Practical large-scale forest stand inventory using small-footprint airborne scanning laser. Scandinavian Journal of Forest Research 19, 164–179.
Næsset, E., 2002. Predicting forest stand characteristics with airborne scanning laser using a practical two-stage procedure and field data.

Remote Sensing of Environment 80, 88–99. doi:10.1016/S0034-4257(01)00290-5

Næsset, E., 1997. Estimating timber volume of forest stands using airborne laser scanner data. Remote Sensing of Environment 61, 246–253. doi:10.1016/S0034-4257(97)00041-2

Næsset, E., Gobakken, T., Holmgren, J., Hyyppä, H., Hyyppä, J., Maltamo, M., Nilsson, M., Olsson, H., Persson, Å., Söderman, U., 2004. Laser scanning of forest resources: the nordic experience. Scandinavian Journal of Forest Research 19, 482–499. doi:10.1080/02827580410019553

Næsset, E., Økland, T., 2002. Estimating tree height and tree crown properties using airborne scanning laser in a boreal nature reserve. Remote Sensing of Environment 79, 105–115. doi:10.1016/S0034-4257(01)00243-7

Newnham, G.J., Armston, J.D., Calders, K., Disney, M.I., Lovell, J.L., Schaaf, C.B., Strahler, A.H., Danson, F.M., 2015. Terrestrial Laser Scanning for Plot-Scale Forest Measurement. Current Forestry Reports 1, 239–251. doi:10.1007/s40725-015-0025-5

Nex, F., Remondino, F., 2014. UAV for 3D mapping applications: A review. Applied Geomatics 6, 1–15. doi:10.1007/s12518-013-0120-x

Niemi, M., Vauhkonen, J., 2016. Extracting Canopy Surface Texture from Airborne Laser Scanning Data for the Supervised and Unsupervised Prediction of Area-Based Forest Characteristics. Remote Sensing 8, 582. doi:10.3390/rs8070582

Nouwakpo, S.K., Huang, C., 2012. A Simplified Close-Range Photogrammetric Technique for Soil Erosion Assessment. Soil Science Society of America Journal 76, 70. doi:10.2136/sssaj2011.0148

Nurminen, K., Karjalainen, M., Yu, X., Hyyppä, J., Honkavaara, E., 2013. Performance of dense digital surface models based on image matching in the estimation of plot-level forest variables. ISPRS Journal of Photogrammetry and Remote Sensing 83, 104–115. doi:10.1016/j.isprsjprs.2013.06.005

O'Farrell, P.J., Anderson, P.M.L., 2010. Sustainable multifunctional landscapes: A review to implementation. Current Opinion in Environmental Sustainability 2, 59–65. doi:10.1016/j.cosust.2010.02.005

Ota, T., Ogawa, M., Shimizu, K., Kajisa, T., Mizoue, N., Yoshida, S., Takao, G., Hirata, Y., Furuya, N., Sano, T., Sokh, H., Ma, V., Ito, E., Toriyama, J., Monda, Y., Saito, H., Kiyono, Y., Chann, S., Ket, N., 2015. Aboveground biomass estimation using structure from motion approach with aerial photographs in a seasonal tropical forest. Forests 6, 3882–3898. doi:10.3390/f6113882

Ozdemir, I., 2008. Estimating stem volume by tree crown area and tree shadow area extracted from pansharpened Quickbird imagery in open Crimean juniper forests. International Journal of Remote Sensing 29, 5643–5655. doi:10.1080/01431160802082155

Paneque-Gálvez, J., McCall, M.K., Napoletano, B.M., Wich, S.A., Koh, L.P., 2014. Small drones for community-based forest monitoring: An assessment of their feasibility and potential in tropical areas. Forests 5, 1481–1507. doi:10.3390/f5061481

Pasumansky, A., 2017. Personal comunication 15 March 2017. Agisoft Technical Support.

Pierzchała, M., Talbot, B., Astrup, R., 2014. Estimating soil displacement from timber extraction trails in steep terrain: Application of an unmanned aircraft for 3D modelling. Forests 5, 1212–1223. doi:10.3390/f5061212

Pretzsch, H., 2009. Forest Dynamics, Growth and Yield. doi:http://doi.org/10.1007/978-3-540-88307-4

Puliti, S., Ene, L.T., Gobakken, T., Næsset, E., 2017a. Use of partial-coverage UAV data in sampling for large scale forest inventories. Remote Sensing of Environment 194, 115–126. doi:10.1016/j.rse.2017.03.019

Puliti, S., Gobakken, T., Ørka, H.O., Næsset, E., 2017b. Assessing 3D point clouds from aerial photographs for species-specific forest inventories. Scandinavian Journal of Forest Research 32:1, 68–79. doi:10.1080/02827581.2016.1186727

Puliti, S., Olerka, H., Gobakken, T., Næsset, E., 2015a. Inventory of Small Forest Areas Using an Unmanned Aerial System. Remote Sensing 7, 9632–9654. doi:10.3390/rs70809632

Pyysalo, U., Hyyppae, H., 2002. Reconstructing Tree Crowns from Laser Scanner Data for Feature Extraction. ISPRS Commission III, Symposium 2002 September 9 - 13, 2002, Graz, Austria B-218 ff (4 pages).

Rahlf, J., Breidenbach, J., Solberg, S., Astrup, R., 2015. Forest parameter prediction using an image-based point cloud: A comparison of semi-ITC with ABA. Forests 6, 4059–4071. doi:10.3390/f6114059

Rahlf, J., Breidenbach, J., Solberg, S., Næsset, E., Astrup, R., 2014. Comparison of four types of 3D data for timber volume estimation. Remote Sensing of Environment 155, 325–333. doi:10.1016/j.rse.2014.08.036

Remondino, F., Spera, M.G., Nocerino, E., Menna, F., Nex, F., 2014. State of the art in high density image matching. The Photogrammetric Record 29, 144–166. doi:10.1111/phor.12063

RIEGL LMS, 2017. RiSCAN PRO Version 2.0. Software Description and User's

Instructions. Available online: http://www.riegl.com/ (accessed on 26 June 2017).
Rothermel, M., Wenzel, K., 2012. SURE - Photogrammetric Surface Reconstruction from Imagery. Proceedings LC3D Workshop 1–21.
Ryding, J., Williams, E., Smith, M.J., Eichhorn, M.P., 2015. Assessing handheld mobile laser scanners for forest surveys. Remote Sensing 7, 1095–1111. doi:10.3390/rs70101095
Sallabanks, R., Haufler, J., Mehl, C., 2006. Influence of Forest Vegetation Structure on Avian Community Composition in West-Central Idaho. Wildlife Society Bulletin 34, 1079–1093.
Shannon, C.E., 1948. A mathematical theory of communication. The Bell System Technical Journal 27, 379–423. doi:10.1145/584091.584093
Solberg, S., Naesset, E., Bollandsas, O.M., 2006. Single Tree Segmentation Using Airborne Laser Scanner Data in a Structurally Heterogeneous Spruce Forest. Photogrammetric Engineering & Remote Sensing 72, 1369–1378. doi:0099-1112/06/7212–1369
Tabacchi, G., Di Cosmo, L., Gasparini, P., Morelli, S., 2011. Stima del volume e della fitomassa delle principali specie forestali italiene, Equazioni di previsione, tavole del volume e tavole della fitomassa arborea epigea.
Talbot, B., Pierzchała, M., Astrup, R., 2016. Applications of Remote and Proximal Sensing for Improved Precision in Forest Operations 327–336.
Taylor, S.E., McDonald, T.P., Veal, M.W., Corley, F.W., Grift, T.E., 2002. Precision Forestry: Operational tactics for today and tomorrow. 25th Annual Meeting of the Council of Forest Engineers 6.
Tonolli, S., Dalponte, M., Vescovo, L., Rodeghiero, M., Bruzzone, L., Gianelle, D., 2011. Mapping and modeling forest tree volume using forest inventory and airborne laser scanning. European Journal of Forest Research 130, 569–577. doi:10.1007/s10342-010-0445-5
Tran, D.., Nguyen, N.V., 2006. The concept and implementation of precision farming and reice integrated crop management systems for sustainable production in the twenty-first century. International Rice Commission Newsletter 55, 103–113.
Trimble, 2017. Trimble RealWorks® 8.0 User Guide.
Turner, D., Lucieer, A., Watson, C., 2012. An automated technique for generating georectified mosaics from ultra-high resolution Unmanned Aerial Vehicle (UAV) imagery, based on Structure from Motion (SFM) point clouds. Remote Sensing 4, 1392–1410. doi:10.3390/rs4051392
Ullah, S., Adler, P., Dees, M., Datta, P., Weinacker, H., Koch, B., 2017. Comparing image-based point clouds and airborne laser scanning data for estimating forest heights. iForest - Biogeosciences and

Forestry 10, e1–e8. doi:10.3832/ifor2077-009
Valbuena, R., Eerik??inen, K., Packalen, P., Maltamo, M., 2016. Gini coefficient predictions from airborne lidar remote sensing display the effect of management intensity on forest structure. Ecological Indicators 60, 574–585. doi:10.1016/j.ecolind.2015.08.001
Valbuena, R., Packalen, P., Mehtätalo, L., García-Abril, A., Maltamo, M., 2013. Characterizing forest structural types and shelterwood dynamics from Lorenz-based indicators predicted by airborne laser scanning. Canadian Journal of Forest Research 43, 1063–1074. doi:10.1139/cjfr-2013-0147
Vastaranta, M., Wulder, M.A., White, J.C., Pekkarinen, A., Tuominen, S., Ginzler, C., Kankare, V., Holopainen, M., Hyyppä, J., Hyyppä, H., 2013. Airborne laser scanning and digital stereo imagery measures of forest structure: comparative results and implications to forest mapping and inventory update. Canadian Journal of Remote Sensing 39, 382–395. doi:10.5589/m13-046
Vericat, D., Smith, M.W., Brasington, J., 2014. Patterns of topographic change in sub-humid badlands determined by high resolution multi-temporal topographic surveys. Catena 120, 164–176. doi:10.1016/j.catena.2014.04.012
Vestjordet, E., 1968. Merchantable volume of Norway spruce and Scots pine based on relative height and diameter at breast height or 2.5 m above stump level., in: Medd. Det Nor. Skogforsøksves, 25. (in Norwegian). pp. 411–459.
Vestjordet, E., 1967. Functions and tables for volume of standing trees. Norway spruce. Meddelelser fra Det Norske Skogforsøksvesen. 1967. Functions and tables for volume Summary., standing trees. Norway spruce. Meddelelser fra Det Norske Skogforsøksvesen. 22:539–574. Norwegian with English.
Vogeler, J.C., Hudak, A.T., Vierling, L.A., Evans, J., Green, P., Vierling, K.T., 2014. Terrain and vegetation structural influences on local avian species richness in two mixed-conifer forests. Remote Sensing of Environment 147, 13–22. doi:10.1016/j.rse.2014.02.006
Wallace, L., Lucieer, A., Malenovský, Z., Turner, D., Vopěnka, P., 2016. Assessment of forest structure using two UAV techniques: A comparison of airborne laser scanning and structure from motion (SfM) point clouds. Forests 7, 1–16. doi:10.3390/f7030062
Warner, W.S., 1995. Mapping a three-dimensional soil surface with hand-held 35 Mm photography. Soil and Tillage Research 34, 187–197.
Waser, L.T., Fischer, C., Wang, Z., Ginzler, C., 2015. Wall-to-wall forest mapping based on digital surface models from image-based point clouds and a NFI forest definition. Forests 6, 4510–4528.

doi:10.3390/f6124386
White, J.C., Coops, N.C., Wulder, M.A., Vastaranta, M., Hilker, T., Tompalski, P., 2016. Remote Sensing Technologies for Enhancing Forest Inventories: A Review. Canadian Journal of Remote Sensing 42, 619–641. doi:10.1080/07038992.2016.1207484
White, J.C., Stepper, C., Tompalski, P., Coops, N.C., Wulder, M.A., 2015. Comparing ALS and image-based point cloud metrics and modelled forest inventory attributes in a complex coastal forest environment. Forests 6, 3704–3732. doi:10.3390/f6103704
White, J.C., Wulder, M.A., Vastaranta, M., Coops, N.C., Pitt, D., Woods, M., 2013. The utility of image-based point clouds for forest inventory: A comparison with airborne laser scanning. Forests 4, 518–536. doi:10.3390/f4030518
Whitehead, K., Hugenholtz, C.H., Myshak, S., Brown, O., LeClair, A., Tamminga, A., Barchyn, T.E., Moorman, B., Eaton, B., 2014. Remote sensing of the environment with small unmanned aircraft systems (UASs), part 1: a review of progress and challenges. Journal of Unmanned Vehicle Systems 2, 86–102. doi:10.1139/juvs-2014-0007
Wulder, M.A., Bater, C.W., Coops, N.C., Hilker, T., White, J.., 2008. The role of LiDAR in sustainable forest management. The Forestry Chronicle 84, 807–826.
Zahawi, R.A., Dandois, J.P., Holl, K.D., Nadwodny, D., Reid, J.L., Ellis, E.C., 2015. Using lightweight unmanned aerial vehicles to monitor tropical forest recovery. Biological Conservation 186, 287–295. doi:10.1016/j.biocon.2015.03.031
Zvoleff, A., 2015. Package "Glcm", 1.2. Available online http://cran.r-project.org/web/packages/glcm/glcm.pdf (accessed on 11 April 2017).

Paper III – UAV photogrammetric DTM-independent variables can be used to predict forest structural indices? A case of study in mixed temperate forests

Francesca Giannetti[a*], *Nicola Puletti*[b], *Stefano Puliti*[c], *Davide Travaglini*[a*], *Gherardo Chirici*[a]

*Corresponding author Francesca Giannetti francesca.giannetti@unifi.it

[a] Università degli Studi di Firenze, Department of Agricultural, Food and Forestry Systems, Via San Bonaventura, 13-50145, Firenze, Italy

[b] Consiglio per la ricerca in agricoltura e l'analisi dell'economia agraria (CREA), Forestry Research Centre, Arezzo, Italy.

[c] Department of Ecology and Natural Resource Management, Norwegian University of Life Sciences

Ecological Indicators

Abstract

In the EU 2020 biodiversity strategy, maintaining and enhancing forest biodiversity is essential. Forest managers and technicians should include biodiversity monitoring as a support for forest management and conservation issues, through the adoption of forest biodiversity indices.

In the last years, the increasing availability of aerial digital and multispectral imagery from Unmanned Aerial Vehicles (UAV) and the advancements in Structure from Motion (SfM) photogrammetry have increased the availability of 3 dimensional (3D) data for forest applications.

The present study investigates the potential of a new type of SfM photogrammetry which does not require the availability of high resolution DTM developed from expensive Airborne Laser Scanning (ALS) surveys. We

used DTM-independent variables calculated on the basis of 3D UAV photogrammetric for the spatial prediction of eight forest structure indices which are commonly used for forest biodiversity monitoring: basal area; mean Diameter at Breast Height (DBH); standard deviation of DBH; DBH Gini coefficient; standard deviation of tree heights; dominant tree height ; Lory's height, and growing stock volume. The experiment was carried out with 80 field surveys acquired in two study areas with mixed temperate forests in Italy. The accuracy of UAV DTM-independent predictions was compared with a benchmark approach based on explanatory variables calculated from traditional ALS data.

The two approaches, in terms of Root Mean Square Error, produced similar predictions. On a total of 16 tests (8 variables in two study areas), in 9 cases DTM-independent estimations were more accurate than those from ALS.

Finally DTM-independent variables were used to construct maps of the forest structure indices in the two test areas to demonstrate the possible operational use of the approach for depicting the spatial pattern of forest biodiversity.

Keyword: Forest inventory, structure from motion, photogrammetry, airborne laser scanner, biodiversity, precision forestry, forest structure.

1. Introduction

New methods and tools for the integration of spatial and temporal dimensions in forest ecosystems monitoring are needed to support sustainable forest management in taking into consideration the wide array of ecosystems services provided by forests (Fotakis et al., 2012; Myronidis and Arabatizis, 2009; Fotakis, 2015). The protection of forest biodiversity is an increasingly important issue at European level (European Environmental Agency, 2012; Fotakis et al., 2012; Arabatzis, 2010; Kurttila, 2001; European Union, 2011). In fact the European Union (2011), in the 2020 strategy for EU biodiversity, indicate how it is essential to increase the contribution of forestry in maintaining and enhancing biodiversity. Moreover it is reported that by 2020 forest management plans, or equivalent instruments, in line with Sustainable Forest Management (SFM), need to provide "*a measurable improvement in the conservation status of forest ecosystems and species and in the provision of related ecosystem services as compared to the EU 2010 Baseline*"(European Union, 2011).

As a consequence forest managers should include biodiversity monitoring in the phase of information acquisition to support forest management choices (Arabatzis, 2010; Ozdemir, 2008; Ozdemir and Karnieli, 2011; Seitz et al., 2008; Baskent et al., 2008); for such a purpose an objective and statistically rigorous systems of forest biodiversity indicators is urgently needed.

Frequently forest biodiversity is described and measured through indicators based on species compositions (Winter et al., 2008; Zellweger et al., 2013), or structural diversity (McElhinny et al., 2005; Mura et al., 2015). Alpha or beta biodiversity indicators based on species composition are well known and established in vegetation science and conservation biology (Noss, 1990). Forest structure indicators are related to the spatial arrangement of the different components of the forest ecosystem, such as

tree heights at different canopy levels, trees spacing and trees dimension (McElhinny et al., 2005). Forest structure is considered one of the most important indicator of forest health (Franklin, 1988; Hunter, 1999; Kolb et al., 1994; Zellweger et al., 2013) and a good predictor of habitat quality for several animal communities (Halaj et al., 2000; McElhinny et al., 2005; McGraw, 1994; Müller et al., 2010, Salter et al., 1985; Shine et al., 2002; Welsh and Lind, 1996). Several authors reported that maintaining and improving the complexity of forest structure is crucial to contrast the loss of biodiversity (Kolb et al., 1994; Zellweger et al., 2013; Winter et al., 2008; Chirici et al., 2011; Chirici et al., 2012; Bottalico et al., 2017).

The most common structure diversity indices are based on simple information collected in plots measured in the field in the framework of forest inventories such as: tree diameters at breast height (DBH) and tree heights (H) (Staudhammer and LeMay, 2001; McElhinny et al., 2005¸Müller and Vierling, 2014; Pommerening, 2002).

Data from active or passive remote sensing (RS) can be used as predictors for deriving wall-to-wall spatial estimation of the variables measured forest inventory plots (Mura et al., 2015; Fotakis et al., 2015; Valbuena et al., 2016; Brosofske et al., 2014; Corona, 2010) including forest biodiversity indicators (Valbuena et al., 2016; Bottalico et al., 2017; Mura et al., 2015). In the context of precision forestry (Taylor et al., 2002), in order to planning and conducting site-specific forest management activities, the demands for global-level and small-scale forest information have increased. Maps that describe the forest environment under different points of view, for instance through multiple biodiversity indicators, are considered crucial to support forest management activities (Corona et al., 2017; Fardusi et al., 2017). Several technics can be used for predicting forest biodiversity indicators with RS.

Some authors have reported that textural metrics (Haralick et al., 1973) derived by high resolution satellite and aerial images, are useful to predict forest structure indices and forest cover changes (Bruniquel-Pinel and Gastellu-Etchegorry, 1998; Gómez et al., 2012; Ozdemir and Karnieli, 2011). For example, St-Onge and Cavayas (1995) yielded to relatively accurate estimates of crown diameter, stand density and percent cover using MEIS-II image with a resolution of 36 cm. Bruniquel-Pinel and Gastellu-Etchegorry, (1998) demonstrated the utility of textural metrics to predict tree position, Leaf Area Index and crown cover from high spatial resolution airborne images acquired by RAMI pushbroom instruments. Moreover, Ozdemir and Karnieli, (2011), demonstrated that Basal Area (G), Standard Deviation of Diameters at Breast Heights ($\sigma_{dbh)}$, and Gini Coefficient (GC), can be predicted and mapped with a reasonable accuracy using the texture features extracted from the spectral bands of WorldView-2 image. Gómez et al., (2012) founded that texture variables derived from imagery captured with QuickBird-2 in a Mediterranean pines forest are also useful to map forest structural diversity indices such as DBH, H, and crown diameters.

Other authors have found that the use metrics calculated from Airborne Laser Scanner (ALS) can produce accurate results in predicting forest structure indices (Evans et al., 2009, Lefsky et al., 2002, Lim et al., 2003, Zimble et al., 2003, Valbuena et al., 2013, 2014, 2016, Mura et al., 2015, 2016; Bottalico et al., 2017, Teobaldelli et al., 2017). Lefsky et al., (2002) and Lim et al., (2003) showed in their review the potential of using ALS returns to estimate canopy structure and function, and to predict forest stands variables such as H, biomass and volume. Zimble et al., (2003) showed that ALS-derived tree heights could be useful in the detection of differences in the continuous, nonthematic nature of vertical forest

structure with acceptable accuracies. Moreover, Evans et al., (2009) underline how ALS returns can be useful to develop different types of metrics for a better comprehension of forest structure and spatial dynamics. Moreover, other authors have found that these ALS metrics can be used as predictors to spatial estimate structure indices (e.g. DBH, H, Growing Stock Volume, σ_{dbh}, GC, Lorenz curve) in different forest types in boreal (Valbuena et al., 2016), Mediterranean (Bottalico et al., 2017; Teobaldelli et al., 2017), and temperate biomes (Mura et al., 2015).

Niemi and Vauhkonen, (2016) and Ozdemir and Donoghue, (2013) reported that the combination of traditionally ALS metrics and textural variables computed on ALS high resolution raster grid Canopy Height Model (CHM) (i.e. pixel size 0.5 m), are useful to improve the estimation accuracy of traditionally forest variables (i.e. stem volume, basal area) as well as for forest structure indicators (i.e. mean diameter, tree height diversity and tree DBH diversity).

New methods in computer vision and stereo-matching algorithms have increased the number of predictors that can be calculated from 3D photogrammetric data (Bohlin et al., 2012; Gobakken et al., 2015; Puliti et al., 2015). The increasing attention to 3D photogrammetry is due, also, to the recent advancements in RS using lightweight unmanned aerial vehicles systems (UAV) equipment with digital cameras. In fact, UAV can provide at forest management scale an alternative low cost option to acquire multi-temporal RS data (Lisein et al., 2013; Puliti et al., 2015; Wallace et al., 2016; Zahawi et al., 2015). Recently, Giannetti et al., (in review) have developed a new set of DTM-independent explanatory variables to predict traditional forest inventory variables (e.g. stem volume, basal area, stem number, Lorey's height and dominant height) from UAV photogrammetric data (i.e. image based point cloud and digital surface model (DSM)).

However, to our knowledge, the potential of UAV photogrammetric DTM-independent explanatory variables have never been investigated to predict structural complexity indices.

1.1 Objective

In this contribution we present the area-based (Nasset,2002) spatial estimation of the following forest structure complexity indices: basal area (G; m^2ha^{-1}); mean DBH (DBH_{mean}; cm); standard deviation of DBH (DBH_{σ}; cm); DBH Gini coefficient (Gini); standard deviation of H ($H_{\sigma h}$; m); dominant height (H_{dom}) and Lory's height (H_l) and stem volume (V m^3 ha^{-1}). Predictors are DTM-independent variables (Giannetti et al., 2017) from 3D UAV photogrammetric imagery. The accuracy of the DTM-independent approach was assessed against a more traditional approach based on ALS data in two forest districts in Italy.

2. Materials

2.1. Study area

The experiment was carried out in two study areas located in central Italy, in the Apennine mountains of Tuscany Region, and in the metropolitan area of Florence (Figure 1).

The first study area (115 ha) is located in the Nature State Reserve of Vallombrosa where biodiversity conservation is the main target of forest management. The Vallombrosa Reserve was not actually managed since 1970 when it was leaved more or less undisturbed to natural evolution.

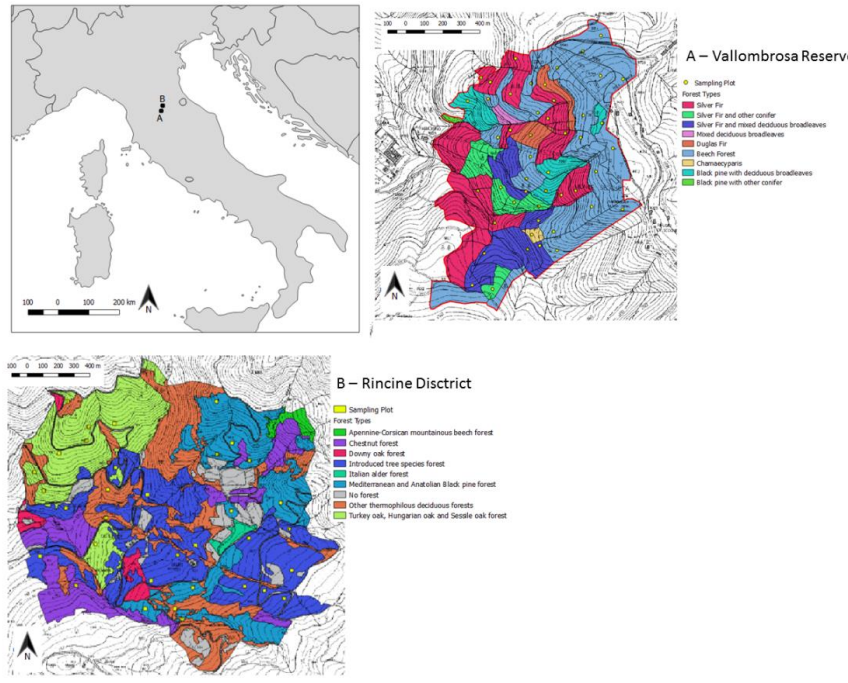

Figure 1: study areas with forest types and location of the field plots.

The Reserve is included in the Site of Community Importance (SCI) "Vallombrosa and S. Antonio Forest" (IT5140012) under the Natura 2000 Network (Habitats Directive 92/43/EC), two priority habitats (9210* and 9220*) are included in the SCI.

The study area is characterized by high slope (mean slope=41 %) and high altitude difference (1080-1432 m a.s.l.), it is dominated by beech (*Fagus sylvatica* L.) whit other broadleaves (Common ash (*Fraxinus excelsior* L.), oaks (*Quercus cerris* L., *Quercus pubescens* L.), European hop-hornbeam (*Ostrya carpinifolia* Scop.), common holly, (*Ilex aquifolium* L.), sycamore (*Acer pseudoplatanus*. L.) and ilex (*Ilex aquifolium* L)) and plantations dominated by Silver Fir (*Abies alba* M.) whit other conifers (.*Pseudotsuga menziesii* Franco, *Pinus Nigra* J.F. Arnold, *Chamaecyparis*, Spach) (Figure 1).

The beech forests are even-aged (155-230 year) and mostly derived by coppice converted to high-forest woodland.

All the conifers plantations are even-age. Silver Fir plantations derived by the traditional management systems carried out in Vallomborsa by local monks for wood production with a traditional rotation period of 80 years. More details about the management history of Vallombrosa Reserve can be found in Bottalico et al., (2014). Duglas fir and Chamecyparis are experimental plantations started in 1926 and 1922 respectively. The Black Pine plantations were carried out in the framework of a reforestation project in low fertility areas for protection of mountain steep zones. The mixed broadleaves forests are mostly coppice forests that were used in the past for firewood production.

The second study area has (290 ha), is located in the District of Rincine (Florence), and it is a public property of the Tuscany Region. The area is located at an altitude ranging between 1200 and 2300 m a.s.l.. Forest habitats are characterized by oaks (*Quercus cerris* L., *Quercus pubescens* L.) mixed whit other broadleaves (*Ostrya Carpinifolia Scop*; *Carpinus betulus* L.; *Fraxinus ornus*, L.; *Prunus avium* L.; *Ulmus*), beech (*Fagus sylvatica* L.) and chestnut (*Castanea Sativa* Mill.), and conifer plantations dominated by *Pinus Nigra* J.F.Arnold and *Pseudotsuga menziesii* Franco with several other non-indigenous species (*Cedrus libani*, A.Rich., *Cupressus Arizzonica*, *Chamaecyparis*, Spach) (Figure 1).

Conifers plantations are even-age experimental plantations started between 1965 and 1975 for pulpwood production. The broadleaves forests are mostly management as coppice for firewood production. The Rincine forest management follows the criteria of Sustainable Forest Management certified by both Forest Stewardship Council (FSC) and by the Programme for the Endorsement of Forest Certification schemes (PEFC)

systems. Rincine disctrict is also a Model Forest (International Model Forest Network (IMFN), 2008). In particular, the objective of the Model Forest is to support the sustainable management of natural resources through a participatory, landscape-level approach that reflects environmental and socio-economic issues from the perspectives of local needs and global concerns (IMFN, 2008).

2.2. Field data

2.2.1 Local forest inventory

In each study area, a local forest inventory was carried out (Figure 1).

In Vallombrosa field measurements were conducted in a total of 30 circular fixed-area sample plots having 13 m radius (each plot covers 530 m^2). Field work was carried out in June 2015. Field plots were selected using a tessellation stratified sampling scheme (Barabesi and Franceschi, 2011) based on a hexagonal grid with hexagons of 1 ha.

Rincine field measurements were carried out in 50 square fixed-area plots. Each plot having a size of 530 m^2. Field work was carried out between June and September 2016. Field plots were selected using the one-per-stratum stratified sampling scheme (Bruss et al., 1999; Barabesi et al., 2012) based on a 23 x 23 m grid. To do this, the study area was partitioned into 50 strata (i.e., polygons based on equal-size strata obtained by means of clusters) and one sample plot was independently and uniformly selected in each stratum.

The fact that the field plots were extracted on the basis of different sampling schemes is not relevant for the purposes of this study since it is developed in model-based framework.

In both study areas, the coordinates of plot centers were recorded using a Global Navigation Satellite Systems (GNSS) receiver Trimble Juno 3 B Handheld with 2–5 m positional accuracy in post-processing. In each plot

the Diameters at Breast Heights (DBH) and top height of all trees (H) with a DBH ≥ 2.5 cm were registered using a caliper and a Haglof Vertex IV device. Field work was carried out in June 2015 in Vallombrosa and between June and October 2016 in Rincine.

2.2.2 Forest structural complexity indices

Field data were used to calculate a set of seven structural complexity indices based on tree DBH and height. The indices considered in this work were selected after a literature review of possible biodiversity drivers (Bottalico et al., 2017; McElhinny et al., 2005; Meng et al., 2016; Mura et al., 2015; Ozdemir and Karnieli, 2011; Valbuena et al., 2016; Ziegler, 2000).

In more details we calculated the following indices: four DBH related indices (basal area, mean DBH, standard deviation of DBH and Gini coefficient); one tree height related index (standard deviation of H) and three indices that combine DBH and H (Lory's height, dominant height, growing stock volume). In the next paragraphs the indices chosen in this study are briefly presented on the basis of the literature review (Table 1).

2.2.2.1 Horizontal structural complexity indices

Basal Area (G) is an historical forest inventory variable that describes the amount of an area occupied by tree stems. G is directly related to growing stock volume and biomass which are important variables supporting traditional forest management approaches oriented to a sustainable wood production as well as for biodiversity conservations proposes (McElhinny et al., 2005).

Mean DBH (DBH_{mean}) is considered an important indicator to describe successional stages and for assessing the type of forest management and the level of naturalness of forest habitat (McElhinny et al., 2005; Uuttera et al., 1998; Ziegler, 2000). In fact, generally the DBH_{mean}

is related to forest stand age (McElhinny et al., 2005; Ziegler, 2000). DBH_{mean} is calculate as

$$\mathrm{DBH_{mean}} = \sqrt{\frac{4G}{\pi n}}$$

where G is the total basal area and *n* is the number of trees in the stand.

The standard deviation of DBH (DBH_{σ}) is a measure of the variability in tree size. It is considered an important indicator of micro-habitat diversity in forest stands (McElhinny et al., 2005; Mura et al., 2015; Ozdemir and Karnieli, 2011). Generally, the high degree of biodiversity is associated to high variation in stem diameters that is related to the presence of different succession stages in a given forest stand (Esseen et al, 1992; Bradsbaw and Lindén, 1997). DBH_{σ} is calculate as

$$\mathrm{DBH_{\sigma}} = \sqrt{\frac{\sum_{i=1}^{n}(DBH_i - \overline{DBH})^2}{n-1}}$$

Where *i* is the tree index, *n* is the number of trees in the plot and $\overline{DBH}$ is the mean plot-level diameter and DBH_i is the diameter of the of *i-th* tree.

Gini coefficient (Gini) is also used for measuring tree size diversity in a forest stand (Lexerød and Eid, 2006; Valbuena et al., 2016). Theoretically, the minimum value of this coefficient is zero when all trees have equal size, while the maximum value is 1 when all trees except one have a value of zero (Meng et al., 2016; Ozdemir and Karnieli, 2011; Valbuena et al., 2016). The index describes tree size inequality for each field plot (Valbuena et al., 2016). Gini coefficient is calculated as

$$\mathrm{Gini} = \frac{\sum_{t=1}^{n}(2t - n - 1)G_t}{\sum_{t=1}^{n} G_t(n-1)}$$

where G_t is the basal area for tree in rank *t* (m^2ha^{-1}) and *t* is the rank of a tree in order from 1,….,n (Meng et al., 2016).

2.2.2.2 Vertical structural complexity indices

The standard deviation of H (H_σ), describes the variation of the trees along the vertical stratum. High variations in tree height are, usually, linked with a variety of tree ages and species in a stand, and can be used as indicator of micro-habitats diversity for wildlife (Bottalico et al., 2017; McElhinny et al., 2005; Mura et al., 2015; Zenner, 2005).

$$\mathrm{H}_\sigma = \sqrt{\frac{\sum_{i=1}^{n}(H_i - \overline{H})^2}{n-1}}$$

Where *i* is the tree index, *n* is the number of trees in the plot and $\overline{H}$ is mean plot-level height and H_i is the height of the *i-th* tree.

2.2.2.3 Combined structural complexity indices

The dominant height (H_{dom}) is an indicator of forest site productivity (Skovsgaard and Vanclay, 2008) and it is calculated as the mean height of the 100 largest trees in terms of DBH per hectares.

The Lory's height (H_l) weights the contribution of trees to the stand height by their basal area. Thus, Lorey's mean height is calculated as:

$$\mathrm{H}_\mathrm{l} = \frac{\sum_{i=1}^{n} G_i * H_i}{G}$$

Where *i*-th is the tree index, *G* is the total basal area in the plot and G_i is the basal area of the i-th tree in the plot and H_i is the height of the *i*-th tree in the plot.

The plot level growing stock volume was calculated on the basis of the equations developed by Tabacchi et al., (2011) in the framework of the 2nd Italian National Forest Inventory based on tree DBH and height.

Table 1: forest structural indices statistical summary from field reference data.

Structural index and Forest biophysical proprieties	Study area	Minimum	Average	Maximum
G [m^2ha^{-1}]	Vallombrosa	13.0	58.9	99
	Rincine	10.2	47.8	69.1
DBH_{mean}[cm]	Vallombrosa	14.4	27.9	37.2
	Rincine	9.6	27.2	46.8
DBH_{σ} [cm]	Vallombrosa	7.5	12.1	22.2
	Rincine	3.4	7.5	15.1
Gini [0,1]	Vallombrosa	0.29	0.46	0.76
	Rincine	0.11	0.33	0.71
H_{dom} [m]	Vallombrosa	11.2	24.8	39.0
	Rincine	12.7	25.1	38.4
H_l [m]	Vallombrosa	6.7	17.1	11.4
	Rincine	9.68	21.3	35.6
H_{σ}[m]	Vallombrosa	2.9	7.1	14.7
	Rincine	1.2	3.7	6.7
V [m^3ha^{-1}]	Vallombrosa	154.2	602.8	1013.2
	Rincine	79.1	495.8	1052.9

2.3 Remotely sensed data

2.3.1 UAV Photogrammetric Data

To acquire aerial images a SenseFly eBee Ag fixed wing UAV equipped with a SONY WX 18.MP RGB camera was used. The UAV flight over Vallombrosa in June 2015 and over Rincine in July 2016, both in leaf-on conditions. In each area, UAV acquisition was completed in one working day.

Before UAV acquisitions, 12 ground control points (GCPs) were placed on the ground in each study area. We used 50 × 50 cm targets with a black and white checkerboard pattern to ensure the largest contrast in

the images. The targets were fixed to the ground in open areas and their coordinates were recorded with a Trimble Geo 7X receiver; data collection lasted for approximately 15 min for each target with a 2-sec logging rate. The recorded coordinates were post-processed with correction data from the nearest ground base station using Pathfinder software. In the two study areas, the post-processed GCP coordinates revealed standard deviations for northing, easting, and height of 0.7 cm, 0.5 cm, and 1.4 cm, respectively.

The flight parameters were the same in the two study areas: flight altitude was 145 m above ground level, the overlap was 85% longitudinal and 75% lateral. The total flight time was 69 minutes in Vallombrosa (169 ha, 1.6 ha/minute) divided into two flights, and 82 minutes in Rincine (290 ha, 3.5 ha/minute) divided into four flights. Flight line spacing was 40 m and the distance between two adjacent photos was 35.7 m. The focal length of the camera was set to 4 mm and the ISO sensibility was ISO-100 with a shutter speed of 1/2000 sec. A total of 228 images were acquired in Vallombrosa and 506 in Rincine with a field of view of 200x150 m.

After visual inspection, the quality of the images acquired in the two study areas was considered good, without any problem related to light and atmospheric conditions, saturation, or blurriness.

Three-dimensional data were extracted from the UAV images using the Agisoft PhotoScan Pro software (Agisoft LLC, 2017).

This software uses Structure from Motion Algorithms and stereo-matching algorithms for image alignment and multi-view stereo reconstruction and it is able to fully automate the photogrammetric workflow to process aerial images and producing 3D and 2D models, which can be exported as georeferenced image based points cloud, Digital Surface Models (DSM) and orthophotos (Agisoft LLC, 2017). This software has been already used for forest analysis (Giannetti et al., 2017; Kachamba et al.,

2016; Lisein et al., 2013; Puliti et al., 2017, 2015; Wallace et al., 2016). In the two study areas, the UAV images were processed as follows: (a) image alignment; (b) mesh building; (c) guided marker positioning and optimization of camera alignment (georeferencing of created scene), (d) dense cloud building and (e) raster grid DSM generation with a resolution of 0.5m x 0.5m. We refer to Puliti et al. (2015) for a detailed description of processing parameters used in Agisoft Photoscan and to Giannetti et al. (submitted) for a detailed description of parameters associated to 3D UAV photogrammetric point-cloud generation. From the SfM photogrammetric work flow we obtained point clouds having a density of 44.25 point m^{-2} in Vallombrosa and 48.36 point m^{-2} in Rincine.

2.3.2 ALS data

In the two study areas the ALS survey was carried out in May 2015 under leaf-on condition using an Eurocopter AS350 B3 equipped with a LiDAR RIEGL LMS-Q680i sensor. The flight height was 1,100 m a.s.l. Full-waveform LiDAR data was registered and discretized to a point density of 10 pts/m^2. Common procedures for pre-processing ALS data (e.g. outliers and noise removal, classification of ground/non-ground, and computation of height on the ground) were carried out with the *LAStools software* (Isenburg, 2017) in order to obtain ALS normalized point clouds. More detailes can be found in Chirici et al. (2017).

3. Methods

3.1 Explanatory variables

To predict forest structure indices, we used a set of photogrammetric DTM-independent predictors variables recently

proposed by Giannetti et al. (2017 submitted) computed just from UAV photogrammetric image base point clouds and DSM. For comparison we calculated more traditionally variables derived from ALS normalized echoes, too.

Both DTM-independent and ALS variables were calculated for each one of the field plots available in the two study areas.

3.1.1 DTM-independent variables from UAV photogrammetric data

DTM-independent predictors variables were calculate in accord with Giannetti et al., (2017 submitted) on the basis of the non-normalized UAV photogrammetric point cloud and raster grid DSM having a resolution of 0.5x0.5 m.

A total of 163 DTM-independent variables were computed. In details, 148 were point cloud variables and 15 were DSM variables.

The point cloud variables were computed on the base of *z*, *z standard*, *intensit*y, *RGB* value and combined *z* and *intensity* (Giannetti et al., submitted).

The DSM variables were calculated on the basis of average and standard deviation statistics of Grey-level co-occurrence matrix textural of mean, variance, homogeneity, contrast, dissimilarity, entropy and second moment (Haralick et al., 1973). In addition, from DSM also the number of local maxima was extracted with a search window of 3x3 pixel, or 1.5x1.5m. A detailed description of the DTM-independent variables used in the current study can be found in Giannetti et al. (submitted). The DTM-independent variables were computed using the R-CRAN package lidR (Roussel, 2017).

A summary of DTM-independent variables is provided in table 2 and 3.

Table 2: Point clouds DTM-independents variables (Giannetti et al., 2017, in review).

Explanatory variables	Description
sd_z	*z* standard deviation
kur_z	*z* kurtosis (Davies and Goldsmith, 1984; McGaughey, 2014)
ske_z	*z* skewness (Davies and Goldsmith, 1984; McGaughey, 2014)
AAD_z	*z* median absolute deviation (McGaughey, 2014)
range_z	Difference between maximum and minimum *z* values
entropy	*z* normalized Shannon diversity index (*entropy*) (Pretzsch, 2009; Shannon, 1948)
z_d1, z_d2,..., z_d9, z_d10	*z* density variables defined as tenths of the distance between the 100th percentile and the lowest *z* value.
z_{st}*_sum*	Sum of z_{st} values
z_p1, z_p2, ..., z_ p95, z_p100	Percentile of 10, 20, 30, 50, 60, 70, 80, 90, 95, 100 z_{st} distribution
max_i	*Intensity* maximum value
min_i	*Intensity* minimum value
avg_i	*Intensity* average value
sd_i	*Intensity* standard deviation
kur_i	*Intensity* kurtosis (Davies and Goldsmith, 1984; McGaughey, 2014)
ske_i	*Intensity* skewness (Davies and Goldsmith, 1984; McGaughey, 2014)
AAD_i	*Intensity* median absolute deviation (McGaughey, 2014)
range_i	Difference between maximum and minimum *Intensity* values
entropy_i	*Intensity* normalized Shannon diversity index (*entropy*) (Pretzsch, 2009; Shannon, 1948)
i_quart_1; i_quart_2; i_quart_3;i_quart_4	Quartile of 25, 50, 75, 100 intensity distribution
i_d1, i_d2, i_d3, i_d4	*Intensity* density calculated for equally intensity layers, defined as quarters of the distance between the 100th percentile and the lowest intensity value.
i_1q_p1,....., i_1q_p100	*z* percentiles of 1st intensity quartiles
Explanatory variables	**Description**
i_1_p50/p25	Ratio between *i_1q_p50/i_1q_p25*
i_2q_p1,....., i_2q_p100	*z* percentiles of 2nd intensity quartiles
i_2_p50/p25	Ratio between *i_2q_p50/i_2q_p25*
i_3q_p1,....., i_3q_p100	*z* percentiles of 3rd intensity quartiles
i_3_p50/p25	Ratio between *i_3q_p50/i_3q_p25*
i_4q_p1,....., i_4q_p100	*z* percentiles of 4th intensity quartiles
i_4_p50/p25	Ratio between *i_4q_p50/i_4q_p25*
i_1q_d1,....., i_1q_d10	*z* density variables of 1st intensity quartiles
i_2q_d1,....., i_2q_d10	*z* density variables of 2nd intensity quartiles
i_3q_d1,..., i_3q_d10	*z* density variables of 3rd intensity quartiles
i_4q_d1,..., i_4q_d10	*z* density variables of 4th intensity quartiles
mean_R, mean_G, mean_B, mean_NIR	Mean value of *R*, *G*, *B* and *NIR* bands

min_R, min_G, min_B, min_NIR	Minimum value of *R*, *G*, *B* and *NIR* bands
max_R, max_G, max_B, max_NIR	Maximum value of *R*, *G*, *B* and *NIR* bands
sd_R, sd_G, sd_B, sd_NIR	Standard deviation of *R*, *G*, *B* and *NIR* bands

Table 3: DSM DTM-independent variables (Giannetti et al., 2017, in rewiev).

Explanatory variables	Description
AVG_mean	Average of GLCM *mean* textural (Haralick et al., 1973)
SD_mean	Standard deviation of GLCM *mean* textural (Haralick et al., 1973)
AVG_variance	Average of GLCM *variance* textural (Haralick et al., 1973)
SD_variance	Standard deviation of GLCM *variance* textural (Haralick et al., 1973)
AVG_ homogeneity	Average of GLCM *homogeneity* textural (Haralick et al., 1973)
SD_ homogeneity	Standard deviation of GLCM *homogeneity* textural (Haralick et al., 1973)
AVG_ contrast	Average of GLCM *contrast* textural (Haralick et al., 1973)
SD_ contrast	Standard deviation of GLCM *contrast* textural (Haralick et al., 1973)
AVG_ dissimilarity	Average of GLCM *dissimilarity* textural (Haralick et al., 1973)
SD_ dissimilarity	Standard deviation of GLCM *dissimilarity* textural (Haralick et al., 1973)
AVG_ entropy	Average of GLCM *entropy* textural (Haralick et al., 1973)
SD_ entropy	Standard deviation of GLCM *entropy* textural (Haralick et al., 1973)
AVG_ second moment	Average of GLCM *second moment* textural (Haralick et al., 1973)
SD_ second moment	Standard deviation of GLCM *second moment* textural (Haralick et al., 1973)
num_max	Number of local maxima

3.1.2 ALS echoes variables

We calculated 32 echo-based predictors variables on the basis of DTM normalized ALS data.

The variables we used are those most typically used for forest estimations (Leas et al., 2011) and included three types of predictors: statistical (McGaughey, 2010), height, and density (Naesset et al., 2004).

The variables were computed using the R-CRAN package lidR (Roussel, 2017).

A summary of ALS explanatory variables is provided in Table 4.

Table 4: ALS echoes variables.

DTM dependent metrics	Descriptive feature
tot	Total Number of point
min	Minimum
max	Maximum
avg	Average
range	Range
sd	Standard deviation
var	Variance
cv	Coefficient of variation
iq	Interquantile distance
sk	Skewness (Davies and Goldsmith, 1984; McGaughey, 2010)
ku	Kurtosis (Davies and Goldsmith, 1984; McGaughey, 2010)
aad	Average absolute deviation (McGaughey, 2010)
p1, p2, ..., p95, p100	percentile of 10, 20, 30, 50, 60, 70, 80, 90, 95, 100 h distribution
p99/p25	Ratio of percentiles
p99/p50	Ratio of percentiles
p99/p75	Ratio of percentiles
d1, d2,….,d9,d10	proportion of points above the 1^{st},…,10^{th} fraction to the total number of points (cutoff=1.30)

3.2 Model development

Multiple linear regression models were used because of their simplicity and efficiency to characterize the relationship between forest attributes and predictors variables from RS (Bottalico et al., 2017; Giannetti et al., 2017; Mura et al., 2015; Puliti et al., 2015).

It is important to note that our aim was to compare the performance of UAV DTM-independent variables versus traditionally ALS echoes variables for predicting forest structural diversity indicators. Not to obtain the best absolute predictions that can be probably reached with more advanced non-parametric methods such as K-nearest neighbors (Chirici et al., 2016) or Random Forest (Yu et al., 2011).

To fit the models we used each forest structure indices as response variables and as independent variables the two set of RS predictors variables from RS: DTM-independent and ALS echoes.

First of all, a correlation analyses between the metrics was carried out to check for the mutually correlated variables using Person's product moment correlation (r) matrix. In case of two metrics with r>0.85 only the one that is at least less correlated with other metrics were used in the models as independent variables.

The best combination of explanatory variables was selected using a subset regression procedure using a branch-and-bound algorithm (Clausen, 1999). The algorithm was addressed to optimize the *Adjusted* R^2 *(Adj.* R^2*)* for each possible predictors combination. The algorithm was set to find at least five explanatory variables that maximized the *Adj.* R^2, searching for one-variable model, two-variables model until five-variables models. This configuration was chased because models that have many predictors usually have a great R^2 but might suffer of overfitting. We chosed the simplest models (those with the smallest number of predictors) because such models are easier to understand and to be evaluated in replicated and cross-validation studies.

The accuracy of the predictions was calculated at plot level on the basis of a Leave-One-Out cross validation approach (LOO). The LOO was carried out by leaving out each *i*th plot iteratively, the model was fitted using the remaining plots.

The selected models were evaluate using the LOO procedure by means of *Adj.* R^2, root mean square error (*RMSE*), relative root mean square error ($RMSE_{\%}$), mean difference (*MD*) and relative mean difference ($MD_{\%}$) and were calculate as:

$$MD = \frac{\sum_{i=1}^{n}(\hat{y}_i - y_i)}{n}$$

$$RMSE = \sqrt{\frac{\sum_{i=1}^{n}(\hat{y}_i - y_i)^2}{n}}$$

Where, $\hat{y}_i$ is the predicted value for the *i-th* plot, y_i is the observed value for the *i-th* plot, *n* is the number of plots. The relative RMSE ($RMSE_{\%}$) was calculated as the percentage of RMSE on the average measured value of the variable in the plot.

3.3 Spatial predictions

We used DTM-independent models, developed as reported in the section 3.2. to create spatial predictions (maps) of the selected diversity indices in the two areas.

The gridded maps are calculated for 23 m x 23 m pixels that mimic the plot area in both the study areas.

4. Results

4.1. Regression Models

Individual models were developed for each of the different set of predictors (UAV DTM-independent vs ALS echoes), for each response variable (the eight indices G, DBH_{mean}, DBH_{σ}, Gini, H_{σ}, H_{dom}, H_I and V) and in both the study areas. The number of explanatory variables selected by the branch-and-bound algorithm ranged between 1 and 5 for both DTM-independent (Table 3) and ALS models (Table 4). DTM-independent models reveled a better fit in Vallombrosa with *Adj.* R^2 ranging between 0.58 and 0.79, compared to Rincine where it ranged between 0.38 and 0.65.

In Vallombrosa the DTM-independent variables resulted in consistently larger *Adj.* R^2 for G, DBH_{mean}, Gini, H_σ , while ALS variables resulted higher *Adj.* R^2 for H_l, while comparable results between the two set of predictors were observed for V, H_{dom}, and DBH_σ (Table 4 and Table 5). In Rincine, among the two sets of variables, DTM-independent variables produced more accurate results with higher *Adj.* R^2 for DBH_σ while ALS resulted in higher *Adj.* R^2 for G, $H_{dom,}$ and H_l. In Rincine comparable results between the two set of variables were observed for GC, $H_{\sigma,}$ and V (Table 5 and 6). The LOO of the selected models revealed that the differences in predictive accuracy in terms of $RMSE_{\%}$ between DTM-independent and ALS models in Vallombrosa ranged between -4.65% and 3.79% while in Rincine ranged between -3.51% and 7.02% (Figure 2).

In all the selected models MD values were relatively small, never higher than 1.3% of the mean reference value measured in the field whit the two-side *t-test* that revealed MD values as never statistically significant (*p-values*≥ 0.82).

The analysis of the residuals revealed no violation of the assumptions of linearity, normality of the residuals, homoscedasticity, and independence for any of the models. The NCV test, the Kolmogorov Smirnov and the Durbin-Watson tests always resulted in *p-values* > 0.05. The assumption are confirmed, also, by the visual analysis of the scatterplot of the field reference against the LOOCV predicted values (Figure 3).

Table 5: variables selections and model accuracies, in terms of RMSE, RMSE% and Adj.R2, for the multiple regression models using as predictors the UAV DTM-independent variables.

Structural index	Study Area	DTM-independent variables	RMSE	RMSE%	Adj. R^2
G [m^2ha^{-1}]	Vallombrosa	*zsd+i_4q_d10+num_max*	7.5	12.8	0.76
	Rincine	*AAD_B+P99P75*	12.9	26.7	0.40

DBH_{mean} [cm]	Vallombrosa	*I_4q_d10+d10+AVG_homogeneity+AVG_mean+num_max*	4.2	15.1	0.66
	Rincine	*I_2q_d5+I_1q_p2*	5.3	19.7	0.71
DBH_{σ} [cm]	Vallombrosa	*z_st_p10+I_2q_p100+p100+SD_entropy+AVG_homogeneity*	2.8	23.2	0.61
	Rincine	*entropy_B+SD_dissimilarity+SD_homogeneity+AVG_dissimilarity+all*	1.7	23.2	0.50
Gini [0,1]	Vallombrosa	*I_2q_d10+AVG_contrast+i_4_p75_p25+i_3_p75_p25+i_1_p75_p25*	0.09	19.1	0.58
	Rincine	*VCI_R+mean_G+SD_homogeneity+d8*	0.07	23.3	0.65
H_{dom} [m]	Vallombrosa	*I_2q_d10+AVG_homogeneity+i_d2+i_mean+i_3_p75_p25*	2.4	33.7	0.40
	Rincine	*AAD+mean_R+SD_mean+d7+qav+d3*	1.0	29.0	0.38
H_I [m]	Vallombrosa	*I_4q_p95+num_max+AVG_homogeneity+AVG_dissimilarity*	3.3	13.5	0.70
	Rincine	*AVG_entropy+SD_entropy+p7+AVG_contrast*	4.0	15.0	0.60
H_{σ} [m]	Vallombrosa	I_ske+i2q_d10+min_B+num_max+ AVG_homogeneity	3.1	15.9	0.64
	Rincine	SD_homogeneity+p7	3.7	16.9	0.65
V [$m3ha^{-1}$]	Vallombrosa	I_quant_1+i_1q_d5+num_max+ AVG_homogeneity	96.1	15.9	0.79
	Rincine	I_1q_p5	122.2	24.3	0.78

Table 6: variables selections and model accuracies, in terms of RMSE, RMSE% and Adj.R2, for the multiple regression models using as predictors the ALS variables.

Structural index	Study Area	ALS variables	RMSE	RMSE%	Adj. R^2
G [m^2ha^{-1}]	Vallombrosa	*p10*	9.40	16.39	0.54
	Rincine	*d7+d8+d9+CV*	9.84	20.58	0.69
DBH_{mean} [cm]	Vallombrosa	*p99*	5.01	18.18	0.39
	Rincine	*p9+all*	4.84	17.80	0.72
DBH [cm]	Vallombrosa	*std+kur+b30+b80*	2.76	22.83	0.61
	Rincine	*p9+d1+CV+AAD+avg*	2.01	26.72	0.42
Gini [0,1]	Vallombrosa	*d2*	0.11	23.79	0.25
	Rincine	*d1+d6+CV*	0.073	22.55	0.71
H_{dom} [m]	Vallombrosa	*p10+d6*	2.13	29.97	0.56
	Rincine	*d3+d2+d1+CV*	1.04	28.56	0.33

H_l	Vallombrosa	*p5*	3.49	14.08	0.71
[m]	Rincine	*p95*	2.44	9.71	0.87
H_σ	Vallombrosa	*p75*	3.01	15.34	0.73
[m]	Rincine	*p95*	2.11	9.90	0.91
V	Vallombrosa	*p5*	100.81	16.72	0.79
[m^3ha^{-1}]	Rincine	*p5*	122.29	24.66	0.76

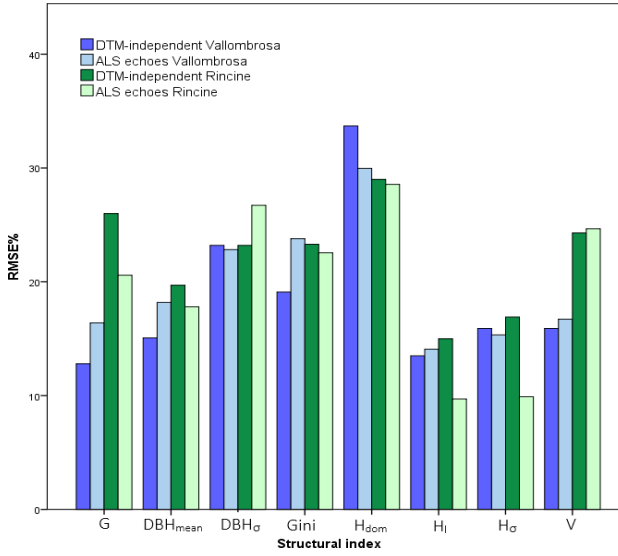

Figure 2: study areas reporting the forest types and the simple plots.

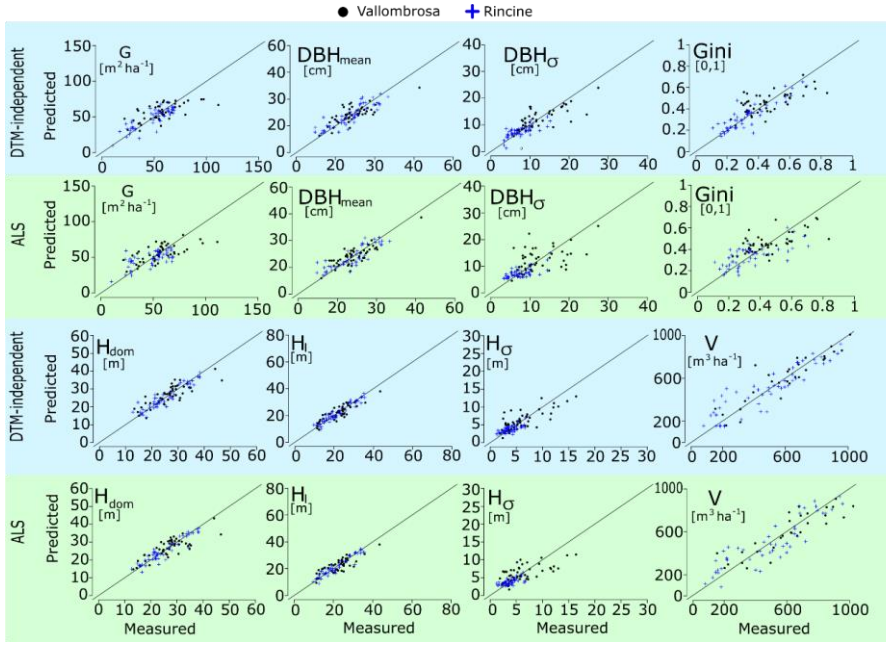

Figure 3: Scatterplot of measured versus predicted values for the models using UAV DTM-independent variables (light blue background) and ALS echoes variables (light green blackground). Black dots represent Vallombrosa while blue crosses are for Rincine.

4.2 Maps

To give an example of the possible application of DTM-independent variables to produce maps to support forest management and biodiversity monitoring we applied the models from Table 3 to create spatially continuous estimations of the 8 indicators in the two study areas (Figure 4). These mapped indices are widly used in forest management for ecological propose and biodiversity monitoring (McElhinny et al., 2005).

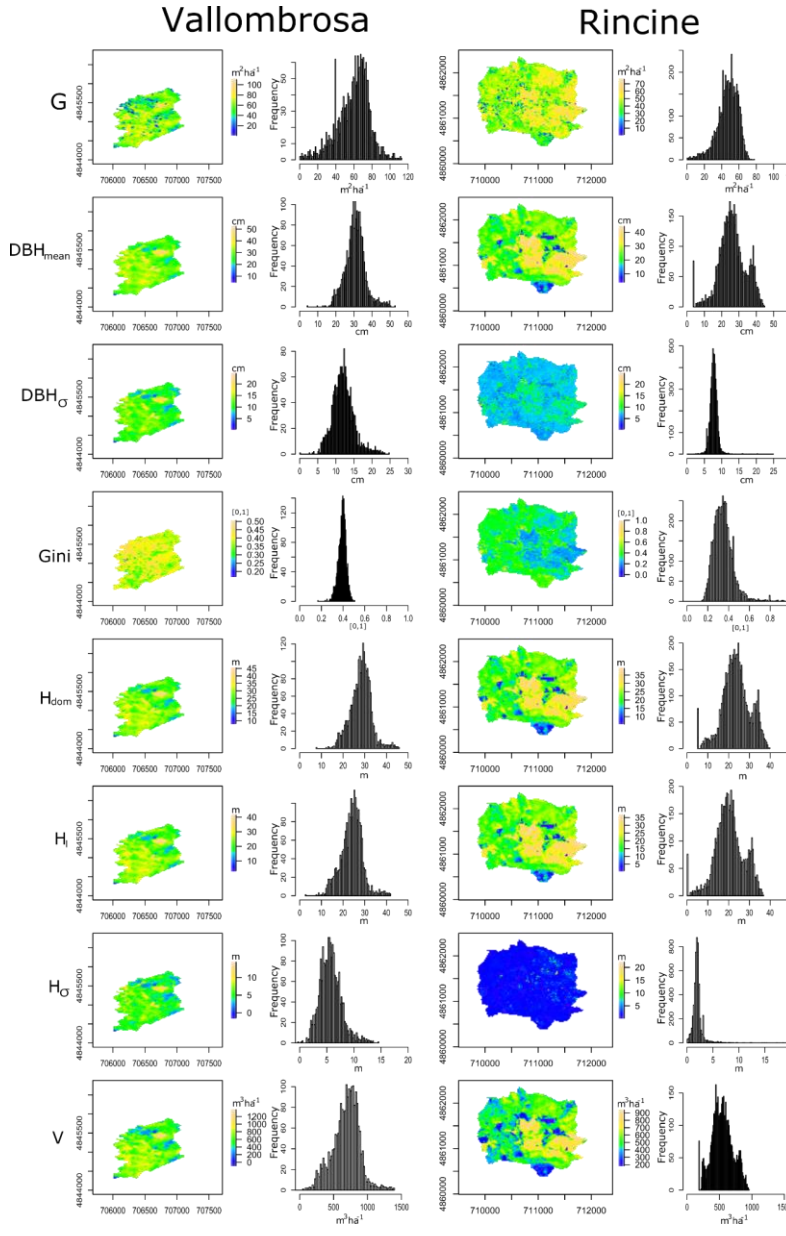

Figure 4: maps and histograms of the eight structure indices calculate on the basis of models based on UAV DTM-independent variables for the two study areas: on the left Vallombrosa on the right Rincine.

5. Discussion

The current study assesses the use of DTM-independent explanatory variables (Giannetti et al., in review) calculate from 3D UAV photogrammetric data to model and map eight forest structure complexity indices (*G,* DBH_{mean}, $DBH_{\sigma,}$ Gini, H_{σ}, H_{dom} $H_{I,}$ and V) in two mixed temperate forests characterized by different types of management systems. The Vallombrosa forest which is mainly left to natural evolution and the Rincine district that is actively managed with a sustainable forest management approach. To the authors' knowledge, the present study is the first one where DTM-independent variables from UAV photogrammetric data are used to model forest structure indices and the first where DTM-independent models are used to create spatial predictions of the feature variables.

The current discussion is focused on comparing the accuracy derived by DTM-independent models in relation to the benchmark method based on ALS data and on comparing the results obtained by previous research in modelling forest structure indices using different types of predictors.

Among the two types of forests, DTM-independent models produced comparable results in terms of *Adj.* R^2 (i.e. Vallombrosa: $0.40 \leq Adj.\ R^2 \leq 0.79$; Rincine: $0.38 \leq Adj.\ R^2 \leq 0.78$), but in terms of $RMSEs_{\%}$ more accurate results were observed in Vallombrosa ($12.81\% \leq RMSE_{\%} \leq 23.29\%$) comparing to those retrieved in Rincine ($15.06\% \leq RMSE_{\%} \leq 29.00\%$) (Figure 3).

In both the areas DTM-independent models produced accurate results in modelling the growing stock volume (Table 3 and Figure 3), even if the models based on ALS achieved slighter better results (Table 4 and Figure 3). In terms of $RMSE_{\%}$, the accuracy of DTM-independent models for both study areas (i.e. Vallombrosa= 15.95% and Rincine=24.34%) is in the

range of previously reported studies based on ALS variables for which $RMSE_{\%}$ typically ranged between 16.7% and 30% (Barbati et al., 2009; Bottalico et al., 2017; Corona and Fattorini, 2008; Tonolli et al., 2011).

Among the two types of forests, DTM-independent models produced more accurate results in terms of $RMSE_{\%}$ and *Adj.* R^2 for G, DBH_{mean}, Gini, and H_{dom} in Vallombrosa and for σ_{dbh} in Rincine comparing to the ones obtained by ALS.

Moreover, the accuracy obtained in the current study using DTM-independent models, in both study areas, was higher or comparable for G, DBH_{mean} DBH_{σ}, H_{σ}, and H_{dom} with those obtained with ALS variables by Bottalico et al., (2017) in a Mediterranean forest and those obtained by Mura et al., (2015) in a temperate forest. For Gini structure indices, the accuracy of DTM-independent models in terms of $RMSE_{\%}$ (Table 3 and 4) is in line with the ones obtained by Valbuena et al., (2016), with ALS variables, in two boreal forests: one unmanaged for conservation purpose (i.e. $RMSE_{\%}$= 20.24%), and one used for maximizing commercial economic returns (i.e. $RMSE_{\%}$= 18.78%). For Gini structure indices, with DTM-independent predictors we obtained better results in Vallombrosa compared to those from Rincine in contrast with the finding of Valbuena et al., (2016). Moreover, we found that the Gini DTM-independent model in Vallombrosa produced an $RMSE_{\%}$ that is 4.65% points lower than those obtained by ALS model, while comparable results between DTM-independent and ALS models were observed in Rincine.

For the indices related to tree height (i.e. H_{dom}, $H_{l,\ and}$ σ_h) ALS produced always better results comparing to those obtained by DTM-independent models. These results were expected because normalized ALS metrics are directly related with tree heights.

We found that the DTM-independent models produced consistent results in monitoring forest structure variables across two different types of management systems also if the variations in forest management lead to some differences in the structural properties of forests (Lilja and Kuuluvainen, 2005; Uuttera et al., 1998).

Adopting the conservative and simple modelling approach based on multiple linear regressions with the lower number of predictors we observed comparable results with the one obtained with more complex exponential and power models (Valbuena et al., 2016; González-Ferreiro et al., 2012). It seems that DTM-independent variables are good predictors for forest structure modelling. The DTM-independent models were also useful to create maps of forest structure indices that can be used for forest management propose. The maps were derived using DTM-independent models of the eight forest structure indices considered in this study in both the study areas.

Comparing the maps of DBHσ, and Hσ indices across the two study areas (Figure 4), it is possible to note that the variability in vertical and horizontal stratum is higher in Vallombrosa than Rincine. These results could be expected because of the different forest management regimes adopted in the two study areas. As reported by Lexerød and Eid, (2006) if tree size diversity in low, almost all trees became mature for productive purpose at the same time, while large tree size diversity ensure a wide range of habitats providing a high level of biodiversity. The maps developed in this study allowed a comprehensive spatially analysis of the structure variability between two temperate mixed forests. Moreover, these indices are often adopted for forest biodiversity monitoring and several authors have underlined how these types of maps are useful to take better decision in the framework of sustainable forest management, forest certification

purposes and for precision forestry (Corona et al., 2017; Valbuena et al., 2016). Moreover, UAV photogrammetric data are less expensive than ALS data and thus they can be more frequently acquired for multitemporal forest ecosystem trend analysis.

6. Conclusion

Several conclusions can draft from this study:

- UAV DTM-independent variables are good predictors for modelling forest structure indices confirming the results obtained by Giannetti et al., (submitted) for growing stock volume modelling.
- UAV DTM-independent models can be used to create maps with spatial predictions of forest structure indices useful for supporting forest management and precision forestry.
- UAV DTM-independent maps can be useful to compare the variability different between different forests.

Authors contributions

Francesca Giannetti designed the experiment, data processing and wrote the manuscript. Francesca Giannetti and Nicola Puletti perfomed the statistical analysis. Davide Travaglini and Gherardo Chirici designed the field sampling schemes. Stefano Puliti, Nicola Puletti, Gherardo Chirici and Davide Travaglini co-authored and revised the manuscript.

Acknowledgments

This research was supported by the LIFE program in the framework of the project "FRESh LIFE—Demonstrating Remote Sensing integration in sustainable forest management" (LIFE14 ENV/IT/000414) and in part by Accademia Italiana di Scienze Forestali in the framework of PhD Student Scholarship given to Francesca Giannetti.

We wish to thank Andrea Barzagli, Barbara Del Perugia and Marta Galluzzi for the fieldwork in Rincine District and all the graduating students of the University of Florence for the help in fieldwork data acquisition in the Vallombrosa forest.

References

Agisoft LLC, 2017. Agisoft PhotoScan User Manual. Available online http://www.agisoft.com/pdf/photoscan-pro_1_3_en.pdf (accessed on 11 April 2017).

Arabatzis, G., 2010. Development of Greek forestry in the framework of the European Union policies. Journal of Environmental Protection and Ecology 11, 682–692.

Barabesi L., Franceschi S. (2011). Sampling properties of spatial total estimators under tessellation stratified designs. Environmetrics 22, 271–278, http://dx.doi.org/10.1002/env.1046.

Barabesi L., Franceschi S., Marcheselli M. (2012). Properties of design-based estimation under stratified spatial sampling with application to canopy coverage estimation. The Annals of Applied Statistics, 6 (1): 210–228. doi: 10.1214/11-AOAS509.

Barbati, A., Chirici, G., Corona, P., Montaghi, A., Travaglini, D., 2009. Area-based assessment of forest standing volume by field measurements and airborne laser scanner data. International Journal of Remote Sensing 30, 5177–5194. doi:10.1080/01431160903023017

Bohlin, J., Wallerman, J., Fransson, J.E.S., 2012. Forest variable estimation using photogrammetric matching of digital aerial images in combination with a high-resolution DEM. Scandinavian Journal of Forest Research 27, 692–699. doi:10.1080/02827581.2012.686625

Bottalico, F., Chirici, G., Giannini, R., Mele, S., Mura, M., Puxeddu, M., McRoberts, R.E., Valbuena, R., Travaglini, D., 2017. Modeling Mediterranean forest structure using airborne laser scanning data. International Journal of Applied Earth Observation and Geoinformation 57, 145–153. doi:10.1016/j.jag.2016.12.013

Bottalico, F., Travaglini, D., Fiorentini, S., Lisa, C., Nocentini, S., 2014. Stand dynamics and natural regeneration in silver fir (Abies alba Mill.) plantations after traditional rotation age. iForest - Biogeosciences and Forestry 7, 313–323. doi:10.3832/ifor0985-007

Bruniquel-Pinel, V., Gastellu-Etchegorry, J.P., 1998. Sensitivity of texture of high resolution images of forest to biophysical and acquisition parameters. Remote Sensing of Environment 65, 61–85. doi:10.1016/S0034-4257(98)00009-1

Chirici, G., Mura, M., McInerney, D., Py, N., Tomppo, E.O., Waser, L.T., Travaglini, D., McRoberts, R.E., 2016. A meta-analysis and review of the literature on the k-Nearest Neighbors technique for forestry applications that use remotely sensed data. Remote Sensing of Environment 176, 282–294. doi:10.1016/j.rse.2016.02.001

Corona, P., Chianucci, F., Quatrini, V., Civitarese, V., Clementel, F., Costa, C., Floris, A., Menesatti, P., Puletti, N., Sperandio, G., Verani, S., Turco, R., Bernardini,

V., Plutino, M., Scrinzi, G., 2017. Precision forestry: concepts, tools and perspectives in Italy. Forest@ - Rivista di Selvicoltura ed Ecologia Forestale 14, 1–12. doi:10.3832/efor2285-014

Corona, P., Fattorini, L., 2008. Area-based lidar-assisted estimation of forest standing volume. Canadian Journal of Forest Research 38, 2911–2916. doi:10.1139/X08-122

Davies, O.L., Goldsmith, P.L., 1984. Statistical methods in research and production : with special reference to the Chemical Industry, Longman. ed. London.

European Environmental Agency, 2012. Streamlining European biodiversity indicators 2020: Building a future on lessons learnt from the SEBI 2010 process. EEA Technical report No 11/2012, Copenhagen, 2012.

European Union, 2011. Q & A on the Communication an EU biodiversity strategy to 2020 1–13.

Fardusi, M.J., Chianucci, F., Barbati, A., 2017. Concept to Practices of Geospatial Information Tools to Assist Forest Management and Planning under Precision Forestry Framework : a review 41, 3–14.

Fotakis, D., Sidiropoulos, E., Myronidis, D., Ioannou, K. (2012) Spatial genetic algorithm for multi-objective forest planning. Forest Policy and Economics, 21, 12–19

Franklin, J.F., 1988. Structural and functional diversity in temperate forests. In: Wilson, E.O. (Ed.), Biodiversity. National Academy Press, Washington, D.C., pp. 166–175

Giannetti, F., Chirici, G., Gobakken, T., Næsset, E., Travaglini, D., Puliti, S., submitted 2017. Development and assessment of DTM-independent variables for prediction of forest biophysical properties using UAV photogrammetric data. submitted.

Gobakken, T., Bollandsås, O.M., Næsset, E., 2015. Comparing biophysical forest characteristics estimated from photogrammetric matching of aerial images and airborne laser scanning data. Scandinavian Journal of Forest Research 30, 73–86. doi:10.1080/02827581.2014.961954

Gómez, C., Wulder, M.A., Montes, F., Delgado, J.A., 2012. Forest structural diversity characterization in Mediterranean pines of central Spain with QuickBird-2 imagery and canonical correlation analysis. Canadian Journal of Remote Sensing 37, 628–642. doi:10.5589/m12-005

Halaj, J.; Ross, D.W., Moldenke A.R. (2000) -Importance of habitat structure to the arthropod food-web in Douglas-fir canopies. Oikos, 90 (1) (2000), pp. 139–152

Haralick, R.M., Shanmugam, K., Dinstein, I., 1973. Textural Features for Image Classification.

Hunter, M.L., 1999. Maintaining Biodiversity in Forest Ecosystems. Cambridge. University Press, Cambridge, UK

International Model Forest Network (IMFN), 2008. Guide to Model Forest Governance.
Kachamba, D., Ørka, H., Gobakken, T., Eid, T., Mwase, W., 2016. Biomass Estimation Using 3D Data from Unmanned Aerial Vehicle Imagery in a Tropical Woodland. Remote Sensing 2016, Vol. 8, Page 968 8, 968. doi:10.3390/RS8110968
Kurttila, M., 2001. The spatial structure of forests in the optimization calculations of forest planning - A landscape ecological perspective. Forest Ecology and Management 142, 129–142. doi:10.1016/S0378-1127(00)00343-1
Lexerød, N.L., Eid, T., 2006. An evaluation of different diameter diversity indices based on criteria related to forest management planning. Forest Ecology and Management 222, 17–28. doi:10.1016/j.foreco.2005.10.046
Lilja, S., Kuuluvainen, T., 2005. Structure of old Pinus sylvestris dominated forest stands along a geographic and human impact gradient in mid-boreal Fennoscandia. Silva Fennica 39, 407–428. doi:10.14214/sf.377
Lisein, J., Pierrot-Deseilligny, M., Bonnet, S., Lejeune, P., 2013. A photogrammetric workflow for the creation of a forest canopy height model from small unmanned aerial system imagery. Forests 4, 922–944. doi:10.3390/f4040922
McElhinny, C., Gibbons, P., Brack, C., Bauhus, J., 2005. Forest and woodland stand structural complexity: Its definition and measurement. Forest Ecology and Management 218, 1–24. doi:10.1016/j.foreco.2005.08.034
McGaughey, R.J., 2014. FUSION/LDV: Software for LIDAR Data Analysis and Visualization 154.
McGraw, S. (1994) Census, habitat preference, and polyspecific associations of six monkeys in the Lomako Forest, Zaire. American Journal of Primatology, 34 (4) (1994), pp. 295–307
Meng, J., Li, S., Wang, W., Liu, Q., Xie, S., Ma, W., 2016. Estimation of forest structural diversity using the spectral and textural information derived from SPOT-5 satellite images. Remote Sensing 8. doi:10.3390/rs8020125
J. Müller, J. Stadler, R. Brandl (2010) - Composition versus physiognomy of vegetation as predictors of bird assemblages: The role of Lidar. Remote Sensing of Environment, 114 (3) (2010), pp. 490–495
Mura, M., McRoberts, R.E., Chirici, G., Marchetti, M., 2015. Estimating and mapping forest structural diversity using airborne laser scanning data. Remote Sensing of Environment 170, 133–142. doi:10.1016/j.rse.2015.09.016
Niemi, M., Vauhkonen, J., 2016. Extracting Canopy Surface Texture from Airborne Laser Scanning Data for the Supervised and Unsupervised Prediction of Area-Based Forest Characteristics. Remote Sensing 8, 582. doi:10.3390/rs8070582
Noss, R.F., 1990. Indicators for monitoring biodiversity: A hierarchical approach.

Conserv. Biol. 4, 355±364.
Ozdemir, I., 2008. Estimating stem volume by tree crown area and tree shadow area extracted from pansharpened Quickbird imagery in open Crimean juniper forests. International Journal of Remote Sensing 29, 5643–5655. doi:10.1080/01431160802082155
Ozdemir, I., Donoghue, D.N.M., 2013. Modelling tree size diversity from airborne laser scanning using canopy height models with image texture measures. Forest Ecology and Management 295, 28–37. doi:10.1016/j.foreco.2012.12.044
Ozdemir, I., Karnieli, A., 2011. Predicting forest structural parameters using the image texture derived from worldview-2 multispectral imagery in a dryland forest, Israel. International Journal of Applied Earth Observation and Geoinformation 13, 701–710. doi:10.1016/j.jag.2011.05.006
Pretzsch, H., 2009. Forest Dynamics, Growth and Yield. doi:http://doi.org/10.1007/978-3-540-88307-4
Puliti, S., Gobakken, T., Ørka, H.O., Næsset, E., 2017. Assessing 3D point clouds from aerial photographs for species-specific forest inventories. Scandinavian Journal of Forest Research 32:1, 68–79. doi:10.1080/02827581.2016.1186727
Puliti, S., Olerka, H., Gobakken, T., Næsset, E., 2015. Inventory of Small Forest Areas Using an Unmanned Aerial System. Remote Sensing 7, 9632–9654. doi:10.3390/rs70809632
R.E. Salter, N.A. Mackenzie, N. Nightingale, K.M. Aken, P.K.P. Chai (1985) Habitat use ranging behavior and food habits of the proboscis monkey nasalis-larvatus in Sarawak. Primates, 26 (4) (1985), pp. 436–451
R. Shine, E.G. Barrott, M.J. Elphick (2002) - Some like it hot: effects of forest clearing on nest temperatures of montane reptiles. Ecology, 83 (10) (2002), pp. 2808–2815
Seitz B., Katzel R., Kowarik I., Schulz P.M. Method for identifying and recording harvest stands of regional provenances of indigenous woody species. Allg. Forst. Jagdztg. 2008;179:70–76
Shannon, C.E., 1948. A mathematical theory of communication. The Bell System Technical Journal 27, 379–423. doi:10.1145/584091.584093
Skovsgaard, J.P., Vanclay, J.K., 2008. Forest site productivity: A review of the evolution of dendrometric concepts for even-aged stands. Forestry 81, 13–31. doi:10.1093/forestry/cpm041
Tabacchi, G., Di Cosmo, L., Gasparini, P., Morelli, S., 2011. Stima del volume e della fitomassa delle principali specie forestali italiene, Equazioni di previsione, tavole del volume e tavole della fitomassa arborea epigea.
Teobaldelli, M., Cona, F., Saulino, L., Migliozzi, A., D'Urso, G., Langella, G., Manna, P., Saracino, A., 2017. Detection of diversity and stand parameters in Mediterranean forests using leaf-off discrete return LiDAR data. Remote

Sensing of Environment 192, 126–138. doi:10.1016/j.rse.2017.02.008
Tonolli, S., Dalponte, M., Vescovo, L., Rodeghiero, M., Bruzzone, L., Gianelle, D., 2011. Mapping and modeling forest tree volume using forest inventory and airborne laser scanning. European Journal of Forest Research 130, 569–577. doi:10.1007/s10342-010-0445-5
Uuttera, J., Haara, A., Tokola, T., Maltamo, M., 1998. Determination of the spatial distribution of trees from digital aerial photographs. Forest Ecology and Management 110, 275–282. doi:10.1016/S0378-1127(98)00292-8
Valbuena, R., Eerik??inen, K., Packalen, P., Maltamo, M., 2016. Gini coefficient predictions from airborne lidar remote sensing display the effect of management intensity on forest structure. Ecological Indicators 60, 574–585. doi:10.1016/j.ecolind.2015.08.001
Wallace, L., Lucieer, A., Malenovský, Z., Turner, D., Vopěnka, P., 2016. Assessment of forest structure using two UAV techniques: A comparison of airborne laser scanning and structure from motion (SfM) point clouds. Forests 7, 1–16. doi:10.3390/f7030062
H.H. Welsh, A.J. Lind (1996) - Habitat correlates of the southern torrent salamander, Rhyacotriton variegatus (Caudata: Rhyacotritonidae), in northwestern California. Journal of Herpetology, 30 (3) (1996), pp. 385–398
Winter, S., Chirici, G; McRoberts, R.E., Hauk, E.,Tomppo E. (2008)- Possibilities for harmonizing national forest inventory data for use in forest biodiversity assessments. Forestry, 81 (1) (2008), pp. 33–44
Yu, X., Hyyppä, J., Vastaranta, M., Holopainen, M., Viitala, R., 2011. Predicting individual tree attributes from airborne laser point clouds based on the random forests technique. ISPRS Journal of Photogrammetry and Remote Sensing 66, 28–37. doi:10.1016/j.isprsjprs.2010.08.003
Zahawi, R.A., Dandois, J.P., Holl, K.D., Nadwodny, D., Reid, J.L., Ellis, E.C., 2015. Using lightweight unmanned aerial vehicles to monitor tropical forest recovery. Biological Conservation 186, 287–295. doi:10.1016/j.biocon.2015.03.031
Zellweger, F.; Braunisch, V.; Baltensweiler A.; Bollmann K. (2013) - Remotely sensed forest structural complexity predicts multi species occurrence at the landscape scale. Forest Ecology and Management 307 (2013) 303–312. http://dx.doi.org/10.1016/j.foreco.2013.07.023
Zenner, E.K., 2005. Investigating scale-dependent stand heterogeneity with structure-area- curves. Forest Ecology and Management 209, 87–100. doi:10.1016/j.foreco.2005.01.004
Ziegler, S.S., 2000. A comparison of structural characteristics between old-growth and postfire second-growth hemlock-hardwood forests in Adirondack Park, New York, U.S.A. Global Ecology and Biogeography 9, 373–389. doi:10.1046/j.1365-2699.2000.00191.x

Paper IV - Assessment of soil disturbance caused by forest operations by means of Portable Laser Scanner and soil physical parameters.

Francesca Giannetti [a], Gherardo Chirici [a], Davide Travaglini [a], Francesca Bottalico [a], Enrico Marchi[*] [a], Martina Cambi [a]

[a] *Dipartimento di Gestione dei Sistemi Agrari, Alimentari e Forestali, Università di Firenze, Via San Bonaventura, 13 50145 Firenze (Italy)*

**Corresponding author: Enrico Marchi (enrico.marchi@unifi.it)*

Published Giannetti, Francesca et al. (2017). "Assessment of Soil Disturbance Caused by Forest Operations by Means of Portable Laser Scanner and Soil Physical Parameters." Soil Science Society of America Journal: 1-9.
DOI: 10.2136/sssaj2017.02.0051

Abstract

Forest operations can cause compaction and rutting, resulting in soil degradation processes. Soil damage is usually assessed through costly and time-consuming manual field measurements. The aim of this study is to investigate the impact of logging operations on soil using traditional ground surveys integrated with laser scanning data acquired by a terrestrial portable laser scanner (PLS). This approach provides an alternative to soil rut manual measurements. Two skid trails, that differed by the numbers of machine passes and slope were sampled. Data collection was performed before and after forest operations. The specific objectives were to: (i) assess soil compaction, and (ii) determine rutting by way of multi-temporal high-resolution digital terrain models (DTM) generated by PLS data. This is the first study to assess changes in soil volume via the PLS. Significant logging impacts were detected using both investigation methods (i.e., physical parameters from traditional surveys and rutting from multi-temporal spatial analysis based on DTM). The PLS method provides a very high sampling

density of the soil surface, permitting detailed spatial analysis of terrain changes. Moreover, the pre-processing cost for PLS-generated DTM is low in comparison to the time needed for traditional survey based on manual field measurements. PLS may be a useful instrument for soil sampling in forest monitoring applications.

Keywords: Forest logging; soil disturbance; soil compaction and rutting, terrestrial portable laser scanning; precision forestry

Abbreviations: BD, soil bulk density; DTM, digital terrain model; PLS, portable laser scanner; PR, soil penetration resistance; TLS, terrestrial laser scanning.

Core Ideas

- Forest operations may cause severe soil disturbances.
- Soil impacts are usually assessed by time consuming methods.
- Our study investigated the use of a portable laser scanner to assess forest soil disturbance.

1. Introduction

Starting in the 1950s, numerous studies have investigated the impact of mechanized forest operations on soil and possible ways to mitigate these impacts or promote post-logging soil recovery (Steinbrenner and Gessel, 1955; Greacen and Sands, 1980; Johnson and Beschta, 1980; Adams and Froehlich, 1981; Jakobsen and Greacen, 1985; Wronski and Murphy, 1994). In recent decades, the use of heavy machinery in forest management has increased significantly (Cambi et al., 2015a). Forest operations (e.g., skidding, forwarding and cable yarding) can have a detrimental impact on forest soil, tree regeneration and residual stand structure (Marchi et al., 2014). Consequently, quantifying soil damage caused by forest operations is important for forest management and monitoring purposes (Cambi et al., 2017). The most common and obvious effects of mechanized forest operations on soil include compaction and rutting (Kozlowski, 1999; Cambi et al., 2015a). These effects are the result of vertical and horizontal soil displacement associated with shearing stresses and soil compression in moist or wet soils (Horn et al., 2007). One of the first visible indicators of soil having been harmed by the movement of vehicle is the excessive deformation of trafficked areas (i.e., rutting) (Najafi et al., 2009).

Rutting occurs when the ground pressure from tires or tracks exceeds the bearing capacity of the soil, thus causing soil compaction. Over time, this compaction develops into a shearing rut due to wheel slippage and soil displacement (Eliasson, 2005). Rutting has several documented negative environmental effects, such as physical root damage and reduced soil porosity (Pierzchala et al., 2015). Several studies have analyzed the interactions between rutting and soil displacement with others factors. For example, Najafi et al. (2009) and Naghdi et al. (2010) studied the relationship between soil type and soil displacement, arguing that soil

displacement caused by vehicle traffic is greater in clay loam soils. Raper (2005) and Cambi et al. (2015b) assert that soil rutting is a function of the moisture content of the soil at the time of logging.

Research on the effects of rutting due to logging operations has traditionally required the manual measurement of crosssectional and longitudinal profiles of skid trails with soil deformation and/or displacement measured by means of the vertical distance between a reference level and the terrain at regular spatial intervals (Bagheri et al., 2013; Koren et al., 2015). The resolution of measurements can be improved by using a specially designed profile meter (Najafi et al., 2009). However, because traditional soil surveys for disturbance assessment are costly and time consuming, there is increased interest in the use of terrestrial laser scanning (TLS), also known as ground-based light detection and ranging (LiDAR) (López-Saez et al., 2011; Lucía et al., 2011; Vericat et al., 2014; Castillo et al., 2015; Koren et al., 2015; Liang et al., 2016).

TLS is a non-intrusive, high-precision tool designed to collect information on the three-dimensional (3-D) spatial characteristics of any object (Nadal-Romero et al., 2015; Liang et al., 2016). Based on LiDAR technology (Liang et al., 2016), TLS provides an accurate measurement of the distance between the device and objects in the surrounding environment. The acquisition process returns a dense 3-D point cloud indicative of LiDAR pulses being reflected off surrounding environmental surfaces (Nadal-Romero et al., 2015; Hayakawa et al., 2016). From these point clouds, it is possible to generate highresolution digital terrain model (DTM) that provides an accurate representation of topographical surfaces (Haubrock et al., 2009; Heritage and Large, 2009). Multi-temporal TLS acquisitions allow for the accurate measurement of changes and deformation in terrain (Haubrock et al., 2009; Heritage and Large, 2009;

Milan et al., 2011), thus providing a measure of volumetric changes (Koren et al., 2015) and facilitating the documentation of surface conditions (e.g., the development of rills, roughness, etc.) (Nadal-Romero et al., 2015).

The time needed for TLS acquisition is relatively short and the precision is sufficient for detailed soil disturbance studies in highly active areas, including landslide monitoring, soil profile extraction (Teza et al., 2008; Dunning et al., 2010) and soil erosion monitoring (Lucía et al., 2011; LópezSaez et al., 2011; Vericat et al., 2014; Castillo et al., 2015). While traditional TLS instruments operate from a fixed point in space for each acquisition, newer kinematic systems can operate while moving (Liang et al., 2016). Mobile laser scanning systems, for example, can be installed in cross-country vehicles, such as an all-terrain vehicle (Hyyppä, 2011; Hyyppä et al., 2013; Liang et al., 2016). A portable laser scanner (PLS), on the other hand, is miniaturized system that can be worn or held by the operator while walking during acquisition (Liang et al., 2016; Ryding et al., 2015).

Several studies have evaluated the use of terrain modelling, using data acquired by traditional TLS systems, to support forest operatios and to quantify soil damage caused by logging operations (Dunning et al., 2010; Pirotti et al., 2012; Korean et al., 2015). However, the use of PLS data to quantify soil displacement and rutting following forest operations has been never tested.

The objectives of this study were to: (i) assess soil compactions, and (ii) determinate the extent of logging-included rutting by way of multi-temporal high resolution DTM generated by PLS data.

The effects of mechanized logging on soil compaction and rutting were investigated along two skid trails, in the Apennine Mountains of central Italy. Traditional soil sampling methods, integrated with laser scanning data from PLS, taken both before and after logging, were used for

this investigation. The results of this analysis and subsequent discussion account for fact that the number of machine passes and slope differ among the two study trails.

2. Materials and methods

2.1 Study area and experimental trails

This study was performed in the Vallombrosa Forest, located in the Apennine Mountains of Florence, Italy (43°47¢07˝ N; 11°31¢32˝ E). The climate is temperate-humid with a rainfall pattern typical of the Mediterranean. The mean annual temperature is 9.7°C and the total annual rainfall is 1337 mm, with an average of 71.2 mm in the summer months (June–August) (Bottalico et al., 2014). Soil in the Vallombrosa Forest developed on sedimentary rocks comprised of sand stone with thin layers of siltstones and rarely marl. Umbrept and Umbric Dytrochrept soils, based on IUSS Working Group (2014), dominate the study area.

The study area is an elevation of about 1000 m asl and is home to a pure even-aged stand of silver fir (Abies alba Mill.) growing in clay loam soil. The stand was completely destroyed by a windstorm on March 2015 (Chirici et al., 2017). Forest operations were performed in June 2016 to remove fallen trees from the forest floor using two types of forest vehicles and two trails. Both skid trails were used by heavy forest vehicles to reach larger windthrow areas (i.e., the vehicles left the trail to venture further into the forest to arrive at the cutting areas). The following data were collected from each trail, herein referred to as Trail 1 and Trail 2 (Figure 1), before and after vehicle trafficking: (i) soil core samples to assess soil compaction, and (ii) laser scanning data to assess soil displacement, with special attention to damage by rutting. Table 1 shows the main characteristics of the experimental trails.

Table 1: Characteristics of the trails and number of passes of forest vehicles in each trail. The number of passes are referred to single passes.

Skid Trail	Total length (m)	Maximum slope (%)	Forest vehicle	Number of passes of forest veichle	Total number of passes
1	116	3	Harvester	15	34
			Forwarder	19	
2	90	37	Forwarder		37

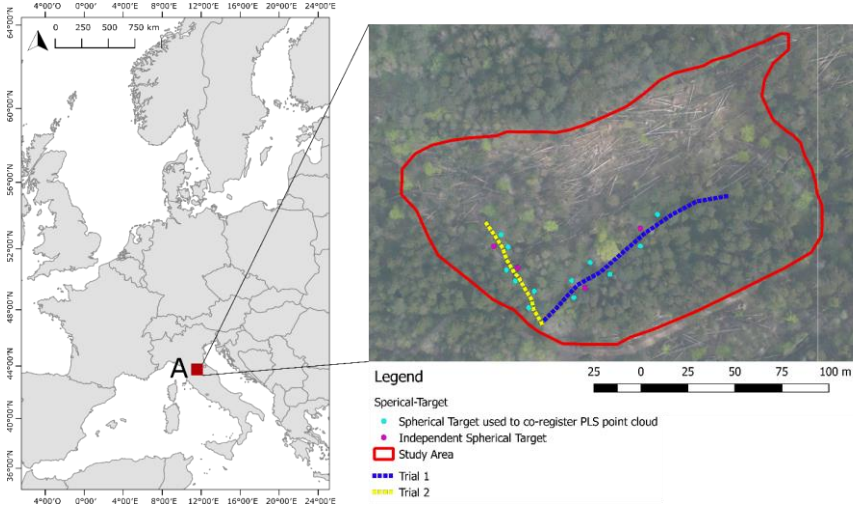

Figure 1: study area with location of the trails and the eight spherical targets; six of which were used post-scanning as control points for point cloud co-registration, while the remaining two were used to assess errors in scan alignment

2.2 Forest vehicles

Two forest vehicles were used in this study. The first vehicle was an 8-wheel forwarder, John Deere 1110 D, with an empty mass of 17.5 t (121 kW engine power), equipped with Nokian Forest Rider tires inflated to

550 kPa, used for timber extraction. The forwarder features a patented balanced bogie system for reduced ground impact and a smooth ride, even when fully loaded. The second vehicle, was a John Deere 1470 E harvester, with an empty mass of 20.7 t (180 kW engine power), used for cutting trees and processing. The number of forest vehicle passes for each trail is shown in Table 1. Additional information on each of the forest vehicles can be found in Table 2. Ground contact pressure was estimated by means of the ratio between the empty or loaded mass of each vehicle and the contact area of the wheels with the ground. The contact area between the tire and the ground was determined by pulling a rope tightly around the portion of the tire on the ground, assuming a circular contact patch (Neri et al., 2007).

Table 2: Main characteristics of the two forest vehicles used to produce forest trail traffic

Characteristic	Forwarder 1110 D				Harvester 1470 E			
	Front		Rear		Front		Rear	
	Empty	Loaded	Empty	Loaded	Empty	Loaded	Empty	Loaded
Mass (kg)	10500	10483	7000	13896.6	20700			
Wheels (n)	4	4	4	4	4		2	
Tires	700/50x26.5	700/50x26.5	700/50x26.5	700/50x26.5	26.5-20		34-16	
Equipment	Chains	Chains	Bogie tracks	Bogie tracks	Bogie tracks		Chains	
Ground pressure data (kPa)	142	260	62	113	56		116	

2.3 Data

2.3.1 Soil samples

Soil sampling was performed to determine the physical parameters of soil before and after logging. Sampling was performed on the first part of each skid trail (i.e., first 30 m from the forest road) due to the uniformity of the soil layer in these areas. The sampling scheme is shown in Figure 2. After trafficking, 14 soil samples were collected from each trail, with 7 samples taken per right and left track. Another 14 samples were

collected from beside each trail. Each soil sample was georeferenced on a local coordinate system with a total station Topcon OS series 103. Before trafficking, the same number of samples were collected from the same area and used for control purposes. Notwithstanding, although we tried to anticipate the position of tracks generated by the wheels of each vehicle, the position of pre-trafficking samples did not correspond with the actual post-trafficking position of the tracks. All soil samples were collected from the top mineral soil layer (max. 10ccm depth) using a rigid metallic cylinder (8.5 cm height and 5.0 cm inner diameter) after litter removal. Close to each sampling point, penetration resistance was measured using an Eijkelkamp TONS/FT2 penetrometer at a depth of about 4 cm. Soil samples were taken in June 2016; during the experiment, soil moisture (determined on a weight/weight basis on oven dried soil) was approximately 22%.

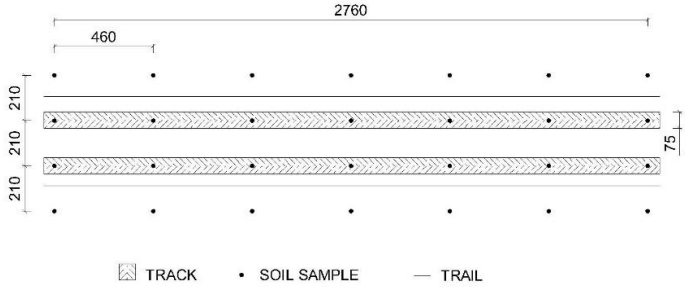

Figure 2: Soil sampling scheme of a trail; Values are in cm.

2.3.2 Laser scanning data collection and pre-processing

Portable laser scanning data were used to estimate the size and volume of ruts and bulges. In each trail, eight spherical targets (diameter = 0.14 m), mounted on a 1.40-m tall pole (Figure 3), were positioned outside the trail before the scan, where they remained throughout the duration of the study. Six of these targets were used after the scan as control points for point cloud co-registration, while the remaining two targets were used to

assess for possible errors in scan alignment. Laser scanning data were collected using a ZEB 1 lightweight portable 3-D laser scanner (GeoSLAM Ltd.). The main characteristics of the ZEB 1, according to the manufacturer, are shown in Table 3, while additional information can be found in Ryding et al. (2015).

Table 3: Characteristics of the ZEB 1 portable laser scanner.

Characteristic	Description
Data acquisition speed:	43200 points/sec
3D measurement accuracy:	+/- 0.1% (typically)
Maximum range:	up to 30 m (15 m outdoors)
Laser safety class:	class 1 Eye Safe
Angular field of view:	+270 x ~ 100 degrees
Weight of scanner head:	665 g
Dimensions of scanner head:	60 x 60 x 360 mm

The scan was performed in each trail with the user slowly walking along the trail (approximately 30 cm s–1). The user walked in straight lines along the center line with the instrument remaining at breast height (1.4 m) throughout. The laser scanning data were collected both before and after logging operation using a closed loop, starting and ending at the same point (Ryding et al., 2015). Before all scanning operations, logging residues, such as branches or logs were removed from the ground suface.

Raw data, registered by ZEB1, was pre-processed to obtained point clouds for the two trails. This procedure uses simultaneous localization and mapping (SLAM) algorithms that combine measurement data from the laser with positional data from the on-board Inertial measurement unit (IMU) to perform cloud-to-cloud registration, using feature recognition to automatically align the scan data (Bosse et al., 2012). Pre-processing was

performed on-line using the GeoSLAM servers. Table 4 shows the time needed for data pre-processing, and its cost. The 3-D point cloud data were generated in '.las' and '.ply' file formats, which are compatible with a variety of software. The post-logging 3-D point cloud were then "cleaned" to remove any non-soil objects, such as rocks, stumps and logs. Six spherical targets were identified in the point clouds by visual interpretation and used as control points to co-register the point clouds taken before and after logging. Point cloud co-registration was performed using the 'Point pair based' alignment tool, available in CloudCompare (version 2.6+) software. This tool aligns two-point clouds using the '4 points Congruent Sets For Robust Registration' algorithm (Aiger et al., 2008). The pre-logging scan for each trail was used as reference model for co-registration. In addition, the root mean square error (RMSE) for vertical and horizontal displacement was assessed using two independent spherical targets to yield statistics on the uncertainty in the alignment.

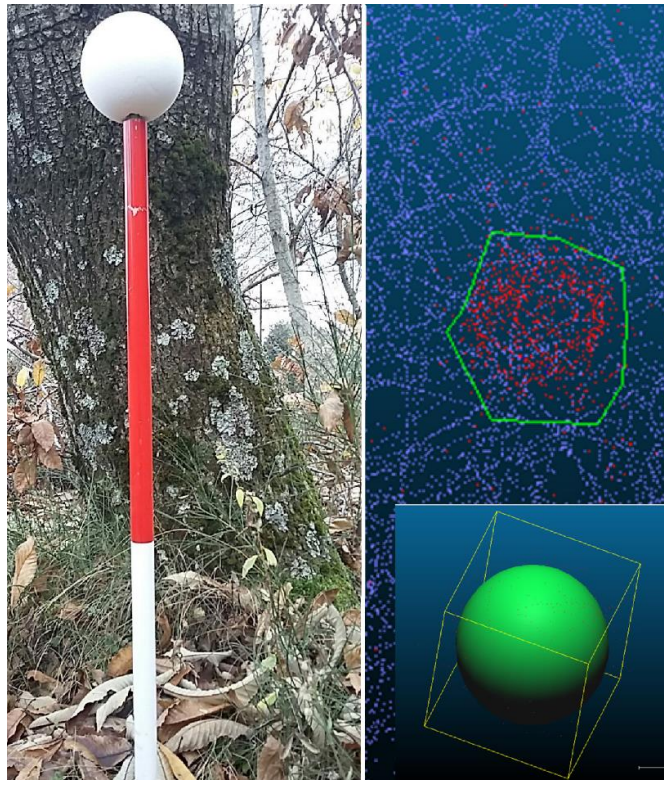

Figure 3: Example of spherical target in the study area (left), and spherical target visible in point cloud produced by a portable laser scanner (right).

Table 4: Details of scans acquisition and data pre-processing.

Trail	Scan date	Acquisition time min	Processing time min	Credit
Trail 1	01.06.2016 (Before logging)	7’	7’	53
Trail 1	15.06.2016 (After logging)	8’	8’	57
Trail 2	15.06.2016 (Before logging)	7’	7’	46
Trail 2	20.06.2016 (After logging)	8’	8’	49

2.4 Data analysis

2.4.1 Soil physical parameters

Bulk density was computed for each soil sample using the method described in Picchio et al. (2012). Statistical analysis were used to test the influence of forest operations on soil bulk density (BD) and penetration resistance (PR). The data were checked for normality using the Kolmogorov–Smirnov test, and homogeneity of variance using the Levene test. Differences in physical parameters (BD and PR) of the soil in both the study trails and control area were assessed using one-way ANOVA. Post-hoc testing was performed using the Tukey's HSD test.

2.4.2 Portable laser scanner

Points produced during each scan were classified as being either ground or non-ground on the basis of the adaptive triangulated irregular network algorithm (Axelsson, 2000). Ground points were rasterized using the rasterize tools present in CloudCompare to create high-resolution (pixel = 1 cm) DTMs for Trail 1 and Trail 2. For each raster cell, the point with the lowest elevation was found and its z coordinates recorded. The DTM before (DTM_1) and after (DTM_2) logging operations were compared using map algebra tools and differences in terrain elevation were computed as $\Delta_{21} = DTM_2 - DTM_1$. Based on this, we calculated for each trail: (i) the volume of ruts (V_L, m^3), where $\Delta_{21} < 0$ (soil volume loss); (ii) the volume of bulges (V_G, m^3), where $\Delta_{21} > 0$ (soil volume gain); and (iii) the total change of soil volume $VT = V_L + V_G$ (m^3). Because Trail 1 and Trail 2 had different sizes, the intensity of the total change of soil volume I_T ($m^3\ m^{-2}$) was estimated to compare the trails, as proposed by Koren et al. (2015):

$$I_T = \frac{V_T}{S} \quad [1]$$

where S is the area of the section considered. The intensity of soil volume loss I_L(m^3 m^{-2}) and the intensity of soil volume gain I_G (m^3 m^{-2}) were computed as well:

$$I_L = \frac{V_L}{S_L} \quad [2]$$

$$I_G = \frac{V_G}{S_G} \quad [3]$$

where S_L is the area of the trail with $\Delta_{21}<0$ and S_G is the area with $\Delta_{21}>0$.

2.4.3 Portable laser scanner and soils physical parameters

To assess the relationship between rut depth and both BD and PR, a correlation analysis was performed. The geographic position of each soil sample was used to determine mean rut depth using the mean value of the Δ_{21} pixels (i.e., surface 19.63 cm^2). Regression analyses were performed between mean rut depth and both BD and PR. To assess the relationship between BD and PR and mean rut depth the coefficient of determination (R^2) was taken into account

3. Results

3.1 Soil compaction

The control BD values were 0.78 and 0.79 g cm^{-3} for Trail 1 and Trail 2, respectively (Table 5). After logging operations, BD within ruts increased about 134% in Trail 1 and 135% in Trail 2. BD beside ruts increased approximately 73% in Trail 1 and 123% in Trail 2. The value of PR increased approximately 47% within ruts and 33% beside ruts in Trail 1, and about 49% within ruts and 32% beside ruts in Trail 2. The results for all parameters

are shown in Table 6. A significant statistical differences was recorded for BD before and after logging, both within and beside trails. A significant statistical differences was also recorded for PR in all trails.

Table 5: Bulk density (BD) and penetration resistance (PR) (mean ± standard deviation) measured for both forest skid trails receiving vehicular traffic. † Values within rows followed by the same letter weree not significantly differenct by Tukey's HSD test ($p<0.05$).

Trails	Parameters	Control	Within ruts	Beside ruts
1	BD (g/cm^3)	0.78 ± 0.07 **a**†	1.83 ± 0.06 **b**	1.35 ± 0.04 **c**
	PR (MPa)	0.36 ± 0.04 **a**	0.53 ± 0.03 **b**	0.48 ± 0.02 **c**
2	BD (g/cm^3)	0.79 ± 0.06 **a**	1.86 ± 0.07 **b**	1.76 ± 0.08 **c**
	PR (MPa)	0.37 ± 0.03 **a**	0.55 ± 0.04 **b**	0.49 ± 0.02 **c**

3.2 Portable laser scanner

The ZEB 1 was used to scan a total area of 1047 m2 and 589 m2 in Trail 1 and Trail 2, respectively. The RMSE for horizontal and vertical displacement assessed with two independent spherical targets was 0.46 and 0.93ccm, respectively. These values represent the level of uncertainty in the ZEB 1 analysis of the soil. In Trail 1, the deepest rut in the terrain due to logging was 39 cm, while the biggest bulge was 44 cm (Figure 4). In Trail 2, the deepest rut reached a depth of 60 cm; the biggest bulge to register was similarly 59 cm (Figure 5). Table 6 shows the volume of soil displacement and intensity of the total change in soil volume computed from multi-temporal analysis of DTMs. Figure 4 shows the spatial distribution of soil disturbance in Trail 1 after 34 forest vehicle passes. The deepest ruts were detected in the initial part of the skid trail (Figure 4: section A of the trail), which coincides with a soil sampling site. The largest

The values of the coefficient of determination (R^2=0.76 for Trail 1 and R^2=0.67 for Trail 2; p-level <0.05) revealed a good relationship between BD

and mean rut depth in both trails (Figure 6); the higher the rut depth the higher the BD. On the contrary, the relationships between PR and mean rut deep were not significant (R^2<0.4, p-level >0.05).

soil bulges (>35 cm) were observed in the remaining part of the skid trail (Figure 4: section B of the trail). Figure 5 shows the spatial distribution of soil disturbances in Trail 2 after 37 forest vehicle passes. Changes in the order of −42 to 20 cm were frequently detected almost everywhere close to the skid trail for Trail 2. Ruts reached an average depth of 42 cm in Trail 2, which was deeper than Trail 1 (i.e., 24 cm).

Moreover, the maximum rut depth in Trail 2 was 60 cm, probably due to the effect of terrain slope, which was higher in Trail 2 (37%) than in Trail 1 (3%).

Table 6: Volume and intensity of soil displacement in Trail 1 and Trail 2.

Parameter	Trail 1	Trail 2
Area (m^2)	1047	589
Slope (%)	3	37
Average rut depth (cm)	24	42
Average rut heights (cm)	27	28
Ruts volume (V_D) (m^3)	5.49	5.90
Bulges volume (V_R) (m^3)	3.53	3.64
Total change of volume ($V_T = V_D + V_R$) (m^3)	9.02	9.54
Intensity of total change of volume (I_T) ($m^3\ m^{-2}$)	0.0086	0.0161
Intensity of volume reduction (I_D) ($m^3\ m^{-2}$)	0.0052	0.0100
Intensity of volume rise (I_R) ($m^3\ m^{-2}$)	0.0034	0.0062

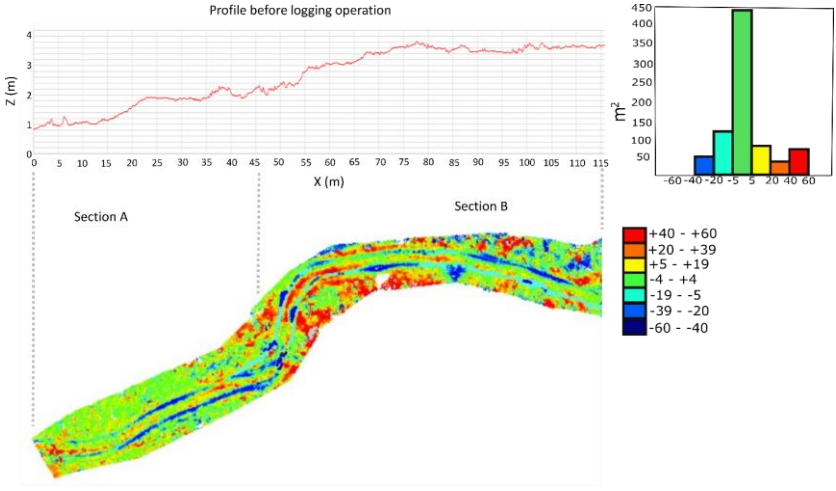

Figure 4: Spatial distribution of soil displacement (Δ21, change in digital terrain elevation) (left), and a histogram of soil surface variation and longitudinal profile for Trail 1 (right); Values are in cm.

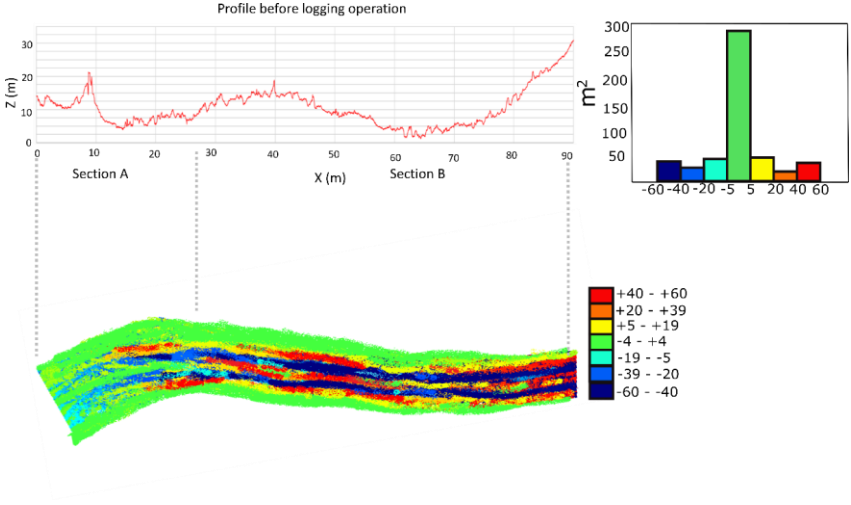

Figure 5: Spatial distribution of soil displacement (Δ21, change in digital terrain elevation) (left), and a histogram of soil surface variation and longitudinal profile for Trail 2 (right); Values are in cm.

3.3. Portable laser scanner and soil physical parameters

The values of the coefficient of determination (R^2 = 0.76 for Trail

1 and $R^2 = 0.67$ for Trail 2; $p < 0.05$) revealed a good relationship between BD and mean rut depth in both trails (Figure 6); the higher the rut depth the higher the BD. On the contrary, the relationships between PR and mean rut deep were not significant ($R^2 < 0.4$; $p > 0.05$)

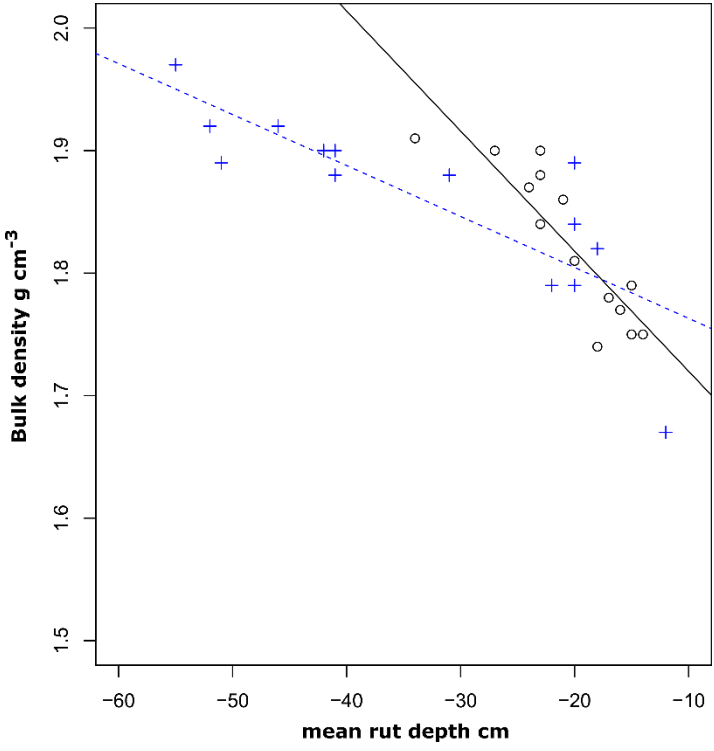

Figure 6: Correlation analysis between mean rut depth derived by the change in digital terrain elevation and soil bulk density. Black dots are Trail 1 data and blue crosses are Trail 2 data. The lines represent the linear regression model between mean rut depth and bulk density

4. Discussion

This pilot study investigated the effects of logging traffic on forest soil, using PLS to assess soil compaction and rutting along two skid trails with different slope gradients. The study focused solely on the effects of

machine trafficking on the selected trails, ignoring the impact on soil throughout the remainder of the harvesting area. Our results, therefore, do not consider soil disturbances within the harvesting area, which according to the literature may vary widely, from 10 to 70% in relation to the system used for harvesting, logging methods and operator skills (Spinelli et al., 2010; Marchi et al., 2014). As reported in other studies, logging operations increased BD and PR (McNabb et al., 2001; Picchio et al., 2012; Marchi et al., 2014; Cambi et al., 2015b) and formed deep ruts (Koren et al., 2015) along the study trails. Similar to results reported by Koren et al. (2015), most of the changes detected in our study were caused by soil compaction and displacement due to logging trafficking. A relationship between BD and mean rut depth was also observed. High BD values were measured in deeper ruts. Lower BD values and mean rut depth were observed in Trail 1, while higher values were observed in Trail 2. Most of the changes in the volume of soil were due to rut formation as a result of soil compaction and displacement caused by forest vehicles, as reported elsewhere (Eliasson 2005; Eliasson and Wästerlund 2007). The observed increase in PR is an indicator of soil deterioration (Panayiotopoulos et al., 1994; Coelho et al., 2000) similar to other studies of machinery-induced effects (Cambi et al., 2015b). In this study PR was investigated only in the top soil layer and an increase was observed on both trails. In our study, increased skid trail slope resulted in higher I_L and I_G (i.e., I_L and I_G were 92 and 82% higher in Trail 2 than in Trail 1). The longitudinal slope can play an important role in the amount of soil displaced (Solgi, 2007). Indeed, we found that rut volumes were greater along the steeper skid trail (Trail 2), similar to other studies that document the effect of slope on rutting during logging (Jourgholami et al., 2014). There was a higher level of soil mixing along section B of Trail 1, likely due to the presence of tree stumps that made the area less uniform.

As the vehicles turned into the cutting area (Section B), the heavy forestry vehicles slowed down, thus contributing to the creation of shallow ruts and soil accumulation outside the skid trail, as observed by Koren et al. (2015). Our study represents the first documented attempt to assess changes in soil volume using data from the PLS. Multi-temporal very high-resolution DTMs were successfully used to measure topographic change, suggesting that use of a PLS has potential to provide rapid and precise analysis of terrain variations due to forestry operations.

The walking method and the subsequent GeoSLAM reconstruction process created a complete point cloud of the investigation area (approximately 1636 m2) in roughly 30 min. Data collection and pre-processing by use of the PLS was simpler and probably faster than traditional TLS systems, which require multiple acquisitions from different points to provide an obstruction and shadow-free scan (Ehbrecht et al., 2016). Data from a PLS can be collected by a single operator, compared with at least two persons needed for field measurements required by laser scanner (Jester and Klik, 2005). However, it is worth noting that the operator must be careful not to alter terrain features during a PLS survey. In conclusion, pre-processing may be more cost effective when compared with the time needed for both traditional surveys based on manual field measurements and TLS. One limitation of both the PLS and TLS approaches is that data post-processing must be done afterward (i.e., not directly in the field), while manual measurement data can be used almost immediately. One further disadvantage of laser scanning is that spatial reference points have to be allotted manually on the ground before scanning (Haas et al., 2016). With regard to the traditional manual survey, Haas et al. (2016) noted that the yardstick must be absolutely perpendicular when collecting data if the measurement values are to be acceptable and error free. Even

miniscule lateral variations from the perpendicular line can lead to distinct errors, which might occur frequently in the transition area of tire tread imprints. Moreover, in the traditional method, the accuracy of the estimation of the rut volume is only approximate because it is based on manual data collected from a limited number of crosssectional and longitudinal profiles of forest trails (Koren et al., 2015). Compared with manual measurement, the PLS provides a much higher sampling density of the soil surface allowing more detailed spatial analysis of terrain changes (Haubrock et al., 2009; Koren et al., 2015). Unlike other methods, the PLS also provides estimates of the volumes transferred from ruts to bulges, and volume loss due to compaction. Additional detailed studies may help develop a relationship between the volume lost by compaction and other soil compaction parameters.

5. Conclusions

Rutting, soil displacement and compaction are problems associated with land use management. In particular, logging operations frequently disturb soil, which may result in soil erosion on steep terrain. Rut depth is often the only variable forest managers consider when assessing soil damage from harvesting operations, yet its measurement require costly, time-consuming field work. In this study, we investigated soil compaction and assessed logging-induced rutting using a PLS, a hand-held terrestrial laser scanning system that acquires data while the operator traverses the study area on foot. Scanner data were used to produce multitemporal high-resolution DTM, before and after logging, thus creating high resolution assessment of soil disturbance. Our results show that the PLS can produce a fast, precise and accurate measurement of the impact of forest operations on soil. In addition, we found a good relationship between rut depth estimated with a PLS and traditional BD measurements. In conclusion, we demonstrated for the first time that PLS technology can be

used to assess soil disturbance caused by forest harvesting machinery. Further studies are needed to compare the PLS against traditional soil disturbance and compaction measurements to determine the utility of using a PLS for soil sampling and monitoring in forest environments. In particular, development of geostatistical models that map soil variables (e.g., BD, PR, soil porosity) based on relation between soil samples and PLS data should benefit sustainable forest management and forest operation planning.

References

Adams, P., Froehlich, H., 1981. Compaction of Forest Soils. PNW 217. A Pacific Northwest Extension Publication. Oregon, Washington, Idaho, USA, p. 16.

Aiger, D., Mitra N.J., Cohen-Or D. 2008. Four-points congruent sets for robust surface registration. ACM Transactions on Graphics (Proc. SIGGRAPH) 27: 1–10. doi:10.1145/1360612.1360684

Axelsson, P. 2000. DEM generation from laser scanner data using adaptive TIN models. ISPRS. 33: 111–118 (B4/1; Part 4).

Bagheri, I., Naghdi, R., Jalali, A.M. 2013. Evaluation of factors affecting soil erosion along skid trails (case study; Shafarood Forest, Northern Iran). CJES. 11: 151–160.

Bosse, M., Zlot, R., Flick, P. 2012. Zebedee: Design of a Spring-Mounted 3-D Range Sensor with Application to Mobile Mapping. IEEE. 28, 5doi: 10.1109/TRO.2012.2200990.

Bottalico, F., Travaglini, D., Fiorentini, S., Lisa, C., Nocentini, S. 2014. Stand dynamics and natural regeneration in silver fir (Abies alba Mill.) plantations after traditional rotation age. iForest. 7: 313–323. doi: 10.3832/ifor0985-007

Cambi, M., Certini, G., Neri, F., Marchi, E. 2015a. The impact of heavy traffic on forest soils: a review. For. Ecol. Manag. 338: 124–138. doi: 10.1016/j.foreco.2014.11.022

Cambi, M., Fabiano, F., Foderi, C., Laschi, A., Picchio, R. 2015b. Impact of wheeled and tracked tractors on soil physical properties. iForest. 9. 89–94. doi: 10.3832/ifor1382-008

Cambi, M., Hoshika, Y., Mariotti, B., Paoletti, E., Picchio, R., Venanzi, R., Marchi, E. 2017. Compaction by a forest machine affects soil quality and Quercus robur L. seedling performance in an experimental field. For. Ecol. Manag. 384: 406–414.

Castillo, C., James, M.R., Redel-Macías, M.D., Pérez, R., and Gómez, J.A. 2015. The SF3M approach to 3-D photo-reconstruction for non-expert users: application to a gully network, SOIL Discuss. 2: 371–399. doi:10.5194/soild-2-371-2015. doi: 10.5194/soild-2-371-2015

Chirici, G., Bottalico, F., Giannetti, F., Rossi, P., Del Perugia, B., Travaglini, D., Nocentini, S., Ruedlinger, E.H.K., Marchi, E., Foderi, F., Fioravanti, M., Fattorini, L., Guariglia, A., Ciancio, O., McRoberts, L.R., Naesset, E., Corona, P., Gozzini, B., 2017. Assessing forest windthrow damages using single-date, post-event airborne laser scanning data. Forestry. Submitted.

Coelho, M.B., Mateos, L., Villalobos, F.J. 2000. Influence of a compacted loam subsoil layer on growth and yield of irrigated cotton in Southern Spain. Soil Till. Res. 57: 129–142. doi: 10.1016/S0167-1987(00)00153-7

Dunning, S.A., Rosser, N.J., Massey, C.I. 2010. The integration of terrestrial laser scanning and numerical modelling in landslide investigations. Q. J. Eng. Geol. Hydrogeol. 43 (2): 233–247. doi: 10.1144/1470-9236/08-069

Ehbrecht, M., Schall, P., Juchheim, J., Ammer, C., Seidel, D. 2016. Effective number of layers: A new measure for quantifying three-dimensional stand structure based on sampling with terrestrial LiDAR. For. Ecol. Manag. 380: 212–223. doi: 10.1016/j.foreco.2016.09.003

Eliasson, L. 2005. Effects of forwarder tyre pressure on rut formation and soil compaction. Silva Fenn. 39 549–557. http://www.metla.fi/silvafennica/full/sf39/sf394549.pdf

Eliasson, L., Wästerlund, I. 2007. Effects of slash reinforcement of strip roads on rutting and soil compaction on a moist fine-grained soil. For. Ecol. Manag. 252 (1–3): 118–123.

Greacen, E.L., Sands, R. 1980. Compaction of forest soils. A review. Aust. J. Soil Res. 18, 163–189. doi:10.1071/SR9800163

Haas, J., Hagge Ellhöft, K., Schack-Kirchner, H., Lang, F. 2016. Using photogrammetry to assess rutting caused by a forwarder—A comparison of different tires and bogie tracks. Soil Till. Res. 163: 14–20. doi: 10.1016/j.still.2016.04.008

Hayakawa, Y.S., Kusumoto, S., Matta, N. 2016. Application of terrestrial laser scanning for detection of ground surface deformation in small mud volcano (Murono, Japan). Earth, Planets Space. 68:114. doi: 10.1186/s40623-016-0495-0

Haubrock, S.N., Kuhnert, M., Chabrillat, S., Güntner, A., Kaufmann, H. 2009. Spatiotemporal variations of soil surface roughness from in-situ laser scanning. Catena. 79 (2): 128–139. doi: doi.org/10.1016/j.catena.2009.06.005

Heritage, G.L., Large, A.R.G. 2009. Laser scanning for the environmental sciences. Wiley-Blackwell, New York.

Hyyppä, J. 2011. Utilizing Individual Tree Information in Laser Assisted Forest Inventory.

Hyyppä, J., Jaakkola, A., Chen, Y., Kukko, A. 2013. Unconventional LIDAR mapping from air, terrestrial and mobile. In: Photogrammetric Week 2013, Stuttgart, Germany, pp. 205–214. http://www.ifp.uni-stuttgart.de/publications/phowo13/180Hyyppae.pdf

Horn, R., Vossbrink, J., Peth, S., Becker, S. 2007. Impact of modern forest vehicles on soil physical properties. For. Ecol. Manag. 248 (1–2): 56–63. doi: 10.1016/j.foreco.2007.02.037

Jourgholami, M., Soltanpour, S., Etehadi Abari, M., Zenner, E.K. 2014. Influence of slope on physical soil disturbance due to farm tractor forwarding in a Hyrcanian forest of northern Iran. iForest. 7: 342–348. doi: 10.3832/ifor1141-007

Koren, M., Slančík, M., Suchomel, J., Dubina, J. 2015. Use of terrestrial laser scanning to evaluate the spatial distribution of soil disturbance by skidding operations. iForest. 8: 386–393. doi:10.3832/ifor1165-007

Kozlowski, T.T. 1999. Soil compaction and growth of woody plants. Scandinavian J. For. Res. 14: 596–619.

Jakobsen, B.F., Greacen, E.L., 1985. Compaction of sandy forest soils by forwarder operations. Soil Till. Res. 5, 55–70. doi.org/10.1016/S0167-1987(85)80016-7

Jester, W., Klik, A. 2005. Soil surface roughness measurement - methods, applicability, and surface representation. Catena. 64: 174–192. doi: 10.1016/j.catena.2005.08.005.

Johnson, M.G., Beschta, R.L., 1980. Logging, infiltration capacity, and surface erodibility in western Oregon. J. Forest. 78, 334–337.

Liang, X., Kankare, V., Hyyppä, J., Wang, Y., Kukko, A., Haggrén, H., Yu X., Kaartinen, H., Jaakkola, A., Guan, F. 2016. Terrestrial laser scanning in forest inventories. ISPRS J. Photogramm. Remote Sens. 115: 63–77. doi.org/10.1016/j.isprsjprs.2016.01.006

Liang, X., Wang, Y., Jaakkola, A., Kukko, A., Kaartinen, H., Hyyppa J., Honkavaara, E., Liu, J. 2015. Forest data collection using terrestrial image-based point clouds from a handheld camera compared to terrestrial and personal laser scanning. IEEE Trans. Geosci. Remote Sens. 53: 5117–5132. doi: 10.1109/TGRS.2015.2417316

López-Saez, J., Corona, C., Stoffel, M., Rovéra, G., Astrade, L., and Berger, F. 2011. Mapping of erosion rates in marly badlands based on a coupling of anatomical changes in exposed roots with slope maps derived from LiDAR data, Earth Surf. Process. Landf., 36: 1162–1171. doi: 10.1002/esp.2141

Lotfalian, M., Parsakhoo, A. 2009. Investigation of forest soil disturbance caused by rubber-tired skidder traffic. International Journal of Natural and Engineering Sciences. 3 (1): 79–82.

Lucía, A., Martín-Duque, J.F., Benjamin Laronne, J., and SanzSantos, M.A. 2011. Geomorphic dynamics of gullies developed in Sandy slopes of Central Spain. Landform Analysis. 17: 91–97. http://geoinfo.amu.edu.pl/sgp/LA/LA17/LA17_091-097.pdf

Marchi, E., Picchio, R., Spinelli, R., Verani, S., Venanzi, R., Certini, G. 2014. Environmental impact assessment of different logging methods in pine forests thinning. Ecol. Eng. 70: 429–436. doi: doi.org/10.1016/j.ecoleng.2014.06.019

Milan, D.J., Heritage, G.L., Large, A.R.G., Fuller, I.C. 2011. Filtering spatial error from DEMs: implications for morphological change estimation. Geomorphology. 125:160–171. doi: 10.1016/j.geomorph.2010.09.012

McNabb, D.H., Startsev, A.D., Nguyen, H. 2001. Soil wetness and traffic level

effects on bulk density and air-filled porosity of compacted boreal forest soils. SSSAJ. 65: 1238–1247. doi: 10.2136/sssaj2001.6541238x

Nadal-Romero, E., Revuelto, J., Errea, P., López-Moreno, J.I. 2015. The application of terrestrial laser scanner and SfM photogrammetry in measuring erosion and deposition processes in two opposite slopes in a humid badlands area (central Spanish Pyrenees). SOIL. 1: 561–573. doi:10.5194/soil-1-561-2015. doi:10.5194/soil-1-561-2015

Naghdi, R., Bagheri, I., Basiri, R. 2010. Soil disturbances due to machinery traffic on steep skid trail in the north mountainous forest of Iran. J. For. Res. 21: 497–502.

Najafi, A., Solgi, A., Sadeghi, S.H. 2009. Soil disturbance following four-wheel rubber skidder logging on the steep trail in the north mountainous forest of Iran. Soil. Till. Res. 103: 165–169. doi:10.1016/j.still.2008.10.003

Neri, F., Spinelli, R., Lyons, J. 2007. Ground pressure forwarder trials: assess benefits in reducing wheel rutting. In proceedings of the Austro2007/FORMEC´07 conference: "Meeting the Needs of Tomorrows´ Forests. New Developments in Forest Engineering", October 7 – 11, 2007, Vienna and Heiligenkreuz, Austria.

Panayiotopoulos, K.P., Papadopoulou, C.P., Hatjiioannidou, A. 1994. Compaction and penetration resistance indicates soil deterioration because it means reduced workability and more difficult soil exploration by roots. Soil. Till. Res. 31: 323–337. doi: 10.1016/0167-1987(94)90039-6

Picchio, R., Neri, F., Petrini, E., Verani, S., Marchi, E., Certini, G. 2012. Machinery–induced soil compaction in thinning two pine stands in central Italy. For. Ecol. Manag. 285: 38–43. doi.org/10.1016/j.foreco.2012.08.008

Pierzchala, M., Talbot, B., Astrup, R. 2015. Measuring wheel ruts with close-range photogrammetry. Forestry. 0: 1–9.

Pirotti, F., Grigolato, S., Lingua, E., Sitzia, T., Tarolli, P. 2012. Laser Scanner Applications in Forest and Environmental Sciences. Italian Journal of Remote Sensing. 44 (1): 109–123.

Pirotti, F., Travaglini, D., Giannetti, F., Kutchartt, E., Bottalico, F., Chirici, G. 2016. Kernel feature cross-correlation for unsupervised quantification of damage from windthrow in forests. The International Archives of the Photogrammetry, Remote Sensing and Spatial Information Sciences, Volume XLI-B7, 2016 XXIII ISPRS Congress, 12–19 July 2016, Prague, Czech Republic: 17–22. doi: 10.5194/isprs-archives-XLI-B7-17-2016.

Raper, R.L. 2005. Agricultural traffic impacts on soil. J. Terramechanics. 42: 259–280. doi.org/10.1016/j.jterra.2004.10.010

Ryding, J., Williams, E., Smith, M.J., Eichhorn, M.P. 2015.Assessing handheld

mobile laser scanners for forest surveys. Remote Sensing, 7 (1): 1095-1111. doi: 10.3390/rs70101095

Solgi, A. 2007. Forest soil disturbance caused by HSM904 wheeled skidder. [M.Sc. Thesis.] Noor, Tarbiat Modares University: 82.

Spinelli, R., Magagnotti, N., Nati, C. 2010. Benchmarking the impact of traditional small-scale logging systems used in Mediterranean forestry. For. Ecol. Manag. 260: 1997–2001. doi.org/10.1016/j.foreco.2010.08.048

Steinbrenner, C.E., Gessel, S.P. 1955. The effect of tractor logging on physical properties of some forest soils in Southwestern Washington. Soil Sci. Soc. Am. J. 19, 372–376. doi:10.2136/sssaj1955.03615995001900030030x

Teza, G., Pesci, A., Genevois, R., Galgaro, A. 2008. Characterization of landslide ground surface kinematics from terrestrial laser scanning and strain field computation. Geomorphology. 97 (3–4): 424–437. doi:10.1016/j.geomorph.2007.09.003

Vericat, D., Smith, M.W., and Brasington, J. 2014. Patterns of topographic change in sub-humid badlands determined by high resolution multi-temporal topographic surveys, Catena. 120: 164–176. doi: 10.1016/j.catena.2014.04.012

Wronski, E.B., Murphy, G. 1994. Responses of forest crops to soil compaction. In: Soane, B. D. and van Ouwerkerk, C. Soil compaction in crop production. Elsevier, Amsterdam: 662 pp.

Paper V - Estimating machine impact on strip roads via close-range photogrammetry and soil parameters: a case study in central Italy.

Martina Cambi[a], **Francesca Giannetti**[a]*, Francesca Bottalico[a], Davide Travaglini[a], Tomas Nordfjell[b], Gherardo Chirici[a], Enrico Marchi[a].

[a] Dipartimento di Gestione dei Sistemi Agrari, Alimentari e Forestali (GESAAF), Università di Firenze. v. S. Bonaventura 13, I-50145 Firenze (Italy)

[b] Department of Forest Biomaterials and Technology, Swedish University of Agricultural Sciences, Skogsmarksgränd, Umeå (Sweden)

Corresponding authors: Francesca Giannetti (francesca.giannetti@unifi.it)

Accepted iForest

Abstract

Several studies have been carried out to investigate the effects of logging vehicle traffic on forest soil, with the objective to ascertain site impacts (soil compaction and rutting). Most of these studies have been based on field measurements and/or soil sampling, involving time consuming methods and punctual surveys. The objective of this study was to measure soil disturbances with application of two methods: via new, image-based models derived by a structure-from-motion (SfM) photogrammetry approach, and traditional soil sampling (bulk density and shear strength). The comparison of image-based models derived by SfM photogrammetry was used to highlight the differences in the shape and distribution of the disturbances along ST and FT. The study was carried out in the Vallombrosa forest (central Italy). Two trails were selected in the logging area, one trafficked by a forwarder (FT) and one trafficked by a skidder (ST). Data collection was conducted before, during and after timber extraction. Results showed that the physical parameters of soil significantly changed due to both FT and ST forest vehicle traffic. This study proved that the use

of SfM photogrammetry may be very useful for improving assessment of the impact of forest operations on soil. Machine passes increased bulk density (111 and 31% for FT and ST, respectively), penetration resistance (29 and 24% for FT and ST, respectively) and shear resistance (14 and 6 % for FT and ST, respectively), whereas porosity decreased (46 and 9 % for FT and ST, respectively). Changes in the physical parameters of soil were significantly lower for ST. After logging, FT clearly showed ruts and bulges, whereas in ST, ruts and bulges were not visible but soil displacement in the direction of extraction was evident and measurable. The results obtained by SfM photogrammetry may revealed information not available via traditional methods, thus improving impact assessment.

Keywords: Forest operation, soil impacts, soil displacement, close range photogrammetry, Digital Terrain Model

1. Introduction

Forest operations are acknowledged to be sources of soil disturbance and erosion, and have been a matter of much research since the 1950s (Cambi et al. 2015). In particular, machine trafficking causes soil compaction (Jamshidi et al. 2008) and rutting, and is one of the major sources of human-induced forest soil degradation (Gomez et al. 2002, Bagheri et al. 2013). The pressure exerted by loaded vehicles passing through is a major factor causing compaction and rut formation (McNabb et al. 2001, Alakukku et al. 2003, Nugent et al. 2003, Eliasson 2005). In the last decades, the weights of forestry machines have increased, thus raising new concern over forest soil degradation (Sheridan 2003). Skid trails are forest areas prone to soil compaction and rutting because they have a road bed that is not naturally compacted and do not have constructed drainage, leading to a reduction in soil porosity, water infiltration and gas exchange, as well as increasing soil erosion, water logging and mudflows (Jansson & Johansson 1998, Grace et al. 2006, Cristopher & Visser 2007).

Most studies concerning soil degradation due to forest operations have examined the physical parameters of soil, such as bulk density, total porosity, macro and micro porosity, shear and penetration resistances, and infiltration capacity (Alakukku et al. 2003, Ampoorter et al. 2007, Jourgulami et al. 2014, Marchi et al. 2014). The physical parameters of soil are usually determined by means of soil sample collection and analysis, or measured using specific instruments, such as penetrometers and scissometers (Picchio et al. 2012, Venanzi et al. 2016), or by means of manual measurements of cross-sectional and longitudinal profiles on skid trails (Koren et al. 2015). Although these methods have been improved over time (Jourgulami et al. 2014), they are time consuming and costly. Moreover, these methods may affect the study area when repeated measurement

methods are applied.

Recently, the field methods used for analysis of geomorphological processes and quantification of soil impacts have seen a change, passing from traditional methods (Lotfalian et al. 2009, Bagheri et al. 2013, Koren et al. 2015) to the use of remote sensing and proximal sensing techniques (D'Oleire-Oltmanns et al. 2012; Talbot et al., 2017) in order to analyse the spatial distribution of soil disturbances (Koren et al. 2015; Giannetti et al., 2017). In recent decades, techniques allowing rapid acquisition of high-density topographic data have proliferated (Nadal-Romero et al. 2015). These techniques include terrestrial laser scanners (TLS; Vericat et al. 2014, Castillo et al. 2015) and photogrammetry techniques (Castillo et al. 2015, Kaiser et al. 2014, Marra et al., submitted), which are used, for example, for the analysis of soil erosion (Micheletti et al. 2015, Nadal-Romero et al. 2015). These techniques make it possible to generate digital elevation models that accurately reproduce topographic surfaces (Vericat et al. 2014, Pierzchala et al. 2014b, Nadal-Romero et al. 2015). Various techniques have been proposed to measure soil surface microtopography (Heng et al. 2010), and their relative strengths and weaknesses have been discussed in recent comparative studies (Jester & Klik 2005, Aguilar et al. 2009). Although the use of close-range photogrammetry in mapping soil surface structure was demonstrated more than 20 years ago (Warner 1995), the advent of structure-from-motion (SfM) photogrammetry (James and Robson, 2012, Marra et al., submitted) has generated an improvement in topographic methods, due to its better accessibility to a wider variety of users, low cost, and increased automatization of routines and workflow (Fonstad et al. 2013, Nadal-Romero et al. 2015). The advantages introduced by SfM in the geosciences were demonstrated by James and Robson (2012), and the reconstruction of high-resolution surface models (Turner et al. 2012) has

opened new possibilities in the applications of geoscience analysis (Castillo et al. 2015), forestry (Pierzchała et al. 2014a, Pierzchała et al. 2014b, Pierzchała et al. 2016) and agriculture (Nouwakpo & Huang 2012).

The objective of this study was to investigate the usefulness of SfM photogrammetry in association with traditional methods for assessing soil disturbance in forest operations. The effects of forest operations on soil were considered for two types of forest machines, forwarder and skidder. The specific objectives of the study were:

(1) to evaluate multitemporal analysis based on the use of image-based high-resolution ground surface models generated through the use of SfM photogrammetry workflow as an instrument to determine rutting and bulges caused by forest operations along all trail surfaces; (2) to assess soil compaction with traditional techniques.

2. Materials and Methods

2.1 Study area

The study was conducted in central Italy, in the Biogenetic reserve of Vallombrosa, which is in the municipality of Reggello (Florence Province) and extends for 5.78 ha. The area is characterised by moderate steep terrain (mean slope = 30%) and is between 920 m and 980 m a.s.l. The forest is characterised by an even-age silver fir (*Abies alba* Mil.) plantation that was completely destroyed by a windstorm on the 5th of March, 2015 (Pirotti et al. 2016, Chirici et al., 2017). The climate is temperate-humid with Mediterranean-type rainfall with a summer minimum and a mean annual temperature of 9.7°C. From 2009-2013, the mean annual precipitation was 1337 mm, with an average of 71.2 mm in June-August (Bottalico et al. 2014). Soil developed on sedimentary rocks of the boulder formation of Chianti, which are comprised of sandstone with thin layers of siltstone and

rarely marl. Soil can be classified as Umbrepts and Umbric Dytrochrepts, based on the USDA Soil Taxonomy (1990). This study was carried out during salvage harvesting of damaged trees.

2.2 Forest machines

Two forestry machines were used in our study. The first was a forwarder John Deere JD1110 D with an empty mass of 17.5 tons (121 kW), which was equipped with 8-wheel Nokian Forest Rider 700/50 x 26.5 tires inflated at 51 kPa. The second machine was a skidder John Deere 548H with an empty mass of 11 tons (96 kW), equipped with 4-wheel Nokian Forest Rider 622/32 x 24.5 tires with chains, inflated to 68 kPa.

2.3 Experimental design

Before logging, two 25 x 3.5 m plots were randomly selected in the study area along the trails designed for timber extraction: one plot in the trail designated to be trafficked by the forwarder (forwarder trail, FT) and one in the trail to be trafficked by the skidder (skidder trail, ST). The mean slopes of the FT and ST plots were 25% and 20%, respectively.

Data collection was carried out at three time points: before forest logging (Time 1), considered as control data; seven working days after the beginning of logging (Time 2); and 13 working days after the beginning of logging (Time 3, i.e. the day after the end of wood extraction). The collected data were compared, taking into account the difference between: *(i)* periods 1 and 2 (Δ_{12}); *(ii)* periods 2 and 3 (Δ_{23}); and *(iii)* periods 1 and 3 (Δ_{13}). The forwarder transported logs up to 6 m in length and the skidder transported whole un-delimbed trees. Extraction was carried out in uphill direction for both machines.

2.4. Data collection

2.4.1. Photogrammetry data

2.4.1.1. Image acquisition

Pictures in FT and ST plots were collected using a consumer reflex camera (Table 1) mounted on a tripod 1.90 m in height. The image points were located at the corner of a rectangular network (Figure 1), and the images were acquired in nadir angle with an overlap and a side lap of 95% every 30 centimetre. The area covered by the images was greater than that of the plots, for a total of ~180 m^2, in order to have a robust model of the trails. A total of 350 images were acquired for each trail in each period. The image acquisition was done in 20 minutes for each trial in each period

Table 1: Details for camera and sensors used in the current study.

Camera model	Nikon D90
Image resolution (pixel)	4288*2848
Focal length (mm)	22
Pixel size (mm)	1*1

2.4.1.2. Ground control points

Ground control points (GCPs) were identified for image geolocation. Two types were measured in each trial: (i) six GCPs to georeference each model and (ii) four permanent GCPs outside the trails that were used to co-register the three models obtained (Figure 1). The X, Y and Z coordinates of each GCP were measured with a total station Leica TCA1800. The GCPs were translocated into the geographic coordinates system (UTM32N-WGS84) using the coordinates of one fixed control point measured by a GPS receiver (Trimble JUNO SERIES 3B). The permanent GCPs were represented in the field by a survey geodetic marker and were protected from the passage of forest machines.

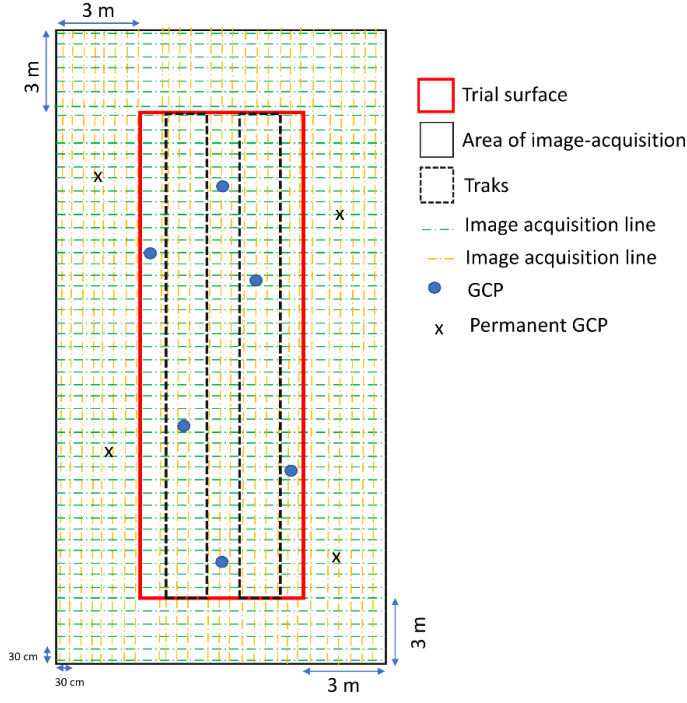

Figure 1: schema of image acquisition and location of ground control points (GCPs). Images were acquired in the intersection of the line acquisition (i.e. every 30 cm).

2.4.1.3. Photogrammetry process

The SfM technique was applied to obtain a 3D georeferenced point cloud from which a digital surface model (DSM) was derived. Data were processed using the Agisoft PhotoScan® Structure for Motion (SfM) photogrammetric software package (http://www.agisoft. com/), which has previously been successfully considered in different analyses (Verhoeven et al. 2012, Javernick et al. 2014, Woodget et al. 2014, Puliti et al. 2015). The workflow was comprised of the following steps: *(i)* image import, *(ii)* image alignment, *(iii)* georeferencing, *(iv)* optimisation of image alignment, *(v)* creation of the point cloud and (*vi*) generation of the DSM. After the

alignment, all photos were oriented, and the raw point cloud was georeferenced. The GCPs were then used to optimise the alignment of camera positions and the orientation of the data, which allowed for better accuracy and reconstruction results. Based on the estimated camera positions and GCPs, Agisoft PhotoScan® calculated depth information for each image, to be combined into a single dense point cloud dataset. The georeferentiation errors calculated by PhotoScan® along the x, y and z coordinates for each 3D point cloud models obtained via the structure-from-motion methodology (i.e. FT1, FT2, FT3, SK1, SK2, SK3) for X, Y and Z coordinate was under centimetric (i.e. < 1 cm)

2.4.1.4. Co-registration of model and difference calculation

The three-dense point clouds obtained by SfM workflow (FT1, FT2, FT3 and SK1, SK2, SK3) were co-registered using the four permanent GCPs outside the trail area by means of a point-based alignment in CloudCompare V2 software. This tool coarsely aligns two-point clouds using the "4 points Congruent Sets For Robust Registration" algorithm (Aiger et al. 2008). After the co-registration process, the point clouds were rasterised with rasterisation tools present in CloudCompare to create very high-resolution digital terrain models (DTMs) of each period for FT (FT-DTM1, FT-DTM2, FT-DTM3) and SK (SK-DTM1, SK-DTM2, SK-DTM3), with pixels of 0.1 x 0.1 cm. For each raster cell, the average elevation of the points in the pixel area was found and recorded in the cell.

The digital terrain models before logging (DTM1), half-way through logging operations (DTM2) and after logging operations (DTM3) were compared using map algebra tools, and differences in terrain elevation (Δz) after forest operations were computed as Δ_{12} = DTM1 – DTM2, Δ_{23} = DTM2 – DTM3 and Δ_{13} = DTM1 – DTM3. Pixels with $\Delta < 0$ were considered to be in

ruts and pixels with $\Delta > 0$ were considered to be in bulges along the surface of the two trails. The average, minimum and standard deviation were computed for $\Delta < 0$ pixels, whereas the average, maximum and standard deviation were computed for $\Delta > 0$ pixels for Δ_{12}, Δ_{23} and Δ_{13}.

2.4.2. Physical parameters

Thirty soil samples were collected at Times 1, 2 and 3, for a total of 90 (30 × 3) samples. These samples were collected (Figure 2) from the top soil layer using a rigid metallic cylinder (8.5-cm height and 5.0-cm inner diameter) after litter removal and were used for determining bulk density. Penetration and shear resistance were measured in triplicate close to each sampling point, using an Eijkelkamp TONS/FT2 penetrometer and a GEONOR 72412 scissometer, respectively. Soil samples were taken where the wheels of the two machines had passed (Figure 1).

All soil samples were weighed in the laboratory before ("moist weight") and after oven drying at 105°C to a constant weight ("dry weight"). Bulk density was determined as the ratio between soil sample dry weight and volume. Soil porosity (PO) was determined via the following equation (1):

$$PO = ((Dp - BD)/Dp*100 \quad (1)$$

where Dp is the particle density measured by a pycnometer (Multipycnometer, Quantachrome, Boynton Beach, FL, USA) on the same soil samples used to determine the bulk density (BD).

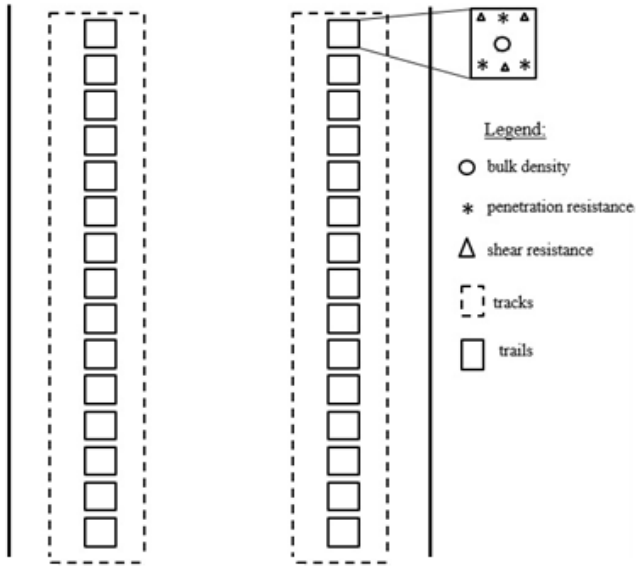

Figure 2: Sampling scheme of soil physical parameters data collection in left and right track caused by a forwarder or skidder.

2.5 Statistical analysis

Statistical analyses were carried out using the software package STATISTICA® ver. 7.1 (StatSoft, Tulsa, OK, USA). All data were checked for normality (Kolmogorov-Smirnov test) and homogeneity of variance (Levene's test) before the analysis. MANOVA analysis and a post hoc Tukey's HSD test were applied to physical parameters to assess the statistical differences among times (1–2, 2–3 and 1–3) and between machines (FT and ST).

A T-test was applied to the values of changes in ground surface level ($\Delta < 0$ = ruts/soil removal and $\Delta > 0$ = bulges/soil increase) between Δ_{12} and Δ_{23} in order to assess statistically significant differences between both times (2 and 3) and machines (FT and ST).

3. Results

The high-resolution surface models were derived by SfM workflow (Figs. 3 and 4; changes in soil surface level after logging are indicated in different colours).

Significant differences ($p < 0.05$) between FT and ST were found when comparing ruts/soil removal and bulges/soil increases at both time intervals Δ_{12} and Δ_{23} (Table 2). Specifically, significant differences in bulge height/soil increase were recorded between vehicles at both time intervals (times Δ_{12} and Δ_{23}), whereas rut depth/soil removal showed significant differences only in the first period (Δ_{12}). FT treatment showed greater rut depth and bulge height than did ST (Table 2). For both FT and ST, the greatest variation in ground surface was recorded in the first period (Δ_{12}). The effects on soil produced by the skidder and forwarder also differed in terms of disturbance type and shape. On FT, the two ruts caused by forwarder passes were clearly visible along the trail and were associated with bulges at both sides of the ruts, but soil displacement along the trail was not detectable (Figure 3). On the contrary, on ST, ruts (wheel tracks) were not visible, but soil displacement was clearly detectable along the trail (Figure 4). On ST, the comparison between time 1 (control) and 2 (seven days of logging) showed soil displacement in the same direction as that of timber extraction. In the second part of logging, from time 2 to 3, soil was further displaced due to the increasing number of passes. Specifically, on ST, a certain quantity of soil was removed at the beginning of the steeper part of the trail and replaced in the flat area at the end of the plot in the skidding direction (Figure 4).

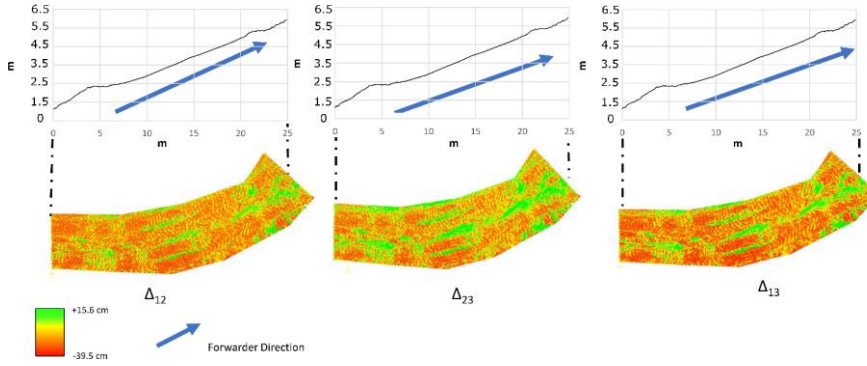

Figure 3: effects on soil produced by forwarder passes between times 1 and 2 (Δ_{12}), times 2 and 3 (Δ_{23}), and between times 1 and 3 (Δ_{13}).

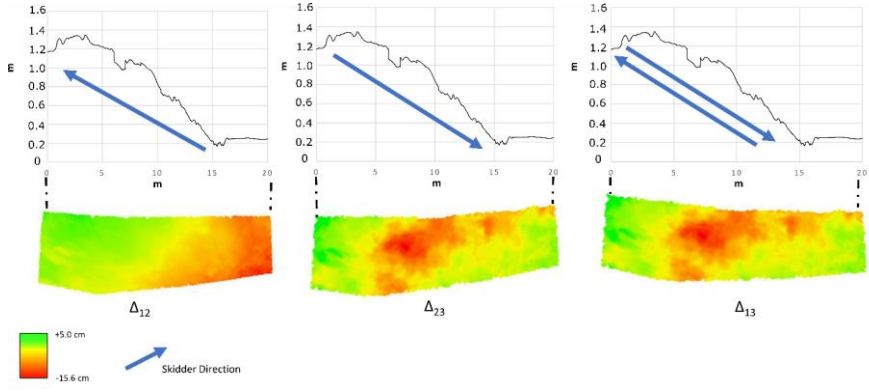

Figure 4: effects on soil produced by skidder passes between times 1 and 2 (Δ_{12}), times 2 and 3 (Δ_{23}), and between times 1 and 3 (Δ_{13}).

On FT, soil moisture, bulk density, porosity, and shear and penetration resistance were significantly higher after logging operations (at times 2 and 3) in comparison with control (time 1). The same parameters did not show significant differences between times 2 and 3, thus suggesting that most of the compaction was reached within the first several logging days. Similar results were obtained on ST, except that soil moisture did not show differences between times 1 and 2 (Table 3).

Table 2: Quantification of the ground surface variation produced by forwarder trails (FT) and skidder trails (ST) after different time periods, calculated considering all $\Delta < 0$ pixels as rutting and all $\Delta > 0$ pixels as bulges. Upper-case letters represent significant differences between FT and ST at the same period, whereas lower-case letters represent significant differences between different periods for the same vehicle (T-test, * $p < 0.05$, **$p<0.001$).

		Ground Surface Variation			
		Rut depth/soil removal $\Delta < 0$		*Bulge/soil increase* $\Delta > 0$	
Trail	*Trail interval*	*Minimum (cm)*	*average ± sd (cm)*	*Maximum (cm)*	*average ± sd (cm)*
FT	Δ_{12}	-36.5	-17.9 ± 12.1a* A*	13.5	9.5 ± 2.5 a * A*
FT	Δ_{23}	-12.3	-4.7 ± 03.6b* A	5.3	3.7 ±2.1 b * A*
FT	Δ_{13}	-39.5	-12.3 ± 8.2	15.6	9.8 ± 2.6
ST	Δ_{12}	-21.4	-8.9 ± 2.9 a ** B*	5.0	4.1 ± 1.0 a* B*
ST	Δ_{23}	-10.7	-4.8 ± 2.5b ** A	1.4	1.1 ± 00.8 b* B*
ST	Δ_{13}	-15.6	-6.1 ± 5.3	3.5	2.2 ± 1.6

Table 3: Results of MANOVA (mean ± standard deviation) to evaluate differences in soil parameters between trails used by different logging vehicles (Wilks test's $F = 42.33$, $p < 0.001$). Different lower-case letters show statistically significant differences between times 1, 2 and 3 (Tukey's HSD tests, $p < 0.05$, $N = 90$). Different upper-case letters show statistically significant differences between FT and ST at the same time (Tukey's HSD tests, $p < 0.05$, $N = 60$). FT = forwarder trail, ST = skidder trail.

Trail	*Time*	*Soil moisture*	*Bulk density*	*Porosity*	*Shear resistance*	*Penetration resistance*
		(%)	*(g cm^{-3})*	*(%)*	*(kPa)*	*(MPa)*
FT	1	19.38 ± 4.86 **a A**	0.81 ± 0.07 **a A**	66.28 ± 6.55 **a A**	68.02 ± 2.54 **a A**	0.35 ± 0.43 **a A**
	2	11.09 ± 1.55 **b A**	1.69 ± 0.24 **b A**	35.89 ± 9.45 **b A**	77.81 ± 7.92 **b A**	0.46 ± 0.34 **b A**
	3	11.13 ± 1.56 **b A**	1.71 ± 0.25 **b A**	35.88 ± 9.44 **b A**	77.80 ± 7.93 **b A**	0.45 ± 0.35 **b A**
ST	1	19.37 ± 4.86 **a A**	0.82 ± 0.07 **a A**	66.26 ± 6.55 **a A**	68.04 ± 2.54 **a A**	0.33 ± 0.43 **a A**
	2	19.24 ± 4.70 **a B**	1.06 ± 0.16 **b B**	61.03 ± 6.59 **b B**	72.40 ± 8.20 **b B**	0.42 ± 0.47 **b B**
	3	19.26 ± 4.72 **a B**	1.07 ± 0.18 **b B**	60.54 ± 6.62 **b B**	72.33 ± 8.23 **b B**	0.41 ± 0.51 **b B**

4. Discussion

At present, the physical parameters of soil are generally assumed to be the most useful for the assessment of impacts on soil due to vehicle traffic (Cambi et al. 2015). This is why we used bulk density, penetration

resistance, shear resistance and soil porosity for measuring soil compaction. In agreement with the results of previous studies (Wang 1997, Williamson & Neilsen 2000, Wallbrink et al. 2002, Han et al. 2009), our findings showed that the investigated physical parameters of soil were significantly affected mainly by the first vehicle passes (comparison between Time 1 and 2). Further machine passes slightly increased or did not affect the physical parameters.

Similar results concerning the impact of forwarder extraction on soil were recorded for the same parameters during timber extraction in the Italian Alps by Cambi et al. (2016). Other studies, however, have found opposing results. Gondard at al. (2003), when assessing the impacts of clear-cutting in Aleppo pine (*Pinus halepensis*) forests in southern France using both forwarders and skidders, observed deep disturbance (i.e. "topsoil removed, subsoil exposed'' according with McMahon's (1995) methods and classification) only when a skidder was used and did not find ruts. Similar results were reported by Deconchat (2001) in mixed oak coppices (Quercus rubber, Q. petraea and Q. pubescens) in southern France under an Oceanic climate. In this study the observed greater soil disturbance due to skidders than forwarders, even though skidders were responsible for less than 1% of ruts. In analysing these results, it should be considered that both studies were based on methods developed for assessing the soil's surface disturbance by means of the simple observation of soil conditions after logging; in other words, methods that cannot immediately detect less visible effects, such as soil compaction (Spinelli et al. 2010). Moreover, it should be considered that the first study was carried out under dry soil conditions, conditions under which soil is highly resistant to compaction, when only the scratching action of dragged logs may have any effect.

Nevertheless, even though our results highlighted a greater compaction caused by forwarders than skidders, it is not possible to draw any general conclusions about differences between the two machines. In fact, in our study it was not possible to collect data about the machine passes, or the wood volumes that had been transported over each trial area. Without, this information any general conclusion could be misleading.

Compaction also depends on machine size, weight and the pressure exerted on soil (Jansson & Johansson 1998, McNabb et al. 2001, Bygdén et al. 2004, Eliasson 2005, Marchi et al. 2014). To measure rutting, manual measurements of cross-sectional and longitudinal profiles are commonly applied (Koren et al. 2015). These methods are used for determining the rut depth at intervals along the trail and, together with rut width measurements, may be used to form a rough estimate of the volume of soil displaced. Our study indicated that the use of SfM photogrammetry may be very useful for the precise measurement of rutting and soil displacement. Analysing the differences in ground surface shape through the use of image-based models derived by SfM may offer detailed information about changes in the characteristics of ruts along the trail and may highlight soil displacement in all directions (e.g. from the tracks to the trail's centre and sides, along the trail). In our study, the results showed that in the first time interval, the FT caused deeper ruts and higher bulges than did the ST (Table 3). In the digital terrain model for FT obtained via SfM photogrammetry, ruts were clearly identifiable, whereas soil displacement along the trail was not detectable. In contrast, ruts were not visible on ST, but soil displacement along the trail was clearly detectable. These difference between FT and ST were likely due to the different types of timber extraction. In fact, rutting is caused by machine wheels both in FT and ST, but in ST, the passing of the top end of the dragged logs (Wood et

al. 2003) may change the impacts on soil in two ways: i) the top ends of the dragged logs reshape the ground after the skidder passes, hiding the rut left by the wheels; ii) the top ends of the dragged logs displace a certain quantity of soil in the dragging direction during each extraction trip. The latter effect may be particularly intense close to slope changes, because the heads of the logs scratch and displace the soil (Williamson & Neilsen 2000, Heninger et al. 2002, Horn et al. 2007, Agherkakli et al. 2010). Soil compaction and soil crumbling and displacement may result in increased water runoff and soil erosion (Williamson & Neilsen 2000, Cambi et al. 2015, Venanzi et al. 2016), with a consequent loss of fertile soil (Venanzi et al. 2016).

Forest soil is extremely fragile in physical terms and the improvement of methods for investigating the effects of soil disturbance is very important (Picchio et al. 2012). With the use of image-based models derived from SfM photogrammetry, the quantification of soil displacement is highly improved in comparison to traditional sampling methods. The use of image-based models allows a new approach to the quantification of soil disturbance, improving analysis concerning soil displacement due to logging, comparable with results obtained by point cloud derived by TLS (Koren et al. 2015). The use of a consumer reflex camera in conjunction with the use of SfM software, however, can produce accuracy models at low cost, with respect to the use of TLS. The use of this methodology (Pierzchala et al. 2014a, Koren et al. 2015) can produce information along the entire trail, not only at the sampling points, and this information is very important for forest managers, allowing the monitoring of soil ecosystems after forest operations and the planning of soil recovery practices (Pinard et al., 2000).

5. Conclusions

This study was conducted with the overall objective of describing

the effects of logging on the depth of ruts, through manual measurements in the field and photogrammetry analysis and on the physical properties of soil. Our findings highlighted how the use of both, image-based models derived via SfM photogrammetry and manual sampling may be very useful for improving the assessment of the impacts of forest operations on soil. Both methods showed significant impacts on soil caused by two different forest machines.

Image-based models turned out to be useful for determining the distribution and types of disturbances, while the physical parameters of soils investigated in this study may be useful in determining local changes in soil characteristics. Our results showed that the image-based models derived via SfM photogrammetric workflow can be useful tools with which to evaluate soil displacement caused by forest machines, improving monitoring and management of impacts upon soil and giving continuous soil displacement measures along the entire trail surface.

Acknowledgement

The authors would like to thank the Vallombrosa Territorial Office for Biodiversity (Carabinieri Forestale) for its support in the research study, Dr. Giovanni Galipò for his help with the field survey and Ms. Ilaria Zorzi, in particular, for her help with the fieldwork.

References

Agherkakli B, Najafi A, Sadeghi S (2010). Ground based operation effects on soil disturbance by steel tracked skidder in a steep slope of forest. Journal of Forest Science 56: 278-284.

Aiger, D, N J Mitra, and D Cohen-Or. (2008). “4-Points Congruent Sets for Robust Surface Registration.” ACM Transactions on Graphics, 27 (3), 1-

10.
Alakukku L, Weisskopf P, Chamen WC, Tijink FG, Van Der Linden J, Pires S, Sommer C, Spoor G (2003). Prevention strategies for field traffic induced subsoil compaction: a review. Soil and Tillage Research 73 145-160. - doi: 10.1016/S01 67-1987(03)00107-7.
Ampoorter E, Goris R, Cornelis WM, Verheyen K (2007). Impact of mechanized logging on compaction status of sandy forest soils. Forest Ecology and Management 241: 162-174.
Bagheri, I., Naghdi, R., Jalali, A.M. 2013. Evaluation of factors affecting soil erosion along skid trails (case study; Shafarood Forest, Northern Iran). CJES. 11: 151–160
Bygdén G, Eliasson L, Wästerlund I (2004). Rut depth, soil compaction and rolling resistance when using bogie tracks. Journal of Terramechanics 40: 179-190. - doi: 10.1016/j.jterra.2003. 12.001.
Cambi M, Certini G, Neri F, Marchi E (2015). The impact of heavy traffic on forest soils: a review. Forest Ecology and Management 338: 124-138. - doi: 10.1016/j.foreco.2014.11.022.
Cambi M, Grigolato S, Neri F, Picchio R, Marchi E (2016). Effects of forwarder operation on soil physical characteristics: a case study in the Italian Alps. Croatian Journal of Forest Engineering 37 (2): 233-239.
Castillo R, James CM, Redel-Macías MD, Pérez R, Gómez JA (2015). SF3M software: 3-D photo-reconstruction for non-expert users and its application to a gully network. SOIL 1: 583-594. - doi:10.5194/soil-1-583-2015.
Chirici, G., Bottalico, F., Giannetti, F., Rossi, P., Del Perugia, B., Travaglini, D., Nocentini, S., Ruedlinger, E.H.K., Marchi, E., Foderi, F., Fioravanti, M., Fattorini, L., Guariglia, A., Ciancio, O., McRoberts, L.R., Naesset, E., Corona, P., Gozzini, B., 2017. Assessing forest windthrow damages using single-date, post-event airborne laser scanning data. Forestry. doi: 10.1093/forestry/cpx029
Christopher E.A., & Visser, R. (2007). Methodology for evaluating post harvest erosion risk for the protection of water quality. N.Z. J. For. 52(2):20–25.
Deconchat M (2001). Effects of logging techniques on the soil surface. Annals of Forest Sciences (France) 58: 653-661.
D'Oleire-Oltmanns S, Marzolff I, Peter K, Ries J (2012). Unmanned Aerial Vehicle (UAV) for monitoring soil erosion in Morocco. Remote Sensing 4: 3390-3416.
Eliasson L (2005). Effects of forwarder tyre pressure on rut formation and soil compaction. Silva Fennica 39: 549-557. - doi: 10.14214/sf.366.
Fonstad M.A., Dietrich J.T., Courville B.C., Jensen J.L., & Carbonneau P.E. (2013). Topographic structure from motion: a new development in

photogrammetfic measurament. Earth Surf. Process. Landforms 38, 421–430

Giannetti, F., Chirici, G., Travaglini, D., Bottalico, F., Marchi, E., Cambi, M. (2017). Assessment of Soil Disturbance Caused by Forest Operations by Means of Portable Laser Scanner and Soil Physical Parameters. Soil Science Society of America Journal, doi:10.2136/sssaj2017.02.0051Gondard H, Romane F, Aronson J, Shater Z (2003). Impact of soil surface disturbances on functional group diversity after clear-cutting in Aleppo pine (Pinus halepensis) forests in southern France. Forest Ecology and Management 180: 165-174.

Gomez, G.A., R.F. Powers, M.J. Singer, and W.R. Horwath. (2002). Nuptake andNstatus in ponderosa pine as affected by soil compation and forest floor removal. Plant Soil 242:263–275

Gondard, Hélène et al. "Impact of Soil Surface Disturbances on Functional Group Diversity after Clear-Cutting in Aleppo Pine (Pinus Halepensis) Forests in Southern France." Forest Ecology and Management 180.1–3 (2003): 165–174.

Grace J. M.; Skaggs R.W.; Cassel D.K. (2006). Soil physical changes associated with forest harvesting operations on a organic soil. Journal of Soil Science Society of America. 70: 503-509

Han SK, Han HS, Page-Dumroese D, Johnson LR (2009). Soil compaction associated with cut-to-length and whole-tree harvesting of a coniferous forest. Canadian Journal of Forest Research 39: 976-989.

Heng, B. C. P., J. H. Chandler, and A. Armstrong (2010), Applying close range digital photogrammetry in soil erosion studies, Photogramm. Rec., 25, 240 – 265, doi:10.1111/j.1477-9730.2010.00584.x.

Heninger R, Scott W, Dobkowski A, Miller R, Anderson H, Duke S (2002). Soil disturbance and 10-year growth response of coast Douglas-fir on non-tilled and tilled skid trails in the Oregon Cascades. Canadian Journal of Forest Research 32: 233-246.

Horn, R., Vossbrink, J., Peth, S., Becker, S. 2007. Impact of modern forest vehicles on soil physical properties. For. Ecol. Manag. 248 (1–2): 56–63. doi: 10.1016/j.foreco.2007.02.037

Kaiser A, Neugirg F, Rock G, Müller C, Haas F, Ries J, Schmidt J (2014). Small-scale surface reconstruction and volume calculation of soil erosion in complex Moroccan gully morphology using structure from motion. Remote Sensing 6(8): 7050-7080.

Koren M, Slančík M, Suchomel J, Dubina J (2015). Use of terrestrial laser scanning to evaluate the spatial distribution of soil disturbance by skidding operations. iForest 8: 386-393.

James, M.R., Robson, S., 2012. Straightforward reconstruction of 3D surfaces and topography with a camera: Accuracy and geoscience

application. Journal of Geophysical Research: Earth Surface 117, 1–17. doi:10.1029/2011JF002289

Jamshidi R, Jaeger D, Raafatnia N, Tabari M (2008). Influence of two ground-based skidding systems on soil compaction under different slope and gradient conditions. International Journal of Engineering Science 19: 9-16. [online] doi: abs/10.1080/14942119.2008.10702554.

Jansson KJ, Johansson J (1998). Soil changes after traffic with a tracked and wheeled forest machine: a case study on a silt loam in Sweden. Forestry 71: 57-66. - doi: 10.1093/forestry/71.1.57.

Javernick L, Brasington B, Caruso B (2014). Modeling the topography of shallow braided rivers using structure-from-motion photogramnmetry. Geomorphology 213: 166-182.

Jester W, Klik A (2005). Soil surface roughness measurement—methods, applicability, and surface representation. Catena 64 (2-3): 174-192.

Jourgholami M., Soltanpour S., Etehadi Abari M., and Zenner, E.K. (2014). Influence of slope on physical soil disturbance due to farm tractor forwarding in a Hyrcanian forest of northern Iran. iForest 7:342–348. doi:10.3832/ifor1141-007

Lotfalian M., & Parsakhoo A. (2009). Investigation of Forest Soil Disturbance Caused by Rubber-tired Skidder Traffic. International Journal of Natural and Engineering Sciences 3 (1), 01-04

Marchi E, Picchio R, Spinelli R, Verani S, Venanzi R, Certini G (2014). Environmental impact assessment of different logging methods in pine forests thinning. Ecological Engineering 70: 429-436.

Marra E, Cambi M, Fernandez Lacruz R, Giannetti F, Marchi E, Nordfjell T (submitted). Photogrammetry Estimation of Wheel Rut Dimension and Soil Compaction Caused by a Forwarder.

McMahon S (1995). A survey method for assessing site disturbance. Project Report 54. Logging Industry Research Organisation, New Zealand, 16 pp.

McNabb DH, Startsev AD, Nguyen H (2001). Soil wetness and traffic level effects on bulk density and air-filled porosity of compacted boreal forest soils. Soil Science Society of America Journal 65: 1238-1247. - doi: 10.2136/sssaj2001.65 41238x.

Micheletti, N., Chandler, J.H., Lane, S.N., 2015. Investigating the geomorphological potential of freely available and accessible structure-from-motion photogrammetry using a smartphone. Earth Surface Processes and Landforms 40, 473–486. doi:10.1002/esp.3648

Nadal-Romero, E., Revuelto, J., Errea, P., López-Moreno, J.I., 2015. The application of terrestrial laser scanner and photogrammetry in measuring erosion and deposition processes in humid badlands in the Central Spanish Pyrenees. SOIL Discussions 2, 337–369.

doi:10.5194/soild-2-337-2015
Nugent C., Kanali C., Owende P.M.O., Nieuwenhuis M., Ward S., 2003. Characteristic site disturbance due to harvesting and extraction machinery traffic on sensitive forest sites with peat soils. Forest Ecology and Management, 180: 85–98
Nouwakpo SK, Huang C (2012). A simplified close-range photogrammetric technique for soil erosion assessment. Soil Science Society of America Journal 76: 70-84.
Picchio R, Neri F, Petrini E, Verani S, Marchi E, Certini G (2012). Machinery-induced soil compaction in thinning two pine stands in central Italy. Forest Ecology and Management 285: 38-43.
Pierzchała M, Talbot B, Astrup RA (2014a). Assessing the quality of a surface model generated from the images obtained from Inexpensive Hobbyist Aircraft (IHA) using structure from motion (SFM). In: Proceedings of the "International Precision Forestry Symposium, Developments in Precision Forestry since 2006." (Ackerman PA, Ham H, Lu C eds). Stellenbosch University (Stellenbosch, South Africa), 1-3 March 2010. Stellenbosch University.
Pierzchała M, Talbot B, Astrup R (2014b). Estimating soil displacement from timber extraction trails in steep terrain: application of an unmanned aircraft for 3D modelling. Forests 5: 1212-1223.
Pierzchała M, Talbot B, Astrup R (2016). Measuring wheel ruts with close-range photogrammetry. Forestry 89: 383-391.
Pinard MA, Barker M, Tay J (2000). Soil disturbance and post-logging forest recovery on bulldozer paths in Sabah, Malaysia. FORECO, 130 (1): 213-225. - doi: 10.1016/S0378-1127(99)00192-9.
Pirotti F, Travaglini D, Giannetti F, Kutchartt E, Bottalico F, Chirici G (2016). Kernel feature cross-correlation for unsupervised quantification of damage from windthrow in forests. The International Archives of the Photogrammetry, Remote Sensing and Spatial Information Sciences, Volume XLI-B7, 2016 XXIII ISPRS Congress, 12–19 July 2016, Prague, Czech Republic: 17-22. - doi: 10.5194/isprs-archives-XLI-B7-17-2016.
Puliti S, Ørka HO, Gobakken T, Næsset E (2015). Inventory of small forest areas using an unmanned aerial system. Remote Sensing 7: 9632-9654. [online] URL: http://dx.doi.org/10.3390/rs70809632
Sheridan GJ (2003). A comparison of rubber-tired and steel-tracked skidders on forest soil physical properties. Australian Journal of Soil Research 41: 1063-1075. - doi: 10.1071/SR02090.
Spinelli R, Magagnotti N, Nati C (2010). Benchmarking the impact of traditional small-scale logging systems used in Mediterranean forestry. Forest Ecology and Management 260: 1997-2001.
Talbot, B., Pierzchała, M., Astrup, R., 2016. Applications of Remote and

Proximal Sensing for Improved Precision in Forest Operations 327–336.

Turner, D., Lucieer, A., Watson, C., 2012. An automated technique for generating georectified mosaics from ultra-high resolution Unmanned Aerial Vehicle (UAV) imagery, based on Structure from Motion (SFM) point clouds. Remote Sensing 4, 1392–1410. doi:10.3390/rs4051392

Venanzi R, Picchio R, Piovesan G (2016). Silvicultural and logging impact on soil characteristics in Chestnut (Castanea sativa Mill.) Mediterranean coppice. Ecological Engineering 92: 82-89. - doi: 10.1016/j.ecoleng.2016.03.034.

Verhoeven G, Doneus M, Briese C, Vermeulen F (2012). Mapping by matching: a computer vision-based approach to fast and accurate georeferencing of archaeological aerial photographs. Journal of Archaeological Science 39: 2060-2070.

Vericat, D., Smith, M.W., Brasington, J., 2014. Patterns of topographic change in sub-humid badlands determined by high resolution multi-temporal topographic surveys. Catena 120, 164–176. doi:10.1016/j.catena.2014.04.012

Wallbrink P J, Roddy B P, and Olley, J M. (2002).A Tracer Bugdet Quantification Soil Redistribution on Hillslopes after Forest Harvesting. Catena 47.3 (2002): 179–201.

Warner WS (1995). Mapping a three-dimensional soil surface with hand-held 35 Mm photography. Soil and Tillage Research 34: 187-197.

Williamson JR, Neilsen WA (2000). The influence of forest site on rate and extent of soil compaction and profile disturbance of skid trails during ground-based harvesting. Canadian Journal of Forest Research 30: 1196-1205. - doi: 10.1139/x00-04.

Wood MJ, Moffat AJ, Carling PA (2003). Improving the design of slash roads used to reduce soil disturbance during mechanized harvesting of coniferous forest plantations in the UK. Journal of Forest Engineering 14: 11-23.

Woodget AS, Carbonneau PE, Visser F, Maddock I (2014). Quantifying submerged fluvial topography using hyperspatial resolution UAS imagery and structure from motion photogrammetry. Earth Surface Processes and Landforms 40 (1): 47-64. - doi: 10.1002/esp.3613.

Other publication and contributions

1. Papers

1. Matteo Mura, Francesca Bottalico, **Francesca Giannetti**, Remo Bertani, Raffaello Giannini, Marco Mancini, Simone Orlandini, Davide Travaglini, Gherardo Chirici (2018). Exploiting the capabilities of the Sentinel-2 multi spectral instrument for predicting growing stock volume in forest ecosystems. International Journal of Applied Earth Observation and Geoinformation 66:126-134, doi:https://doi.org/10.1016/j.jag.2017.11.013
2. **Francesca Giannetti**, Anna Barbati, Leone Davide Mancini, Davide Travaglini, Annemarie Bastrup-Birk, Roberto Canullo, Susanna Nocentini, Gherardo Chirici (accepted). European Forest Types: toward an automated classification. Annals of Forest Science.DOI:10.1007/s13595-017-0674-6
3. Nicola Puletti, **Francesca Giannetti**, Gherardo Chirici & Roberto Canullo. To cite this article: Nicola Puletti, Francesca Giannetti, Gherardo Chirici & Roberto Canullo (2017). Deadwood distribution in European forests, Journal of Maps, 13:2, 733-736,http://dx.doi.org/10.1080/17445647.2017.1369184
4. Francesca Bottalico, Davide Travaglini, Gherardo Chirici, Vittorio Garfì, **Francesca Giannetti**, Alessandra De Marco, Silvano Fares, Marco Marchetti, Susanna Nocentini, Elena Paoletti, Fabio Salbitano, Giovanni Sanesi (2017). A spatially-explicit method to assess the dry deposition of air pollution by urban forests in the city of Florence, Italy. Urban Forestry & Urban Greening, Volume 27, October 2017, Pages 221-234. https://doi.org/10.1016/j.ufug.2017.08.013
5. Gherardo Chirici, Francesca Bottalico, **Francesca Giannetti**, Barbara Del Perugia, Davide Travaglini, Susanna Nocentini, Erico Kutchartt, Enrico Marchi, Cristiano Foderi, Marco Fioravanti, Lorenzo Fattorini, Lorenzo Bottai, Ronald E. McRoberts, Erik Næsset Piermaria Corona, Bernardo Gozzini (2017). Assessing forest windthrow damage using single-date, post-event airborne laser scanning data. Forestry: An International Journal of Forest Research. https://doi.org/10.1093/forestry/cpx029
6. Chirici, G., Bottalico, F., **Giannetti, F.,** Rossi, P., Del Perugia, B., Travaglini, D.,……, Gozzini, B. (2017) Stima dei danni da vento ai soprassuoli forestali in Regione Toscana a seguito dell'evento del 5 marzo 2015. L Italia Forestale e Montana 71(4):197-213 DOI: http://10.4129/ifm.2016.4.02

7. Pirotti, Francesco; Travaglini, Davide; **Giannetti, Francesca**; Kutchartt, Erico; Bottalico, Francesca; Chirici, Gherardo (2016). Kernel feature cross-correlation for unsupervised quantification of damage from windthrow in forests. In: XXIII ISPRS Congress, Prague, Czech Republic, 12–19 July 2016, ISPRS, pp. 17-22. DOI:10.5194/isprsarchives-XLI-B7- 17-2016
8. **Francesca Giannetti**, Gherardo Chirici, Elena Paoletti, Marco Borghetti, Gabriele Bucci (2016) Assessing the bibliometric productivity of forest scientists in Italy. Annals of Selvicultural Research, 40 (1), 19-30. DOI: http://dx.doi.org/10.12899/asr-1211
9. Francesca Bottalico, Gherardo Chirici, **Francesca Giannetti**, Alessandro De Marco, Susanna Nocentini, Elena Paoletti, Fabio Salbitano, Giovanni Sanesi, Chiara Serenelli, Davide Travaglini (2016) Air Pollution Removal by Green Infrastructures and Urban Forests in the City of Florence. Agricolture and Agricoltural Science Procedia, 8, 243-251

2. Book Chapter

1. Giovanni Caudullo, Salvatore Claudio Pasta, **Francesca Giannetti**, Anna Barbati, Gherardo Chirici. Chapter: European Forest classifications in "European Atlas of Forest Tree Species", Book · March 2016, Publisher: Publications Office of the European Union, Luxembourg, Editor: Jesús San-Miguel-Ayanz, Daniele de Rigo, Giovanni Caudullo, Tracy Houston Durrant, Achille Mauri, ISBN: 9789279367403
2. Mario Pividori, **Francesca Giannetti**, Anna Barbati, Gherardo Chirici. Chapter: European Forest Types: tree species matrix in "European Atlas of Forest Tree Species", Book · March 4 2016, Publisher: Publications Office of the European Union, Luxembourg, Editor: Jesús SanMiguel-Ayanz, Daniele de Rigo, Giovanni Caudullo, Tracy Houston Durrant, Achille Mauri, ISBN: 9789279367403

3. Conference Proceedings

1. Travaglini, D., Corona P., Del Perugia B., **Giannetti F.**, Chirici, G. (2017). "*Rilievi inventariali con laser scanner terrestre mobile: un confronto con rilievi classici in castagneti da frutto*". In: Proceedings of the XI SISEF National Congress "La Foresta che Cambia: qualità della vita e opportunità in un paese che cambia" (Fares S, Alivernini, A, Ferrara C, Marchi M, Sallustio L, Chianucci F, Bucci G, eds). Rome (Italy, 10-13 Sept 2017. Abstract-book URL: http://www.sisef.it/sisef/xi-congresso/

2. **Giannetti, F**, Puliti, S., Gobakken, T., Næsset, E, Travaglini D., Chirici, G., (2017) "*DTM-independent variables to predict forest inventory variables using 3D UAV photogrammetric data*". In: Proceedings of the XI SISEF National Congress "La Foresta che Cambia: qualità della vita e opportunità in un paese che cambia" (Fares S, Alivernini, A, Ferrara C, Marchi M, Sallustio L, Chianucci F, Bucci G, eds). Rome (Italy, 10-13 Sept 2017. Abstract-book URL: http://www.sisef.it/sisef/xi-congresso/
3. Cambi, M, **Giannetti F.,** Travaglini D., Chirici, G., Marchi, E., (2017) "*Utilizzo di tecnologie proximal sensing per quantificare il danno al suolo dovuto alle operazioni di esposto*". In: Proceedings of the XI SISEF National Congress "La Foresta che Cambia: qualità della vita e opportunità in un paese che cambia" (Fares S, Alivernini, A, Ferrara C, Marchi M, Sallustio L, Chianucci F, Bucci G, eds). Rome (Italy, 10-13 Sept 2017. Abstract-book URL: http://www.sisef.it/sisef/xi-congresso/
4. Del Perugia B., Travaglini D., Barbati A., Barzagli A., **Giannetti F.,** Lasserre B., Nocentini S., Santopuoli, G., Chirici G., (2017) "*Classificazione delle specie forestali con dati multispettrali e laser scanning multipiattaforma".* In: Proceedings of the XI SISEF National Congress "La Foresta che Cambia: qualità della vita e opportunità in un paese che cambia" (Fares S, Alivernini, A, Ferrara C, Marchi M, Sallustio L, Chianucci F, Bucci G, eds). Rome (Italy, 10-13 Sept 2017. Abstract-book URL: http://www.sisef.it/sisef/xi-congresso/
5. Puletti, N., Chirici G., Barbati A., **Giannetti F**., Grotti M., Morletti A., Ventre T, Corona P., Fattorini L., (2017) "*Stima di risorse forestali ad alta risoluzione tramite informazioni telerilevate multipiattaforma*". In: Proceedings of the XI SISEF National Congress "La Foresta che Cambia: qualità della vita e opportunità in un paese che cambia" (Fares S, Alivernini, A, Ferrara C, Marchi M, Sallustio L, Chianucci F, Bucci G, eds). Rome (Italy, 10-13 Sept 2017. Abstract-book URL: http://www.sisef.it/sisef/xi-congresso/
6. **Giannetti, F.,** Travaglini D., Chirici, G., (2017) "*Use of UAV photogrammetric 3D data for forestry invetory: a case of study*". In: Proceedings of the XI SISEF National Congress "La Foresta che Cambia: qualità della vita e opportunità in un paese che cambia" (Fares S, Alivernini, A, Ferrara C, Marchi M, Sallustio L, Chianucci F, Bucci G, eds). Rome (Italy, 10-13 Sept 2017. Abstract-book URL: http://www.sisef.it/sisef/xi-congresso/
7. Giuliarelli D., Barbati A., Del Perugia B., Ferrari B., **Giannetti F.,** Lasserre B., Mattioli W., Oreti L., Santopuoli G., Tomao A., Travaglini D., Chirici G., (2017) "*Mappatura degli European Forest Types da*

drone e applicazioni per la stima di indicatori di biodiversità forestale". In: Proceedings of the XI SISEF National Congress "La Foresta che Cambia: qualità della vita e opportunità in un paese che cambia" (Fares S, Alivernini, A, Ferrara C, Marchi M, Sallustio L, Chianucci F, Bucci G, eds). Rome (Italy, 10-13 Sept 2017. Abstract-book URL: http://www.sisef.it/sisef/xi-congresso/

8. Balsi, M., Esposito S., Fallavollita P., **Giannetti F.,** Chirici G., (2017) "*High-density Aerial LiDAR Survay for the FREShLife Project*". In: Proceedings of the XI SISEF National Congress "La Foresta che Cambia: qualità della vita e opportunità in un paese che cambia" (Fares S, Alivernini, A, Ferrara C, Marchi M, Sallustio L, Chianucci F, Bucci G, eds). Rome (Italy, 10-13 Sept 2017. Abstract-book URL: http://www.sisef.it/sisef/xi-congresso/
9. D. Travaglini, A. Barbati, A. Barzagli, B. Del Perugia, **F. Giannetti**, D. Giuliarelli, B. Lasserre, M. Marchetti, G. Santopuoli, A. Tomao, G. Chirici "*Integrazione di dati inventariali e dati telerilevati con sistemi a pilotaggio remoto per la stima di indicatori della gestione forestale sostenibile*". XIV ATTI CONVEGNO AISSA, Campobasso, 16-17 Febbraio 2017
10. M. Cambi, **F. Giannetti**, D. Travaglini, G. Chirici, E. Marchi "*Valutazione dei danni al suolo prodotti da utilizzazioni forestali attraverso l'analisi multi-temporale di campioni di suolo e scansioni laser scanner portile terreste*". XIV ATTI CONVEGNO AISSA, Campobasso, 16-17 Febbraio 2017
11. Chirici G., Barzagli A., **Giannetti F.**, Travaglini D., Balsi M., Esposito S., Bottalico F. *"Structure From Motion e Airborne Laser Scanning tramite SAPR per la stima di variabili di interesse forestale"*Conferenza . XX Conferenza Nazionale ASITA, Cagliari, 8-9 Novembre 2016 http://atti.asita.it/ASITA2016/Pdf/092.pdf
12. Alessandro Errico, Francesca Giannetti, Pasquino, V., Giannecchini, L., Solari, L. Gherardo Chirici, Federico Preti (2016). *"The effect of flexible vegetation on flow in drainage channels – field surveys for roughness coefficients estimation".* XXXV CONVEGNO NAZIONALE DI IDRAULICA E COSTRUZIONI IDRAULICHE, Bologna, 14-16 Settembre 2016
13. Martina Cambi, **Francesca Giannetti**, Francesca Bottalico, Gherardo Chirici, Enrico Marchi. *"Estimating rutting and soil displacement in skid trails by soil sampling and 3D Structure for Motion (SfM) photogrammetry modelling: first trial in Vallombrosa forest (Italy)".* 49th International Symposium on Forestry Mechanization (FORMEC) - 4-7 September 2016, Warsaw (Poland)

14. Gherardo Chirici, Andrea Barzagli, **Francesca Giannetti**, Davide Travaglini, Marco Balsi, Francesca Bottalico (2016). *"Telerilevamento LiDAR e ottico tramite SAPR per il monitoraggio delle risorse forestali*". Convegno AIT 2016. Palermo, 22-24 June 2016.
15. **Giannetti F.**, Cambi M., Bottalico F., Chirici G., Marchi E. (2015) *"Trend analysis of sustainability of forest wood production in Tuscany Regions"*, XIV World Forestry Congress FAO, Durban, South Africa, 7-11 September 2015
16. Bottalico F., Chirici G., **Giannetti F.**, De Marco A., Nocentini S., Paoletti E., Salbitano F., Sanesi G., Serenelli C., Travaglini D. (2015) *"Air pollution removal by infrastructures and urban forest in the city of Florence*". Florence SWIF, Sustainability of Well-being International Forum 2015: Food for sustainability and not just food, Florence, 7 June 2015
17. Chirici, G., Barbati A., **Giannetti F.**, Travaglini D., Canullo R. (2015) *"The Use of ICP Forests Level I BIOSOIL – BIODIVERSITY plots for pan-European estimation of forest variables".* In: 4th ICP Forests Scientific Conference, Ljubljana, 19-20 May 2015. The Silva Slovenica Publishing Centre, pp 17, ISBN:978-961-6425-87-2
18. F. Bottalico, G. Chirici, A. De Marco, V. Garfì, **F. Giannetti.**, S. Nocentini, E. Paoletti, F. Salbitano, G. Sanesi, C. Serenelli, D. Travaglini (2015). Urban forest and air pollutants removal: a matter of quality of life. In: Proceedings of the 10th SISEF National Congress "Sostenere il pianeta, boschi per la vita - Ricerca e innovazione per la tutela e la valorizzazione delle risorse forestali" (Travaglini D, Rossi P, Bucci G eds). Firenze (Italy) 15-18 Sep 2015. Abstract-book: Comunicazioni orali, Paper #c10.9.6., pp. 97, [online] URL: http://www.sisef.it/sisef/x-congresso/
19. G. Chirici, L. Bottai, F. Bottalico, A. Bronzi, C. Chiostri, O. Ciancio, M. Fioravanti, M. Germani, **F. Giannetti**, B. Gozzini, E. Gravano, A.M. Melara, S. Nocentini, D. Travaglini (2015). Attività di monitoraggio dei danni da vento ai comprensori forestali della Regione Toscana a seguito dell'evento del 5 marzo 2015. In: Proceedings of the 10th SISEF National Congress "Sostenere il pianeta, boschi per la vita - Ricerca e innovazione per la tutela e la valorizzazione delle risorse forestali" (Travaglini D, Rossi P, Bucci G eds). Firenze (Italy) 15-18 Sep 2015. Abstract-book: Comunicazioni orali, Paper #c10.7.4., pp. 75, [online] URL: http://www.sisef.it/sisef/x-congresso/
20. **F. Giannetti**, A. Barbati, L.D. Mancini, D. Travaglini, G. Chirici (2015). GIS-based automatic classification of BIOSOIL project forest sample plots into the European Forest Types. In: Proceedings of the 10th

SISEF National Congress "Sostenere il pianeta, boschi per la vita - Ricerca e innovazione per la tutela e la valorizzazione delle risorse forestali" (Travaglini D, Rossi P, Bucci G eds). Firenze (Italy) 15-18 Sep 2015. Abstract-book: Comunicazioni orali, Paper #c10.7.3., pp. 74, [online] URL: http://www.sisef.it/sisef/x-congresso/

4. Conference talks and seminars

1. Chirici Gherardo, **Giannetti** Francesca, Travaglini Davide. "*Integrating airborne and terrestrial laser scanning in designing new approaches to forest inventory sampling*". IUFRO 125th Anniversary Congress, 18-22 Freiburg, Germany, 2017
2. Marra E., Cambi Martina, Fernandez Lacruz R., **Giannetti** Francesca, Marchi E., Nordfjell T. *"Photogrammetry estimation of wheel ruts dimension and soil compaction caused by a forwarder*".IUFRO 125th Anniversary Congress, 18-22 Freiburg, Germany, 2017
3. Barbati A., Bravo-Oviedo Andrés, **Giannetti** Francesca, Mancini Leone Davide, Corona P. "*European Mixed forests in Europe: towards an estimation*". IUFRO 125th Anniversary Congress, 18-22 Freiburg, Germany, 2017
4. Galluzzi Marta, Chirici G. (Italy), Selvi F., **Giannetti** Francesca, Mura M., Travaglini D., Canullo R., Bastrup-Birk Annemarie, Valbuena R., Barbati Anna. "Pan-European forest biodiversity monitoring through the ICP-level I network. First results from the BIOSOIL-BIODIVERSITY project". IUFRO 125th Anniversary Congress, 18-22 Freiburg, Germany, 2017
5. Travaglini, D., Chirici, G., Del Perugia, B., **Giannetti**, F., Bottai, L., Gozzini, B., Corona, P. "*Metodologia per il rilievo dei castagneti da frutto IGP*". Giornata di studio: metodologie innovative per l'aggiornamento dell'inventario castanicolo nazionale. Accademia dei Georgofili, Firenze, 6 Febbraio, 2017
6. Travaglini, D., **Giannetti**, F., Chirici, G. "*Potenzialità di impiego dei sistemi laser scannner terrestre mobili nel rilievo delle risorse forestali: prime esperienze in Toscana*". Seminario "Fight Fire With Fire, combatti il fuoco con il fuoco", Rincine, 11 ottobre 2016
7. Chirici G., Barzagli A., **Giannetti F.**, Travaglini D., Balsi M., Esposito S., Bottalico F. *"Structure From Motion e Airborne Laser Scanning tramite SAPR per la stima di variabili di interesse forestale".*XX Conferenza Nazionale ASITA, 2016, Cagliari, 8-10 November, 2016
8. **Giannetti**, F., Travaglini, D., Chirici, C. "*Portable Laser Scanner Application and image acquired by SAPR to Monitoring Forest Ecosystem*". Vista delegazione Ministero delle Risorse Agrarie ed Idriche Iracheno, Firenze 5 ottobre 2016

9. Martina Cambi, **Francesca Giannetti**, Francesca Bottalico, Gherardo Chirici, Enrico Marchi. *"Estimating rutting and soil displacement in skid trails by soil sampling and 3D Structure for Motion (SfM) photogrammetry modelling: first trial in Vallombrosa forest (Italy)"*. 49th International Symposium on Forestry Mechanization (FORMEC) - 4-7 September 2016, Warsaw (Poland)
10. **Giannetti**, F., Chirici. G. Applicazioni SAPR per la Selvicoltura di Precisione. Seminario "*Sistemi a pilotaggio remoto per l'agricoltura di precisione. Esperienze e applicazioni in colture agricole e forestali*", Arezzo, 24 giugno 2016
11. **Giannetti F.,** Chirici G., Paoletti E., Borghetti M., Corona, P., Bucci G. *"Assessing the scientific productivity of the Italian forestry community*". X Congresso Nazionale SISEF – Boschi per la vita, 15-18 Settembre 2015, Firenze
12. Cibecchini D., Aminti G., Antonello L., Bracalini M., Cambi M., Carrai E., Croci F., Errico A., Foderi C., Frassinelli N., Giambastiani Y., **Giannetti F.**, Iacobelli S., Laschi A., Racanelli V., Sassoli M., Migliorini D. "*Unusual meterological phenomena: Vallombrosa forest windthrow caused by the storm of March 5th. Analyses and evaluations*". X Congresso Nazionale SISEF – Boschi per la vita, 15-18 Settembre 2015, Firenze
13. Chirici G., Bottai L., Bottalico F., Bronzi A., Chiostri C., Ciancio O., Fioravanti M., Germani M., Giannetti F., Gozzini B., Gravano E., Melara A.M., Nocentini S., Travaglini D. *"Attività di monitoraggio dei danni da vento ai comprensori forestali della Regione Toscana a seguito dell'evento del 5 marzo 2015*". X Congresso Nazionale SISEF – Boschi per la vita, 15-18 Settembre 2015, Firenze
14. Bottalico F., Chirici G., De Marco A., Garfì V., **Giannetti F**., Nocentini S., Paoletti E., Salbitano F., Sanesi G., Serenelli C., Travaglini D. "*Urban Forest and air pollutants removal: a mattar of quality of life*". X Congresso Nazionale SISEF – Boschi per la vita, 15-18 Settembre 2015, Firenze

Aword

Best presentation XI SISEF National Congress 2017 "La Foresta che Cambia: qualità della vita e opportunità in un paese che cambia", Rome 10-13 October 2017. **Giannetti F**, Puliti S, Gobakken T, Næsset E, Travaglini D, Chirici G - **"DTM-independent variables to predict forest inventory variables using 3D UAV photogrammetric data".**